LIMNOTEK Perairan Darat Tropis di Indonesia
transforming into the Journal of Limnology and Water Resources
p-ISSN: 0854-8390 e-ISSN: 2549-8029
https://ejournal.brin.go.id/limnotek

Volume 30, Number 1, 2024

National Research and Innovation Agency (BRIN)

Indonesian Limnology Society (MLI)

p-ISSN: 0854-8390
e-ISSN: 2549-8029
LIMNOTEK
Perairan Darat Tropis di Indonesia,
***transforming into the* Journal of Limnology and Water Resources**

Volume 30, Number 1, June 2024

DOI: https://doi.org/10.55981/limnotek.v30i1

Published by: National Research and Innovation Agency (BRIN) and Indonesian Limnology Society (MLI)

Advancing Sustainable Water Management in the spirit of Water for Shared Prosperity

Recalling the successful 10th World Water Forum (WWF) 2024, held in the spirit of "Water for Shared Prosperity," Indonesia prioritized three key areas. First, the proposal of a World Lake Day, to commemorate lakes as a vital source of water that supports humans while providing social and economic benefits to society. Second, establishing a Center of Excellence for Water Security and Climate, aimed at capacity building, knowledge sharing, and utilizing superior facilities. Third, raising the issue of integrated water resources management on small islands.

The declaration aligns with our Limnotek transforming into Journal of Limnology and Water Resources (JLWR) focus and scope in establishing an integrated understanding of the interface between natural processes of water resources and inland water ecosystems with their human domains. Hence, it increased our motivation to continue exploring the intricate challenges and emerging opportunities in sustainable water and aquatic ecosystem management.

In this 2024 (1) volume, we present five research papers on key environmental and water resource issues, including the impact of weather changes on sulfide distribution in a tectonic deep lake, heavy metal contamination in a tropical lake, phosphate dynamics in coastal ecosystems, the efficacy of natural bentonite for dye removal in textile wastewater to address river pollution and flood routing dynamics in the challenging topographic using UAV data. Hopefully, our publications offer valuable insights and foster a sustainable and harmonious relationship with our aquatic environment.

In alignment with our ethos of perpetual education, life, and growth, we extend an invitation to our readers to unite in our efforts to ensure that clean water becomes a symbol of our shared commitment to the well-being of our only one earth.

Reviewers:

1. Prof. Dr. Cynthia Henny (Research Centre for Limnology and Water Resources, National Research and Innovation Agency - BRIN, Indonesia)
2. Dr. Yustiawati, S.Si., M.Sc. (Research Centre for Limnology and Water Resources, National Research and Innovation Agency - BRIN, Indonesia)
3. Arianto Budi Santoso, Ph.D. (Research Centre for Limnology and Water Resources, National Research and Innovation Agency - BRIN, Indonesia)
4. Dr. rer. nat Sulung Nomosatryo (Research Centre for Limnology and Water Resources, National Research and Innovation Agency - BRIN, Indonesia)
5. Dr. Iwan Ridwansyah, S.T., M.Sc. (Research Centre for Limnology and Water Resources, National Research and Innovation Agency - BRIN, Indonesia)
6. Siti Rachmawati, S.ST., M.Si. (Universitas Sebelas Maret, Indonesia)
7. Dr. Atriyon Julzarika (Research Centre for Limnology and Water Resources, National Research and Innovation Agency - BRIN, Indonesia)
8. Dr. Hidayat (Research Centre for Limnology and Water Resources, National Research and Innovation Agency - BRIN, Indonesia)
9. Prof. Dr. Tri Retnaningsih Soeprobowati, MAppSc (Universitas Diponegoro, Semarang, Indonesia)
10. Dr. Ir. Ery Suhartanto, ST. MT. (Brawijaya University, Malang, Indonesia)

Secretary:

1. Relita Novianti, M.Si
2. Dewi Verawati, S.Si,
3. Elenora Gita Alamanda Sapan, S.T., M.Eng.

IT Supports: Ira Akhdiana, M.Si.

Email: jlwrjournal@gmail.com

Website: https://ejournal.brin.go.id/limnotek

Mailing Address: Pusat Riset Limnologi dan Sumber Daya Air, BRIN, KST Soekarno,
Jl. Raya Bogor Km 46, Cibinong, Jawa Barat, 16911, Indonesia
phone: +62 811 1064 6825

Accreditation: SINTA-2 period 2020-2025**,** *Surat Keputusan Direktur Jenderal Pendidikan Tinggi, Riset dan Teknologi - Kementerian Pendidikan, Kebudayaan, Riset dan Teknologi Nomor 105/E/KPT/2022,* dated 7 April 2022

Cover Image: Fisherman at Lake Maninjau by Hendro Wibowo (Research Centre for Limnology and Water Resources, National Research and Innovation Agency-BRIN, Indonesia)

p-ISSN: 0854-8390
e-ISSN: 2549-8029
LIMNOTEK
Perairan Darat Tropis di Indonesia,
transforming into the Journal of Limnology and Water Resources

Volume 30, Number 1, 30 June 2024

DOI: https://doi.org/10.55981/limnotek.v30i1

Articles:

LIMNOTEK Perairan Darat Tropis di Indonesia
transforming into the Journal of Limnology and Water Resources
p-ISSN: 0854-8390 e-ISSN: 2549-8029
https://ejournal.brin.go.id/limnotek

The Impact of Weather Condition Changes on Vertical Distribution of Sulfides in Lake Maninjau Based on Observation Data

Mutiara Rachmat Putri[1,2*], Taofik Jasalesmana[1,4], Mirzam Abdurrachman[3], Cynthia Henny[4], Sulung Nomosatryo[4], Alif Shidqie Albani[2]

[1]Earth Science Doctor Program, Faculty of Earth Sciences and Technology, Bandung Institute of Technology, Bandung, Indonesia,
[2]Research Group of Oceanography, Faculty of Earth Sciences and Technology, Bandung Institute of Technology, Bandung, Indonesia,
[3]Geological Engineering Study Program, Faculty of Earth Sciences and Technology, Bandung Institute of Technology, Bandung, Indonesia,
[4]Research Center for Limnology and Water Resources, National Research and Innovation Agency (BRIN), Cibinong 16911, West Java, Indonesia

*Corresponding author's e-mail: mutiara.putri@itb.ac.id

Received: 10 October 2023; Accepted: 05 February 2024; Published: 30 June 2024

Abstract: Sulfide is a crucial parameter in volcanic lakes, as its levels and fluctuations in the lake determine the origin of sulfide and the extent of its impact on the lake ecosystem. In stratified lakes, the sulfide produced tends to be retained beneath the oxic layer. The sulfides rise towards the surface as the oxic layer thins triggered by decreased water column thermal stratification. Meanwhile, the strength or weakness of thermal stratification is greatly influenced by weather conditions. Lake Maninjau is a volcanic lake with a relatively high sulfide content. Its vertical distribution in the water column is highly dependent on the stratification of the water column. When stratification disappears, sulfide rises to the surface (locally known as *tubo belerang*) and has a negative impact on surface biota. The objective of this study is to examine the distribution of sulfides in the water column of Lake Maninjau under two different weather conditions. We perform two surveys to measure physicochemical parameters and sulfide concentration on 26–29 November 2022 and 25–26 August 2023 considering the seasonal pattern. We found that air temperatures and sunshine duration combined with precipitation and wind speed drive the thermal stratification of the water column. The lower air temperature, shorter sunshine duration, higher precipitation, and stronger wind speed in the first survey (west monsoon) compared with the second survey (east monsoon) resulted in lower stratification and triggered the elevated sulfide to the surface. In the middle of the lake, the surface sulfide measured during the first survey was 4.16 µg/L. Meanwhile, in the second survey, it was only observed at 1.16 µg/L. The distribution of sulfides within the water column of Lake Maninjau is regulated by the stratification of the water column, a process directly impacted by weather conditions.

Keywords: Lake Maninjau, thermal stratification, Sulfide concentration, air temperature, rainfall

https://doi.org/10.55981/limnotek.2024.2203

1. Introduction

Sulfide is a foul-smelling gas that is toxic to aquatic life (Boyd, 2014; Piranti *et al.*, 2018). In active volcanic lakes, sulfide can originate from acidic gases emanating from channels connected to the magma system (Aguilera *et al.*, 2000). However, in dormant

volcanic lakes, sulfide arises from sulfate reduction processes and the decomposition of organic matter (Henny, 2009; Dunnette *et al.*, 1985). Sulfide in a lake plays a crucial role in the dynamics of nutrients, metals, and dissolved oxygen (DO) in the water column (Jasalesmana *et al.*, 2023; Henny & Nomosatryo, 2012). Concerning DO, sulfide can reduce the oxic layer at the lake surface and may even eliminate the oxic layer if the DO content in that layer cannot counterbalance the amount of sulfide (Henny, 2009). This condition poses a threat to aquatic organisms because, in addition to the lack of oxygen for respiration, the existing sulfide becomes toxic to the biota.

Studies on the fluctuations of sulfide concentrations (Wardhani & Sugiarti, 2022; Riki Saputra *et al.*, 2017; Sagala & Radiarta, 2012; Handayani *et al.*, 2011) and their impact on nutrient dynamics (Henny & Nomosatryo, 2012) in various freshwater in Indonesia have been widely conducted. Similarly, the consequences of sulfide rising to the surface, leading to fish mortality, have been explored. However, there is limited research specifically examining the physical factors that drive the upward movement of sulfide in lakes. This study provides crucial information about the relationship between climatology and sulfide dynamics in the case of Lake Maninjau.

Lake Maninjau is located in Agam Regency, West Sumatra. This lake was formed due to a volcanic eruption around 52000 years ago (Alloway et al., 2004; Pribadi et al., 2007). This lake has several functions: tourism activities, fisheries, aquaculture, and hydroelectric power generation (PLTA). However, deteriorating water quality has caused the tourism sector to become unpopular. The decline in water quality is characterized by frequent eutrophication and the rise of sulfide from the bottom to the surface resulting in the death of fish in Floating Net Cages (FNC). From 1997 to 2019, losses due to fish deaths reached Rp. 212,175,000,000 (Makmur *et al.*, 2020).

As a volcanic lake, volcanic activity may contribute to sulfide production in Lake Maninjau. However, a previous study reported that sulfide in Lake Maninjau was produced from the sulfate reduction process by sulfate-reducing bacteria (Henny, 2009). The speed of sulfate reduction to sulfide depends on organic carbon, inorganic carbon, or hydrogen as an electron donor and sulfate as an electron acceptor (Henny, 2009). Therefore, increased organic matter from KJA activity has triggered increased sulfide concentrations in Lake Maninjau (Henny & Nomosatryo, 2012, 2016; Henny, 2009). The resulting sulfide will accumulate in the anoxic base layer. Sulfides can rise to the surface, but when they meet the oxic layer, the sulfides are immediately oxidized back to sulfate, potentially depleting the oxygen in the layer (Dunnette *et al.*, 1985).

The distribution of sulfides in the water column is highly dependent on the stratification of the water column, which is directly influenced by weather conditions (Henny, 2009). Stratification inhibits the mixing process between molecules in the hypolimnion and epilimnion layers (Elci, 2016). Consequently, this causes the accumulation of molecules produced in the hypolimnion layer, including sulfide, carbon dioxide, and ammonia (Shi *et al.*, 2021; Kusakabe *et al.*, 2008). However when strong winds and air temperature decrease, the stratification of the column disappears, causing sulfides and other molecules to rise to the surface (Katsev et al., 2010; Santoso et al., 2018; Fukushima et al., 2017, 2021).

Previous studies of sulfide distribution in the water column of Lake Maninjau have not linked it directly to weather conditions (Henny & Nomosatryo, 2012, 2016; Henny, 2009). Therefore, this study aims to examine the distribution of sulfides in the water column of Lake Maninjau under two different weather conditions: high rainfall intensity and high light intensity.

2. Materials and Methods

2.1. Sampling Location and Sulfide - Analysis

The survey at Lake Maninjau was carried out on 26 – 29 November 2022 and 25 – 26 August 2023 (hereafter we call it "Survey 1" and "Survey 2") at seven (7) sampling points (Figure 1). The selection of these two times will represent weather conditions during rainfall (west monsoon), (November 2022) and high sunlight intensity (east monsoon), (August 2023). Temperature and dissolved oxygen (DO) measurements in survey 1 were

conducted using a CTD Rinko Profiler, while survey 2 utilized a ProDO YSI© International. Oxidation-reduction potential (ORP) and pH were measured in both survey 1 and 2 using HORIBA©U-52. Sulfide was measured from water samples taken using a 5 L Niskin Bottle water sampler from a depth of 0.5 m, 2 m, 10 m, 60 m and maximum depth on November 2022 and depth of 0.5 m, 2 m, 10 m, 60 m, and maximum depth on August 2023. The maximum depth varies based on sampling point. Sulfide concentrations were analyzed using the Methylene Blue Method (8131 Method) with the following stages (Manual, 2007): 1. Water samples are taken from a 5 L Niskin Bottle water sampler using a 50 ml syringe and filtered with a 0.45 µm filter. 2. The water sample was quickly transferred to a 10 ml tube to which ZnAc had been added. 3. The water sample is then added to reagents I and II. 4. The sulfide concentration in the sample was then measured using a DR3900 portable spectrophotometer (Manual, 2007).

2.2. Meteorological Data

Air temperature, wind, sun duration (SD), and rainfall on a daily scale were taken from the Padang Panjang Geophysics Station (0° 27' 58.68" S, 100° 22' 46.92" E), which has been published at https://dataonline.bmkg.go.id/data_iklim (Pusat Database-BMKG). Data taken from January 2022 to August 2023. SD is a climatological element used to express solar power exceeding 120 Wm^{-2} (Hamdi, 2014).

2.3. Data Analysis

Relative Thermal Resistance to Mixing (RTRM) is used to assess changes in the stratification strength of the lake water column against weather changes. RTRM is a straightforward approach for quantifying stratification caused by temperature differences (Kunz & Wildman, 2019; Kortmann, 1981). RTRM is calculated with the equation:

$$RTRM = \frac{\text{density of upper layer} - \text{density of lower layer}}{\text{density at 5℃} - \text{density at 4℃}} \quad \text{....Eq. 1}$$

The water density (ρ_T) of the water layer was calculated from the average temperature (T) of the water layer at each measurement point. Water density is calculated by the equation (Ji, 2017):

$$\rho_T = 999.842594 + 6.793952 \times 10^{-2} T - 9.095290 \times 10^{-3} T^2 + 1.001685 \times 10^{-4} T^3 - 1.120083 \times 10^{-6} T^4 + 6.536332 \times 10^{-9} T^5 \quad \text{....Eq. 2}$$

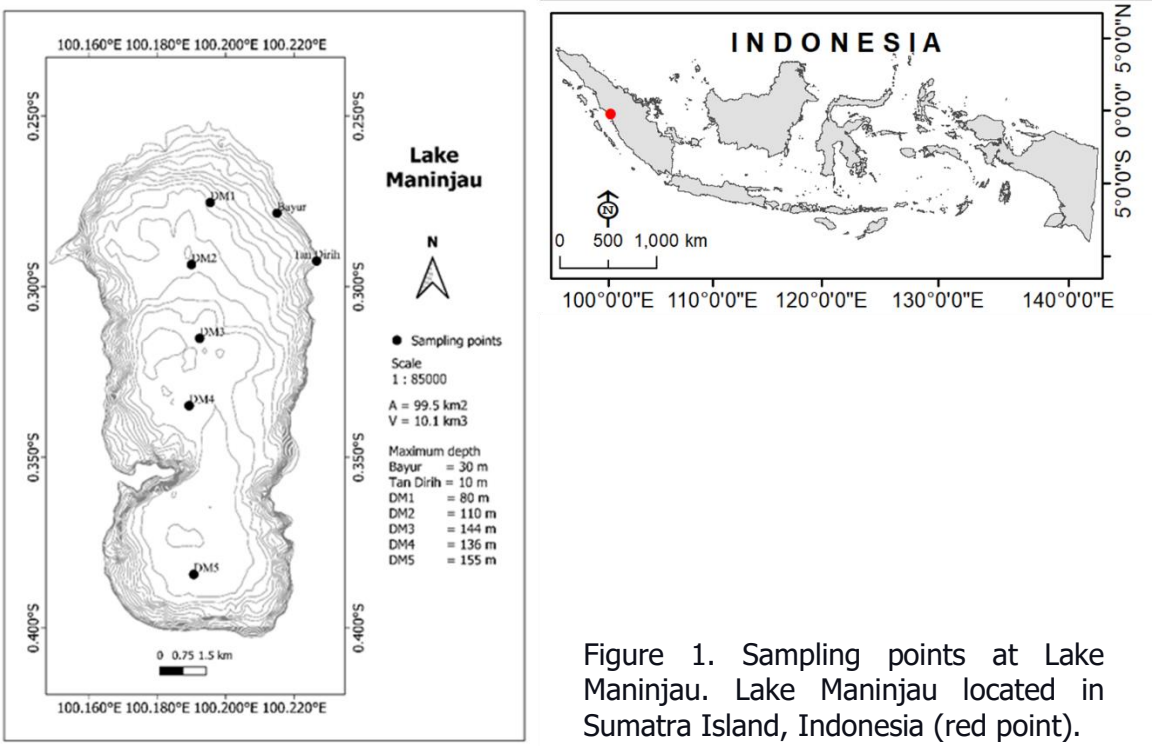

Figure 1. Sampling points at Lake Maninjau. Lake Maninjau located in Sumatra Island, Indonesia (red point).

3. Results and discussion

3.1. Physicochemical Profile of Water Column

The temperature profile of the water column in survey 1 and survey 2 is shown in Figure 2. The temperature profile of the water column in survey 1 relatively looks homogeneous. In contrast, in survey 2 appears stratified, as indicated by the differences in average temperature between the surface and the bottom, with a higher value of 2,2 °C compared to survey 1 is 1.16 °C. Based on the two temperature profiles, the hypolimnion layer of the water column in survey 2 starts from a much deeper depth (29.7 m) compared to survey 1 (1.28 m). The homogeneous temperature profile structure in survey 1 indicates that the Lake Maninjau water column experienced mixing at that time.

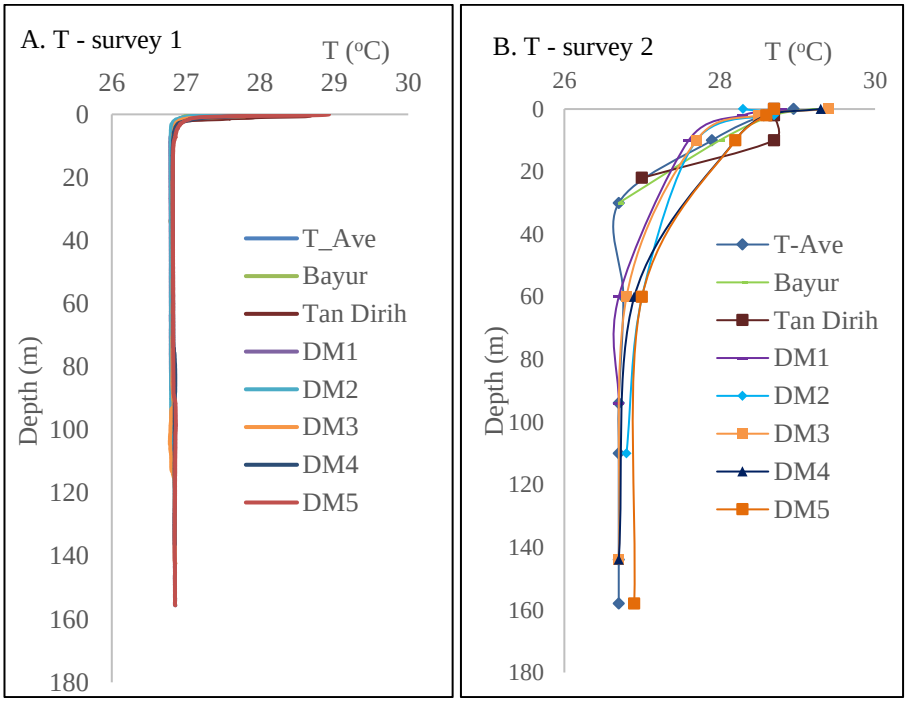

Figure 2. Water column temperature profile in (A) Survey 1 and (B) Survey 2. T-ave is the average temperature of the water column from each station.

The dissolved oxygen (DO) profile also indicates mixing conditions in the water column during survey 1. In survey 1, the water column's DO profile exhibits homogeneity from the surface to the bottom, with an average surface DO concentration of 0.74 mg/L, and its structure is similar to the temperature profile. Conversely, in the second observation, the water column displayed a high DO content, with an average surface DO concentration of 7.64 mg/L. The anoxic layer in the first observation, which was entirely in every layer of the water column, shifted to a depth of 10 in the second observation. This condition can be caused by the production of oxygen from the photosynthesis process by phytoplankton taking place optimally and sulfide as an oxygen reducer remaining in the bottom layer so that it does not reduce the oxygen content at the surface.

Fluctuations in the ups and downs of oxygen levels in the surface layer of Lake Maninjau can occur within a short time (up to an hour scale). In fact (Santoso & Triwisesa, 2020) stated that DO deficiency in Lake Maninjau could occur at any time, significantly if the loading of organic matter from KJA activities increases. However, in long-time observations, the anoxic layer of Lake Maninjau's water column tends to approach the surface (Subehi *et al.*, 2021; Fukushima *et al.*, 2017).

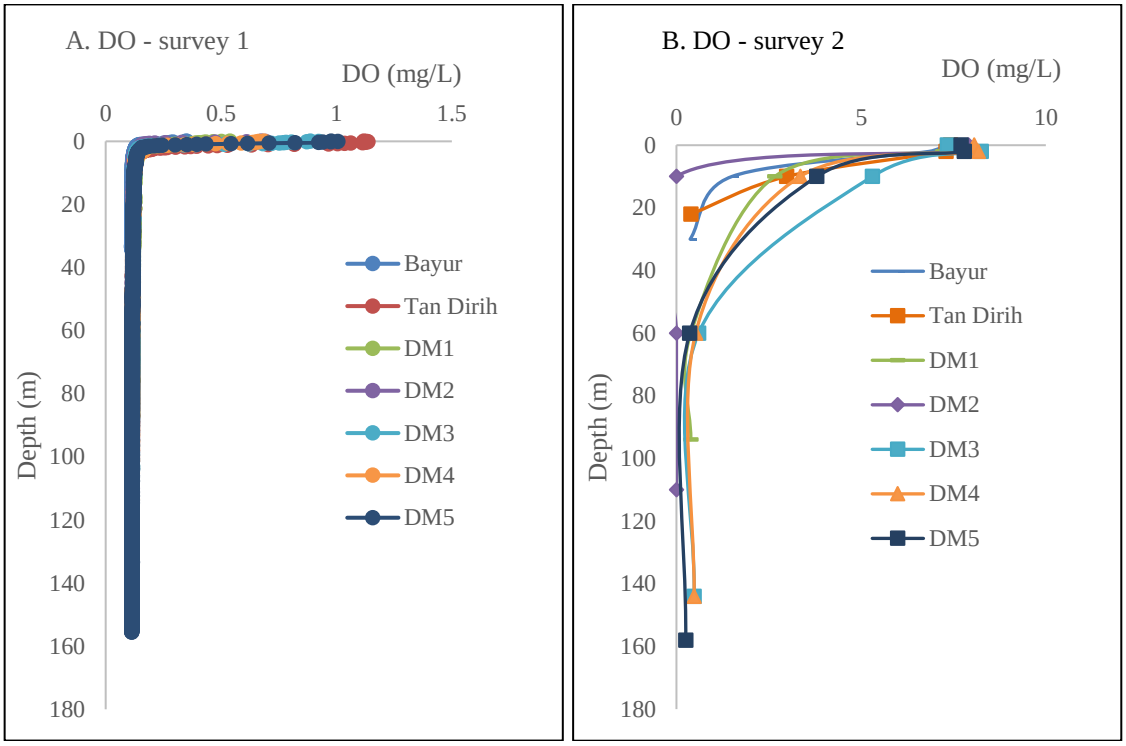

Figure 3. DO profile of the Maninjau Lake water column A) Survey 1 and B) Survey 2. DO water column in survey 1 appears to be homogeneous from the surface to the bottom with a low level. This differs from the water column in survey 2, which has a high DO concentration in the epilimnion layer.

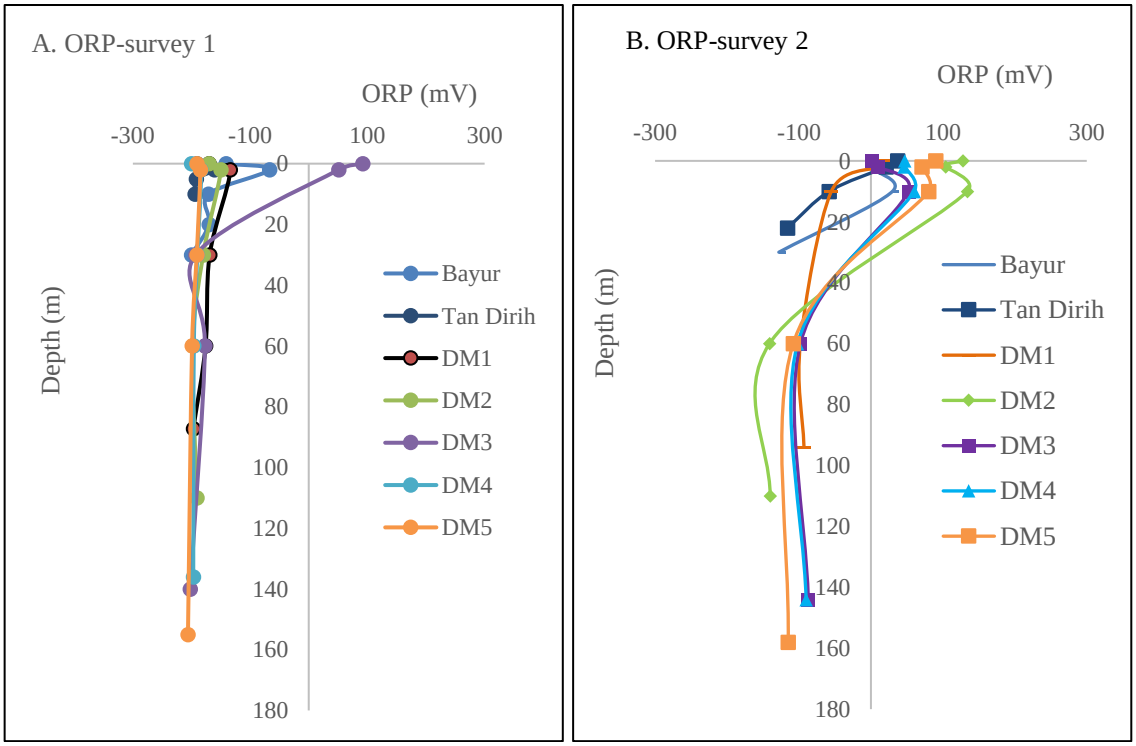

Figure 4. ORP profile of Lake Maninjau water column in (A) survey 1, (B) survey 2.

The significant difference in DO levels in the water column between the first and second survey periods indicates two different redox conditions. This can be seen from the ORP profile in the water column. Figure 4. A shows the ORP of the water column in the first survey period, which is generally negative from the surface to the bottom. In the second survey, the average ORP is negative from a water depth of 10 m (Fig. 4.B). A negative ORP indicates that much oxygen is used for the reduction process, so the oxygen content in the water column decreases drastically. Based on Figure 4.A it can be explained that each layer of the water column in the first survey period is in a reduced state, while the water column in the second survey is in a reduced state starting at a depth of 10 m.

3.2. Sulfide Distribution in Water Column

The physicochemical characteristics of the lake, as demonstrated by the temperature, dissolved oxygen (DO), and oxidation-reduction potential (ORP) profiles in each survey, have an impact on the sulfide profile in the water column. The homogeneity in temperature and DO throughout the water column in survey 1 indicates the absence of stratification, facilitating the movement of various molecules and gases, including sulfides, from the bottom to the surface. Figure 5 displays the distribution of sulfide in the water column of Lake Maninjau during survey 1 and survey 2. Based on Figure 5. A, sulfide in survey 1 is found at the surface with a concentration of 4.16 µg/L, suggesting that sulfides can rapidly rise to the surface due to the absence of thermal stratification. The sulfide concentration in the lake exceeded the class III water quality (for aquaculture) standard set at 2.0 µg/L (Piranti *et al.*, 2018). In contrast, as depicted by the sulfide profile in survey 2 (Figure 5.B), the average sulfide concentration on the surface is only 1.16 µg/L. However, the sulfide concentration in the lower layers is higher compared to the findings from survey 1. By comparing the sulfide concentration at a depth of 60 m, it can be seen that the sulfide in the survey 2 is on average 6 times greater than the sulfide in survey 1.

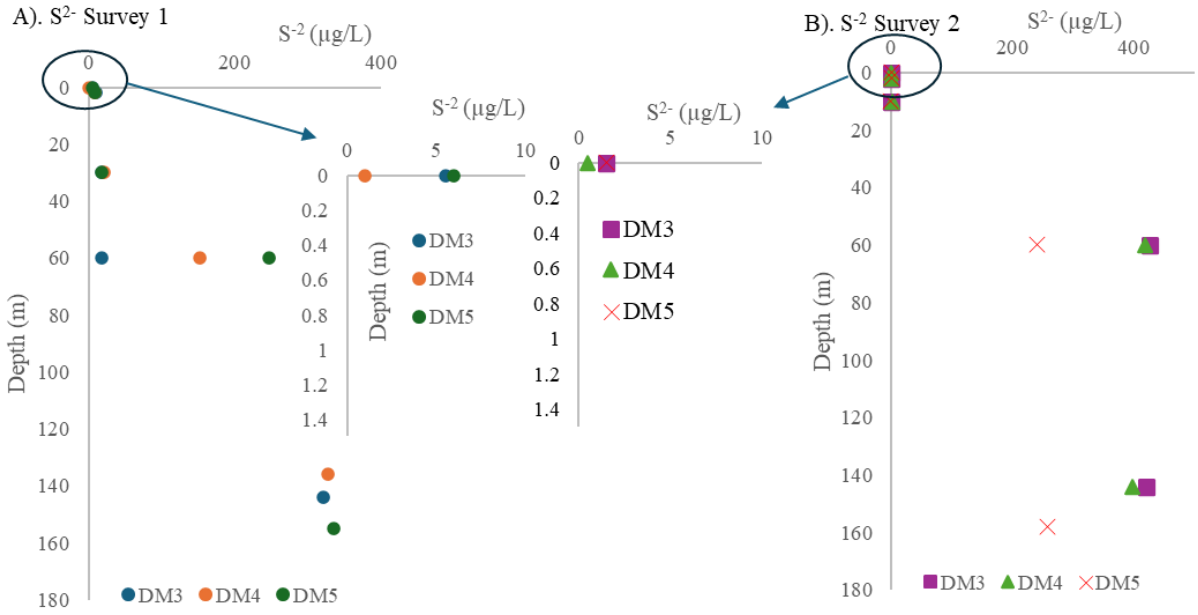

Figure 5. Distribution of sulfide in the water column of Lake Maninjau in (A) survey 1 and (B) survey 2. Small graphs provide snapshot of sulfide levels at the surface.

The elevated sulfide levels in the lower layer during survey 2 indicate that the temperature stratification of the water column during this survey restricted the upward movement of sulfide from the bottom layer to the surface. Simultaneously, the process of sulfate reduction to sulfide by sulfate-reducing bacteria persisted in the bottom layer, leading to the accumulation of sulfide in these lower layers. This is shown by the sulfide

concentration in bottom layer during survey 2 was higher than in survey 1. In contrast, the lower sulfide concentrations in the lower layer during survey 1 resulted from the upward movement of sulfide to the surface as thermal stratification disappeared. Consequently, the dynamics of water column stratification play a crucial role in controlling the distribution of sulfides in Lake Maninjau's water column.

3.3. The Effect of Weather on the Sulfide Distribution

The lake's physical factor most significantly influenced by meteorological parameters is temperature. The temperature of the lake water column will be strongly stratified when the lake absorbs a large amount of heat energy from the atmosphere. When the stratification of the water column is strong, the lake water column will be stable from the mixing process, either through diffusion or convection (Read *et al.*, 2011).

Figure 6 shows the air temperature taken from the Padang Panjang BMKG station in 2022 and 2023. Visually, it can be seen that the air temperature in November 2022 is slightly lower than the air temperature in August 2023 with average temperatures of 22.43 and 22.94 °C, respectively. Even though the air temperature did not differ significantly, the rainfall between the two observation periods differed significantly. The average daily rainfall in the first observation was 21.34 mm, while in the second observation, it was 12.46 mm (Figure 7). Liu et al. (2020) reported that rain can reduce the lake's surface temperature; therefore, the decrease in lake surface temperature in survey 1 was more drastic than in survey 2. This will cause a temperature difference between the surface layer (which is usually warmer), and the bottom layer (which is cooler) becomes smaller, and even the temperature of the water column becomes homogeneous.

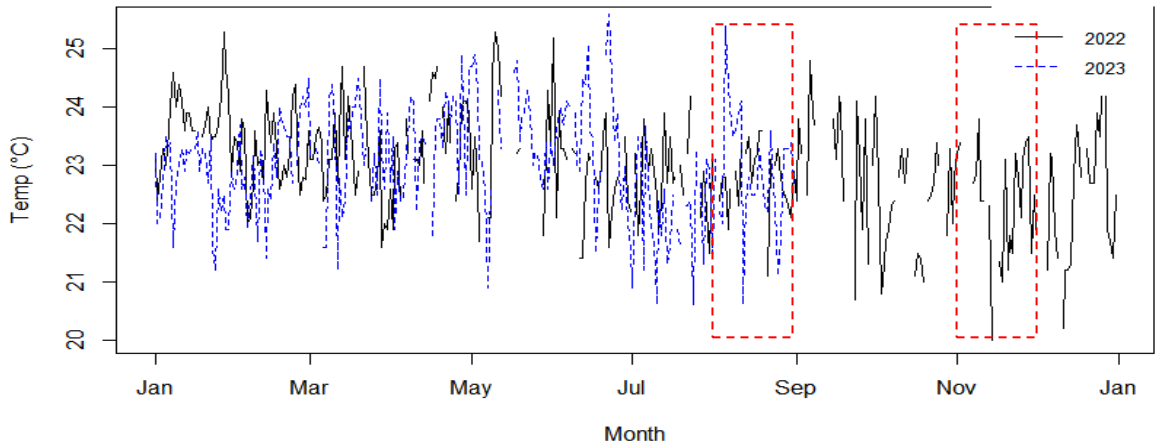

Figure 6. The average air temperature in 2022 and 2023. The black line shows the average air temperature in 2022, and the dotted blue line shows the average air temperature in 2023. The air temperature in 2023 can be found on the website https://dataonline. bmkg.go.id/data_iklim is only available until August.

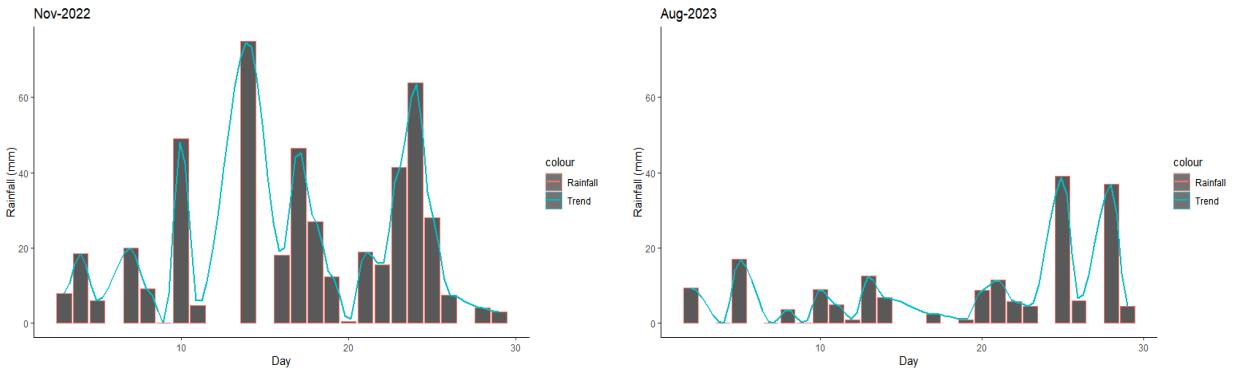

Figure 7. Daily rainfall in November 2022 (left) and August 2023 (right). In general, the average rainfall in November 2022 is higher than August 2023.

Apart from rainfall and air temperature, wind, and solar radiation significantly influence the regulation of water column stratification (Santoso *et al.*, 2018). Figure 8 illustrates the maximum wind speed and sunshine duration (SD) in November 2022 and August 2023. While the average wind speed in November 2022 (v = 3.80 m/s) is not markedly different from that in August 2023 (v = 3.90 m/s), the figure reveals that the wind speed during survey 1 was higher than in survey 2. Conversely, the sunshine duration in November 2022 (1.07 hours) was lower than in August 2023 (SD = 4.41 hours). Therefore, the combination of high rainfall, low air temperature, high wind speed, and low sunshine duration during survey 1 led to a weakening of water column stratification, while the opposite occurred in survey 2.

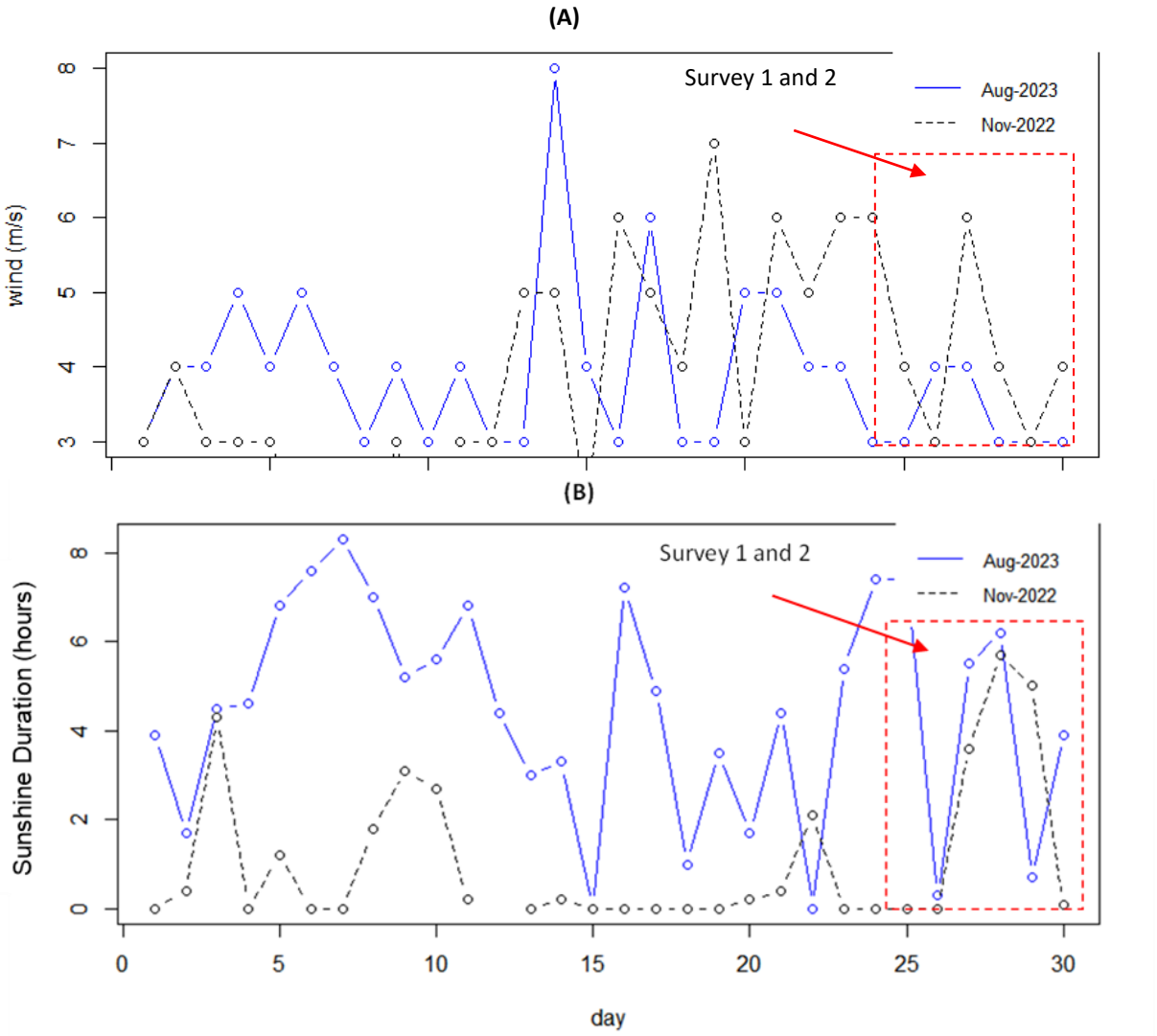

Figure 8. Comparison of (A) Maximum wind speed and (B) sunshine duration in November 2022 and August 2023

The differences in meteorological parameters between the first and second observations impact the stratification of the water column and, at the same time, impact the distribution of sulfides in Lake Maninjau. The sulfide detection on the surface in survey 1 was caused by weakening stratification forces in the water column due to low air temperatures and high rainfall. This condition can be seen from the RTRM profile of the water column in survey 1 (Figure 8.A). Based on Figure 9. A, the RTRM value for the total water column in survey 1 was 36.39, while the RTRM for each water layer varied between -0.16 – 5.60. The water column RTRM in survey 1 was lower than survey 2, which had a total RTRM of 77.50, with the

RTRM of each layer varying in the range -0.13 – 13.59 (Figure 9 B).

The RTRM in survey 1, which is lower than that in survey 2, indicates that the water column in survey 1 experienced mixing, while the water column in survey 2 appeared relatively more stable Visually it can also be seen that the RTRM in survey 1 is zero in almost every layer. Only the water column at a depth of 0 - 1.2 m has an RTRM of more than 1. Because the depth of RTRM > 0 is deeper than the depth of the hypolimnion (29.7 m), as a result, the epilimnion and hypolimnion layers in survey 2 did not undergo mixing. The depth of 32 m to the bottom can be expressed as a mixed hypolimnion layer, where reduction reactions occur, with zero DO content and high sulfides.

The lower RTRM in survey 1, compared to survey 2, indicates that water column stratification is strongly influenced by weather conditions. The low RTRM of the water column in survey 1 facilitated the rise of sulfide to the surface. On the other hand, the high RTRM water column in survey 2 prevents sulfide from rising to the surface as a result it accumulates in the hypolimnion layer, as shown in Figure 5 B.

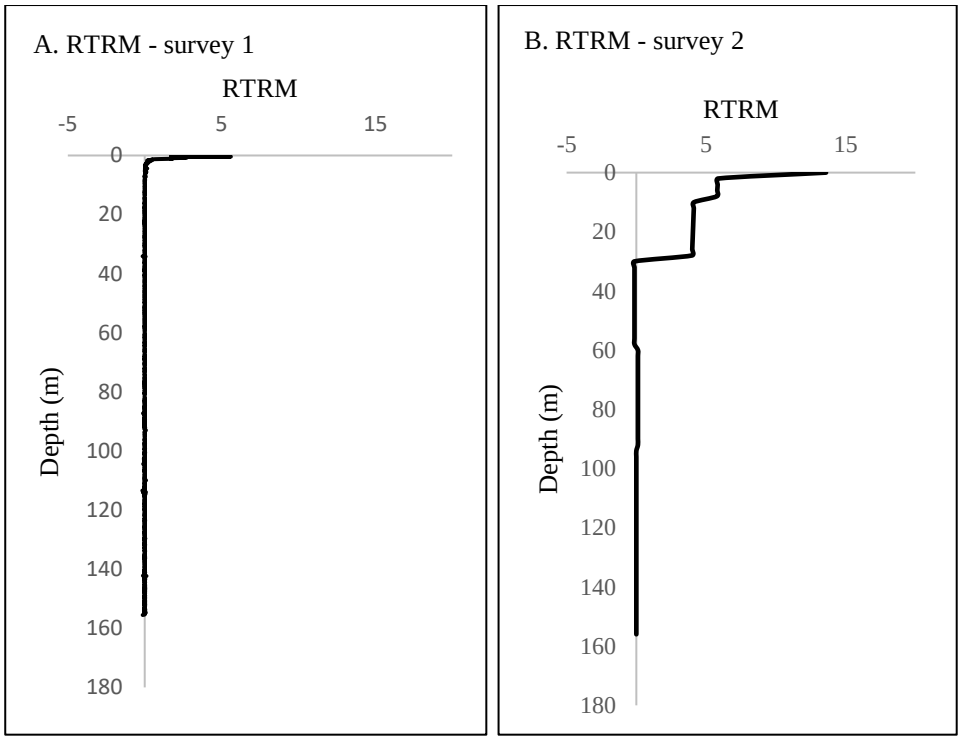

Figure 9. Relative thermal resistance to mixing (RTRM) of water column in Survey 1 and Survey 2

4. Conclusion

This research highlights the importance of characterizing climatological parameters (patterns and magnitudes) as driving factors for the changes in the thermal stratification of a lake. The alteration of thermal stratification due to weather changes has implications for the distribution of sulfide in the water column. The combination of high rainfall and wind speed, along with low sunshine duration and air temperature in survey 1, led to the disappearance of water column stratification, resulting in the upward movement of sulfides to the surface. Conversely, when the air temperature and sunshine duration are high, and the rainfall and wind speed are low, the water stratification will be strong, resulting sulfides remaining in the hypolimnion layer and continuing to increase. This research can be applied to similar lakes and serve as a basis for the development of early warning systems to prevent fish kill event caused by the rise of sulfide to the surface.

Data availability statement

All data used in this study are primary and secondary data. The secondary data is climatological data, which can be accessed openly on the website Pusat Data-BMKG

Funding Agencies

This research was supported in part by SAINTEK scholarship from the minister of research and technology-BRIN and Research Program of the Ministry of Education, Culture, Research, and Technology 2023, contract number: 110/E5/PG.02.00.PL/2023.

Conflict of interests

All authors declare that there are no conflicts of interest in this study.

Author's Contribution

MRP was the team leader of the project. **MRP** and **TJ** developed the idea for this manuscript. **MRP**, **MA** and **CH** provided substantial intellectual contributions to the manuscript. **TJ**, **SN**, and **ASA** contributed on survey and data preparation. All co-authors reviewed and consented to the final version of the document.

References

Aguilera E, Chiodini G, Cioni R, Guidi M, Marini L, Raco B. 2000. Water chemistry of Lake Quilotoa (Ecuador) and assessment of natural hazards. *Journal of Volcanology and Geothermal Research* 97: 271–285. DOI: 10.1016/S0377-0273(99)00168-7

Alloway B V., Pribadi A, Westgate JA, Bird M, Fifield LK, Hogg A, Smith I. 2004. Correspondence between glass-FT and 14C ages of silicic pyroclastic flow deposits sourced from Maninjau caldera, west-central Sumatra. *Earth and Planetary Science Letters* 227: 121–133. DOI: 10.1016/j.epsl.2004.08.014

Boyd C. 2014. Hydrogen Sulfide Toxic, But Manageable. *Global Aquaculture Advocate* 17: 34–36

Dunnette D, Chynoweth D, Mancy K. 1985. The Source of Hydrogen Sulfide in Anoxic Sediment. *Water* 19: 875–884

Elci S. 2016. Effects of thermal stratification and mixing on reservoir water quality. DOI: 10.1007/s10201-008-0240-x

Fukushima T, Matsushita B, Subehi L, Setiawan F, Wibowo H. 2017. Will hypolimnetic waters become anoxic in all deep tropical lakes? *Scientific Reports* 7: 1–8. DOI: 10.1038/srep45320

Fukushima T, Setiawan F, Subehi L, Fakhrudin M, Triwisesa E, Dianto A, Matsushita B. 2021. Convection of waters in Lakes Maninjau and Singkarak, tropical oligomictic lakes. *Limnology*. DOI: 10.1007/s10201-021-00686-8

Hamdi S. 2014. Mengenal Lama Penyinaran Matahari Sebagai Salah Satu Parameter Klimatologi. *Berita Dirgantara* 15: 7–15. DOI: 10.20885/unisia.vol28.iss56.art12

Handayani CIM, Arthana IW, Merit IN. 2011. Identifikasi Sumber Pencemar dan Tingkat Pencemaran Air di Danau Batur Kabupaten Bangli. *Ecotrophic* 6: 37–43

Henny C. 2009. Dynamics of Biogeochemisrty of Sulfur in Lake Maninjau. *Limnotek* XVI: 74–87

Henny C, Nomosatryo S. 2012. Sulfide Dynamics in Lake Maninjau: The Implication on Phosphate Release in the Hypolimnion. *Limnotek : perairan darat tropis di Indonesia* 19: 102–112

Henny C, Nomosatryo S. 2016. Changes in water quality and trophic status associated with cage aquaculture in Lake Maninjau, Indonesia. *IOP Conference Series: Earth and Environmental Science* 31. DOI: 10.1088/1755-1315/31/1/012027

Jasalesmana T, Putri MR, Abdurrachman M. 2023. Water Quality Assessment of Lake Maninjau After the Mass Fish Kill Event. *IOP Conf. Series: Earth and Environmental Science*

Ji ZG. 2017. *Hydrodynamics and water quality: Modeling rivers, lakes, and estuaries*. *Hydrodynamics and Water Quality: Modeling Rivers, Lakes, and Estuaries*. DOI: 10.1002/9781119371946

Katsev S, Crowe SA, Mucci A, Sundby B, Nomosatryo S, Douglas Haffner G, Fowle DA. 2010. Mixing and its effects on biogeochemistry in the persistently stratified, deep, tropical Lake Matano, Indonesia. *Limnology and Oceanography* 55: 763–776. DOI: 10.4319/lo.2009.55.2.0763

Kortmann RW. 1981. RTRM. *LakeLine. Ecosystem Consulting Services, Inc.* 7–10

Kunz K, Wildman R. 2019. Effects of Solar Radiation and Air Temp on Thermal Stratification of Lakes. 0–3

Kusakabe M, Ohba T, Issa, Yoshida Y, Satake H, Ohizumi T, Evans WC, Tanyileke G, Kling GW. 2008. Evolution of CO2 in lakes Monoun and Nyos, Cameroon, before and during controlled degassing. *Geochemical Journal* 42: 93–118. DOI: 10.2343/geochemj.42.93

Liu M, Zhang Y, Shi K, Zhang Y, Zhou Y, Zhu M, Zhu G, Wu Z, Liu M. 2020. Effects of rainfall on

thermal stratification and dissolved oxygen in a deep drinking water reservoir. *Hydrological Processes* 34: 3387–3399. DOI: 10.1002/hyp.13826

Makmur S, Muthmainnah D, Subagdja. 2020. Fishery activities and environmental condition of Maninjau Lake, West Sumatra. *IOP Conference Series: Earth and Environmental Science* 564. DOI: 10.1088/1755-1315/564/1/012025

Manual. 2007. *DR 2800 Spectrophotometer*.

Piranti AS, Rahayu DRUS, Waluyo G. 2018. Evaluasi Status Mutu Air Danau Rawapening. *Jurnal Pengelolaan Sumberdaya Alam dan Lingkungan (Journal of Natural Resources and Environmental Management)* 8: 151–160. DOI: 10.29244/jpsl.8.2.151-160

Pribadi A, Mulyadi E, Indyo P. 2007. Mekanisme erupsi ignimbrit Kaldera Maninjau , Sumatera Barat. *Jurnal Geologi Indonesia* 2: 31–41

Pusat Data -BMKG. (n.d.). *Pusat Database – BMKG. DataOnline https://dataonline.bmkg.go.id/data_iklim*. (last acessed on 30 August 2023)

Read JS, Hamilton DP, Jones ID, Muraoka K, Winslow LA, Kroiss R, Wu CH, Gaiser E. 2011. Derivation of lake mixing and stratification indices from high-resolution lake buoy data. *Environmental Modelling and Software* 26: 1325–1336. DOI: 10.1016/j.envsoft.2011.05.006

Riki Saputra IWR, Restu IW, Ayu Pratiwi M. 2017. Analisis Kualitas Air Danau Sebagai Dasar Perbaikan Manajemen Budidaya Perikanan Di Danau Buyan Kabupaten Buleleng, Provinsi Bali. *ECOTROPHIC : Jurnal Ilmu Lingkungan (Journal of Environmental Science)* 11: 1. DOI: 10.24843/ejes.2017.v11.i01.p01

Sagala S, Radiarta IN. 2012. Vertical-Horizontal Water Quality Profiles of Batur Lake, Bangli District, Bali Supporting Sustainable Lake Management. *Indonesian Aquaculture Journal* 7: 157. DOI: 10.15578/iaj.7.2.2012.157-169

Santoso AB, Triwisesa E. 2020. Ecosystem Metabolism and Oxygen Deficit in Lake Maninjau: Insight From High-Frequency Measurement. *Limnotek : perairan darat tropis di Indonesia* 27: 93–102. DOI: 10.14203/limnotek.v27i2.306

Santoso AB, Triwisesa E, Fakhrudin M, Harsono E, Rustini HA. 2018. What do we know about Indonesian tropical lakes? Insights from high frequency measurement. *IOP Conference Series: Earth and Environmental Science* 118: 0–5. DOI: 10.1088/1755-1315/118/1/012024

Shi J, Wang L, Yang Y, Huang T. 2021. Effects of seasonal thermal stratification on ammonia nitrogen transformation in a source water reservoir. *Processes* 9: 1–12. DOI: 10.3390/pr9122218

Subehi L, Ridwansyah I, Fukushima T. 2021. Dissolved Oxygen Profiles and Its Problems at Lake Maninjau, West Sumatra – Indonesia. *Indonesian Journal of Limnology* 1. DOI: 10.51264/inajl.v1i1.3

Wardhani E, Sugiarti ZA. 2022. Depth Profiles of Dissolved Oxygen (DO) and Hydrogen Sulfide (H2S) Concentration in a Tropical Freshwater Reservoir. *Jurnal Presipitasi : Media Komunikasi dan Pengembangan Teknik Lingkungan* 19: 316–329. DOI: 10.14710/presipitasi.v19i2.316-329

LIMNOTEK Perairan Darat Tropis di Indonesia
transforming into the Journal of Limnology and Water Resources
p-ISSN: 0854-8390 e-ISSN: 2549-8029
https://ejournal.brin.go.id/limnotek

Characteristics of Phosphate Sorption on Surface Sediments: A Study in Kendari Bay

Siti Aisyah[1,2], Eti Rohaeti[1], Arianto Budi Santoso[2], Mohamad Rafi[1]

[1] Department of Chemistry, Faculty of Mathematics and Natural Sciences, Bogor Agriculture Institute, Darmaga Bogor, 16680, Indonesia
[2]Research Centre for Limnology and Water Resources, National Research and Innovation Agency, KST Soekarno – BRIN, Bogor, Indonesia

*Corresponding author's e-mail: aisyah_siti@apps.ipb.ac.id

Received: 10 October 2023; Accepted: 05 February 2024; Published: 30 June 2024

Abstract: Phosphate adsorption and desorption are significant processes that influence the presence of phosphate in aquatic ecosystems and regulate the concentration of phosphate at the water-sediment interface. This research aims to investigate the characteristics of phosphate adsorption and desorption in Kendari Bay sediments, study the relationship between adsorption capacity and sediment characteristics and its phosphorus fraction, and evaluate its potential contribution to the overlying water column. Physicochemical measurements of the water and sediments were performed in the sampling location and the laboratory. Two types of adsorption-desorption kinetics models and two types of isothermal adsorption models were used to estimate the adsorption rate and capacity of the surface sediments. Adsorption kinetics and desorption kinetics experiments produced pseudo-second-order kinetic model equations with regression coefficients (R2) of 0.865–0.936 and 0.886–0.947, respectively. The isothermal adsorption experiment follows the Langmuir equation model with R^2 = 0.964. The maximum adsorption capacity (Q_{max}) value was 156.3–227.3 mg/kg, and the phosphate concentration value at zero equilibrium (EPC_0) was 0.0026–0.0047 mgP/L. Notably, the EPC_0 value was higher than the SRP concentration, indicating that the resuspension of phosphate ions from sediment into the water column could occur. Furthermore, there was a correlation between Q_{max} values with OP, Al-P, Fe-P, clay particles, and organic materials. Potential practical applications may include integrating sediment adsorption capacity data into ecosystem models to inform nutrient management strategies and promote sustainable coastal development in Kendari Bay and beyond.

Keywords: phosphate adsorption, desorption kinetics, water-sediment interface, coastal development, Kendari Bay

DOI: https://doi.org/10.55981/limnotek.2024.2019

1. Introduction

Phosphorus is one of the anthropogenic pollutants that causes eutrophication. Eutrophication can trigger the growth of algae, thereby reducing water quality, which has become a serious threat over the last few decades (Axinte *et al.*, 2015). This phenomenon can result in reduced biodiversity due to reduced dissolved oxygen content. Dissolved inorganic phosphorus (DIP) is a phosphorus fraction that is easily utilized by algae and is a rate-limiting nutrient for phytoplankton primary productivity (Wang *et al.*, 2018). Particulate inorganic phosphorus is in the mineral phase, which is the result of DIP adsorption by particles in the water.

As a crucial element for life on earth, phosphorus regulates a variety of biogeochemical reactions in freshwater and marine systems. Phosphorus in water exists in

dissolved and particulate forms Particulate phosphorus compounds can be found in the form of calcium salt (Ca-phosphate), iron (Fe-phosphate) or complex salts of aluminum (Al-phosphate), and organic phosphorus (OP) (Bramha *et al*., 2014). Phosphorus dissolved or soluble reactive phosphorus (SRP) is commonly known as orthophosphate. Orthophosphate is a form of phosphate that can be used directly by phytoplankton. Loosely adsorbed P is often referred to as exchangeable P. Mobilization of particulate P in a form available to phytoplankton occurs through organic matter degradation, desorption, and mineral dissolution reactions.

In the water column, the phosphate ions will interact with the surrounding particles (Maslukah *et al*., 2017). Naturally, the phosphate ions bind to particles by adsorption, leading to larger aggregates and deposition (Zhang *et al*., 2015). The phosphate ions will be released into the water column below by a desorption process if the ambient conditions of the water change (pH, oxygen content, salinity). Therefore sediments can act as a source of internal phosphorus.

The hazardous potential of phosphorus in sediments is related not only to the total phosphorus (TP) content. but also to the presence of other fractional forms of phosphorus in the sediments. The adsorption-desorption characteristics of phosphate are mainly influenced by the physicochemical characteristics of the sediment, the phosphorus fraction, and the water column at the sediment-water interface. Sediments with different characteristics have different adsorption characteristics. The form of the phosphorus fraction plays a significant role as a cause of the eutrophication of water bodies (Gerard, 2016; Wang *et al*., 2015). Other studies have reported that pH, macro elements, particle size, and organic matter have an impact on the adsorption of phosphate ions in soil and sediment (Zhu *et al*., 2015; Cao *et al*., 2016).

Kendari Bay which is located in Southeast Sulawesi, has significant potential as a habitat for various organisms that live in the aquatic. Around 13 rivers in the city of Kendari flow into the bay area, including the Wanggu River and the Kambu River. Various anthropogenic pollutants resulting from activities along river basins are carried through river flows or urban drainage to the bay area. As a result, the waters of Kendari Bay have become a place for the accumulation of pollutants, including phosphorus and macro elements, especially iron (Armid *et al*., 2017; Asriyana and Irawati, 2019).

Several studies in Kendari Bay have only studied the processes of sedimentation, trophic status, heavy metals pollution and water quality (Armid *et al*., 2017; Asriyana and Irawati, 2019; Alfiani *et al*., 2019; Makkawaru *et al*., 2021). Adsorption and desorption are important processes and factors that influence the presence of phosphate in aquatic ecosystems and control their concentration at the water-sediment interface (Zhang *et al*., 2015; Li *et al*., 2017). Therefore, the study of phosphate adsorption-desorption is crucial to identifying the source phosphate in the sediment. The objectives of this study are to investigate the phosphate adsorption-desorption in Kendari Bay sediments, analyze the correlation between adsorption capacity with sediment characteristics alongside phosphorus fraction, and evaluate the potential for phosphate release into the overlying water column.

2. Materials and Methods

2.1. Time and Location of Research

The study was carried out from May 2022 to October 2022 and consisted of in situ observations, laboratory analysis, and laboratory experiments. Samples were taken in Kendari Bay, Southeast Sulawesi, using a purposive sampling method which considered that the sampling location was influenced by rivers, especially large rivers (Wanggu River and Kambu River) and the areas connected to the open sea. Therefore, five sampling points have been selected, three sampling points were located near the river mouth (TK.1, TK.2, and TK.3) and two sampling points were located near the bay's mouth or the open sea (TK.4 and TK.5). Geographically, Kendari Bay is located at 3°57'59.37" N, 3°59'32.39" S, and 122°31'38.07" E, 122°35'55.93" W (Figure 1). The experiment of adsorption-desorption and sample analysis was carried out at the Genomics Laboratory and Sedimentation

Laboratory, National Research and Innovation Agency (BRIN), Cibinong, Indonesia.

2.2. Water sampling and analysis

The water samples were the water collected from the sediment-water interface. Physicochemical parameters such as pH, Dissolved Oxygen (DO), salinity, and turbidity were measured in situ using a water quality checker. Water samples were collected using a water sampler and then filtered using 0.45 µm pores filter paper to determine the concentration of orthophosphate or Soluble Reactive Phosphate (SRP) and as a material for adsorption-desorption examinations.

The sediment samples were taken using a Wildco Petite Ponar Grab with a capacity of 2.4 liters and stored in tightly closed bags at a cold temperature (±4 °C) during the trip to the laboratory. In the laboratory, the sediment sample was dried in the oven at 40 °C for two days, ground, and sieved until a dry sediment of <2 µm was obtained. The fine sediments were used for the analysis of particle composition (sand, silt, and clay), Organic Matter (OM), macro element content (iron (Fe), aluminum (Al), and calcium (Ca), Mangan (Mn)), phosphorus fractioning, and adsorption-desorption experiments. Sediment particles were analyzed using the hydrometry method in the technical guide for soil/sediment analysis (Eviati and Sulaeman, 2009).

The organic matter content was analyzed using the Gravimetry method (Mucha *et al.*, 2003). The macro elements composition was analyzed by the method of Atomic Adsorption Spectroscopy (AAS) with wet deconstruction (U.S. EPA, 1996). Phosphorus fractioning uses chemical extraction and sequential methods (Yilmaz *et al.,* 2012).

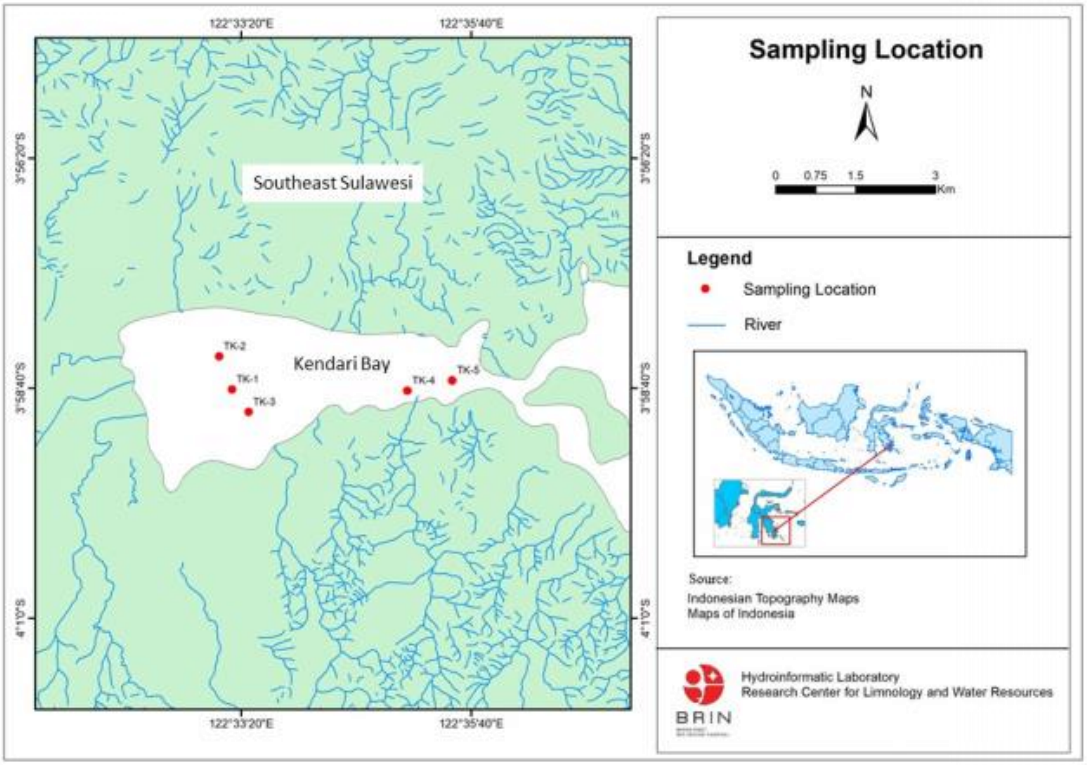

Figure 1. Map of sampling location in Kendari Bay, Sulawei Island, Indonesia

2.2.1. Adsorption-desorption kinetics experiments

Adsorption-desorption kinetics experiments for all samples were carried out according to the method used by Wang *et al.*, (2018). 0.5 g of dry sediment samples and 25 ml of 1 mgP/L solution were placed in a series of 125 mL conical flasks and mixed well using a shaker at 25 ± 1 °C with a speed of 150 rpm for different time intervals (0; 0.25; 0.5; 1; 2; 4; 6; 10; 24; 36; 48; and 60 hours). As an inhibitor of bacterial activity, 1–2 drops of Chloroform were added to the sample solution. 15 ml of suspension solution was

separated using a centrifuge for 15 minutes at a speed of 5,000 rpm. The supernatant was filtered with 0.45 µm pore filter paper and analyzed as SRP. The phosphate adsorption rate by sediment was obtained by entering the SRP concentration value into *the pseudo-first-order* and *pseudo-second-order* kinetic model equations.

The pseudo-First-Order Model assumes that in this model, the rate of adsorption at time t is proportional to the difference between the equilibrium amount adsorbed Q_e and the amount adsorbed at this instant Q_t and that the adsorption is reversible. The constant rate is given in the following Equation 1, by Lagergren (Ho and McKay, 1999):

$$\mathrm{Ln}(Q_e - Q_t) = \ln(Q_e) - k_1 t, \quad \text{....(1)}$$

where Q_t is the amount of phosphorus adsorbed at the instant (t) (mg/g), Q_e is the amount of phosphorus adsorbed at equilibrium (mg/g), and k_1 is the pseudo-first-order rate constant of adsorption (min−1).

Pseudo-Second-Order Model characterizes the adsorption kinetics, by considering both the case of rapid solutes fixation on the most reactive sites and that of a slow fixation on the low-energy sites. This model suggests the existence of a chemisorption. The expression of the pseudo-second-order reaction model was obtained by the equation proposed by Ho and McKay (1999):

$$\frac{t}{Q_t} = \frac{1}{k_2 Q_e^2} + \frac{1}{Q_e} t, \quad \text{....(2)}$$

where k_2 is the pseudo-second-order rate constant of adsorption (g/mg/min). From Equation 2, the adsorbed quantity at equilibrium Q_e and the pseudo-second-order constant k_2 can be determined experimentally from the slope and the ordinate at the origin of t/Q_t as a function of t.

Desorption kinetics experiments were carried out by serially mixing 0.5 g of dry sediment samples and 25 ml of 1 mg P/l solution into a 125 ml Erlenmeyer flask and 1–2 drops of chloroform as an inhibitor of bacterial activity. Next, the sample solution was shaken using a rotary shaker at room temperature (25 ± 1 °C) at a speed of 150 rpm for 36 hours. The suspension solution was separated using a centrifuge at 5000 rpm for 15 minutes and filtered using filter paper with a 0.45 µm pore. The residue was added with 25 ml of ion-free water and shaken again with a rotary shaker for different intervals (0, 0.25, 0.5, 1, 2, 4, 6, 10, 24, 36, 48, and 60 hours). A total of 15 ml of suspension solution was separated using a centrifuge for 15 minutes at a speed of 5000 rpm. The supernatant was filtered with 0.45 µm pore filter paper and analyzed as SRP. The rate of phosphate adsorption by sediment was obtained by entering the SRP concentration value into the pseudo-first-order and pseudo-second-order kinetic model equations.

2.2.2. Isotherm phosphate adsorption

Isothermal adsorption experiments using a modified Wang *et al.* (2018). A sample of water from the study site was filtered using Millipore 0.2 µm filter paper. A quantity of 0.5 g of dry sediment is weighed into Erlenmeyer 100 ml and 40 ml of water samples have been added to KH_2PO_4 solution with concentration variations of 0; 0,1; 0,25; 0,5; 1,0; 2,0; 4,0; 6,0; 8,0 mg P/l. All suspension solutions are shaken using an orbital shaker at room temperature at a rate of 150 rpm for 24 hours. A total of 15 ml of the suspension is centrifugated for 15 minutes at a speed of 5000 rpm, filtered using Millipore 0.45 µm filter paper, and analyzed as SRP. The sediment adsorption capacity was obtained by putting the SRP concentration values into the Freundlich and Langmuir isothermal equation model. The equations are described in Equations 3 and 4 respectively:

$$\ln Q_e = \ln K_F + \frac{1}{n} \ln C_e, \quad \text{....(3)}$$

$$\frac{C_e}{Q_e} = \frac{C_e}{Q_m} + \frac{1}{K_L Q_m}, \quad \text{....(4)}$$

where K_F is the Freundlich adsorption constant (mg/g) (L/mg)$^{1/n}$, n *is* the intensity factor, Qm is the maximum adsorption capacity (mg/g), and K_L is the Langmuir adsorption constant (l/mg).

2.3. Data analysis

The Pearson Correlation analysis was used to perform a quantitative assessment of the relationship between the adsorption-desorption phosphate parameters and sediment characteristics. Minitab version 16 software was utilized for further comprehensive data analysis on the potential dependencies and interactions within the studied variables, aiding in understanding the underlying patterns and dynamics governing phosphate behavior in the sediment system.

3. Results and discussion

3.1. *Water physicochemical properties*

The result of measurement for the physicochemical parameters in the water-sediment interface of Kendari Bay is shown in Table 1. The data revealed that the normal temperature values for tropical waters ranged from 30.0 °C to 30.9 °C, and the pH of water tends to be alkaline, ranging from 8.8 to 9.1 (8.97 ± 0.12). The concentration of dissolved oxygen was low even though it was still in aerobic condition with a range of 2.6 mg/L to 4.0 mg/L, while the SRP concentration value was very low (<0.001 mg/L). The values were lower than in the previous study in the same location (Asriyana and Irawati, 2019)

The pH parameter is significant in the adsorption process because it affects the bond between phosphate ions and the surface of the sediment. On the alkaline condition, the sediment surface will be dominated by negatively charged ions, consequently, it will tend to be more repellent to phosphate ions. The average pH value was in the range of 8.82 to 9.12. The relatively high pH value is thought to be due to the presence of CaCO3, which originates from biogenic apatite and carbonate fluorapatite (CFA) compounds. These compounds come from the bones and teeth of dead marine organisms (Zhuang *et al.*, 2014). In the presence of carbonate compounds, a high pH value will cause phosphate adsorption or coprecipitation with carbonate (Omari *et al.*, 2019).

Table 1. The average value and standard deviation of the physicochemical characteristic of the water at Kendari Bay

Location	TK.1	TK.2	TK.3	TK.4	TK.5
Temperature (°C)	30.1±0.09	30.9±0.11	30.2±0.09	30.1±0.09	30.0±0.10
pH	8.9±0.08	8.8±0.09	8.9±0.09	9.0±0.08	9.1±0.09
Salinity (ppt)	16.3±1.54	17.7±1.87	16.5±2.01	16.6±1.98	16.5±2.41
DO (mg/L)	4.00±0.82	3.75±1.03	3.25±0.95	3.65±0.71	2.60±0.63
SRP (mg/L)	<0.001	<0.001	<0.001	<0.001	<0.001

The low SRP value is also supported by the salinity concentration value. Ca bonds with phosphate ions will be stable and easily released into the water column because Ca will not dissolve in environmental conditions with high salinity (Van Diggelen *et al.*, 2014). The DO values ranging from 2.6 to 4.0 mg/L indicated that it was still in an aerobic condition where it was allowing phosphate ions to bind to metal oxides.

3.2. Sediment physicochemical - properties

The results of sediment functional group analysis at five locations showed that TK.1, TK.2, TK.3, and TK.5 create nearly identical spectrum profiles. However, TK.4 has a slightly different spectrum profile (Figure 2). The spectrum located between 3600 cm^{-1} to 3700 cm^{-1} is the O-H group, which indicates the presence of clay minerals (Veerasingam and Venkatachalapathy, 2014). The spectrum located at 3393 cm^{-1} was thought to be the amine and amide groups of organic compounds containing nitrogen (N).

The appearance of the 1634 cm-1 spectrum confirms the presence of C=C and C=O groups originating from biological materials (Veerasingam and Venkatachalapathy, 2014). The peak from 900 cm-1 to 1100 cm-1 was thought to be related

to Al-OH bending and Si-O stretching vibrations of eroded silicate layers, particularly illite and kaolinite, whereas the spectral band from 693 cm-1 to 776 cm-1 is associated with the presence of quartz grains (Veerasingam and Venkatachalapathy, 2014).

The results of sediment particle size analysis showed the composition of sand, silt, and clay particles as shown in Figure 2. The silt fraction was the most dominant sediment particle, with an average percentage in the range of 74.8% to 79.25%. The distribution of silt particles is evenly distributed throughout all sampling locations.

The abundance of finer sediments at all sites reflects relatively weak hydrodynamic energy (Vicente *et al.*, 2016). In research conducted by Putra *et al.* (2021), the current velocity value in the area of Kendari Bay is relatively lower compared to the outside area of the bay, with an average value of 5.26 cm/second. This showed that the hydrodynamic energy in Kendari Bay was relatively weak. This condition is supported by the morphometry of Kendari Bay, which resembles an estuary where processes such as flocculation occur more intensely due to reduced turbulence so that finer sediment is dominant (Vicente *et al.*, 2016), as shown in Table 2.

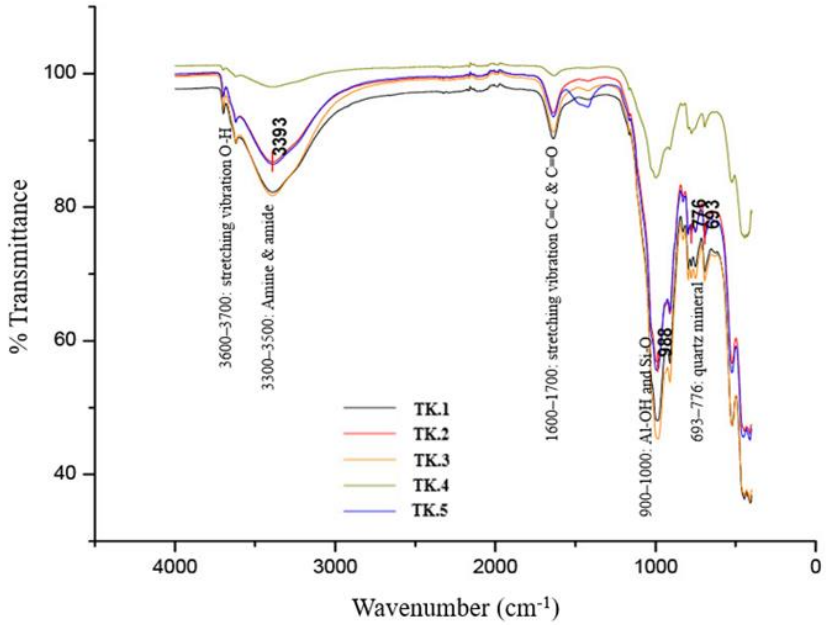

Figure 2. Collection of ATR-FTIR spectra from surface sediments at five sampling locations in the waters of Kendari Bay. Instrument conditions: nominal resolution of 4 cm^{-1} and 16 accumulated scans per adsorption band. The color of the lines indicates the sampling points: TK.1 (black), TK.2 (red), TK.3 (orange), TK.4 (light green), and TK.5 (blue).

The differences in the particle compositions in the sediment will result in differences in the ratio of surface area to mass. Li *et al.* (2021) reported that sediment particles with a finer size (silt and clay) have a larger surface-to-mass ratio when compared to larger particles, thus providing a greater adsorption capacity.

The dominance of the fine particle size of Kendari Bay sediments supports the high concentration of organic matter at this research location, which ranges from 25.16% to 68.44% (Table 2). This phenomenon was reported by Meng *et al.* (2014) and Simanjuntak *et al.* (2020), who found that sediments with a high proportion of fine particles tend to have a high organic material content. Figure 3. shows the relationship between organic matter and fine sediment particles, with a value of R^2 = 0.9068.

The results of macroelement analysis show that Fe is the element with the highest concentration compared to other macroelements, with values ranging from

5.496 to 9.077 mg/g (Table 2). This phenomenon was similar, as reported by Armid *et al*. (2017), at the same locations. The high Fe content in the waters of Kendari Bay is influenced by rivers entering the bay area, which carry anthropogenic pollutants, which originate from untreated mining and industrial waste. According to the CBSSS (2015), as many as 136 ore mining companies is operating in North Konawe, Konawe, and South Konawe Regencies, where the entire district is crossed by the Wanggu River (Armid *et al*., 2017).

Table 2. The average and standard deviation of physicochemical characteristics of surface sediments at Kendari Bay

Location	TK.1	TK.2	TK.3	TK.4	TK.5
Sand (%)	3.8±1.93	2.8±1.74	2.9±1.54	7.8±2.71	4.5±2.32
Silt (%)	76.3±1.76	77.7±1.82	75.8±1.67	79.3±1.97	74.8±1.46
Clay (%)	20.0±3.43	19.4±3.17	21.3±3.95	12.9±2.56	20.7±3.73
Org. matter (%)	68.4±21.81	62.6±17.50	64.4±20.82	25.2±77.45	57.9±19.89
Al (mg/g)	0.268±0.12	0.125±0.06	0.210±0.07	0.088±0.02	0.230±0.10
Ca (mg/g)	2,408±0,98	1,737±0,31	2,422±1,21	2,182±0,52	4,100±1,37
Fe (mg/g)	9,077±2,50	5,498±1,90	5,570±2,21	4,520±1,18	5,100±1,41
Mn (mg/g)	0.292±0.18	0.166±0.13	0.320±0.21	0.066±0.01	0.480±0.28

Macroelements such as Fe, Mn, Al, and Ca play important roles in the cycle of phosphorus compounds in water. Additionally, these elements play a role in the adsorption and desorption of phosphate ions in sediments. The iron content in Kendari Bay sediments was significantly higher when compared to other oligotrophic coastal waters in Indonesia, such as Jepara coastal waters in Central Java (Maslukah *et al*., 2019)

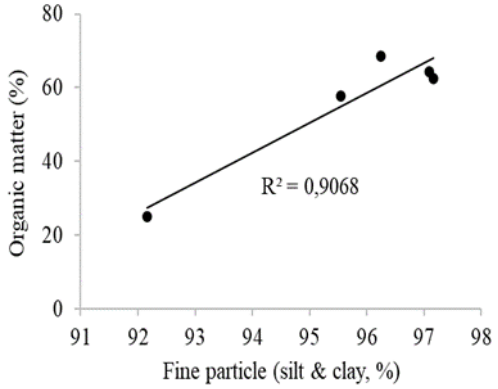

Figure 3. Relationship between fine sediment fraction and organic matter content

The concentrations of Mn and Al were in the range from 0.066 mg/g to 0.480 mg/g and 0.88 mg/g to 0.268 mg/g dry sediment, respectively. Meanwhile, the concentration of Ca was the second highest concentration after Fe, in the ranges from 0.737 mg/g to 4.100 mg/g of dry sediment. Ca can bind phosphate ions to form apatite mineral deposits. Phosphate ions that bind to Ca will be more occluded and dissolved when the pH of water is lower. Meanwhile, the oxidized Fe, Mn, and Al will fall to the bottom of the bay in the solid form of sediment or minerals that have high adsorption capacity for phosphate ions. Therefore, these elements play an important role in the phosphorus cycle at the sediment-water interface.

3.3. Phosphorus fractions

The fractionation of phosphorus compounds in sediment is an important parameter to estimate the internal input of phosphorus compounds into the water column. Vicente *et al*. (2016) stated that phosphorus concentration is an important aspect in assessing the level of eutrophication in water. Phosphorus concentration in waters is mainly regulated by the release from sediment, which depends on the form of different phosphorus fractions because not all phosphorus compounds can be released from sediment. Barik *et al*. (2019) revealed that the composition of different P fractions affects the mobility of sediment phosphorus. The distribution of different P fractions in sediments needs to be known to assess the

risk of eutrophication in aquatic ecosystems (Aydin *et al.*, 2018).

The distribution of phosphate fraction concentrations in each sediment sample varies greatly (Figure 4). The total concentration of phosphorus (TP) in this study ranges from 0.300 to 0.410 mgP/g with an average of 0.360 mgP/g. The concentration of organic phosphorus (OP) was in the ranges from 0.026 to 0.133 mgP/g, contributing 21.5% to TP. Relatively low OP content was observed at the location of TK.4 and TK.5, where the area is close to the open sea. Therefore, the accumulation of higher anthropogenic inputs occurred inside the bay, near the estuary (TK.1, TK.2, and TK.3). Organic P in marine sediments comes from the mineralization of organic materials containing phosphates, such as nucleic acids, lipids, and sugars bound to phosphorus (Li *et al.*, 2017; Tu *et al.*, 2019). Increased organic matter causing an increase in OP has been reported from several research sites (Vicente *et al.*, 2016; Yang *et al.*, 2019; Li *et al.*, 2017).

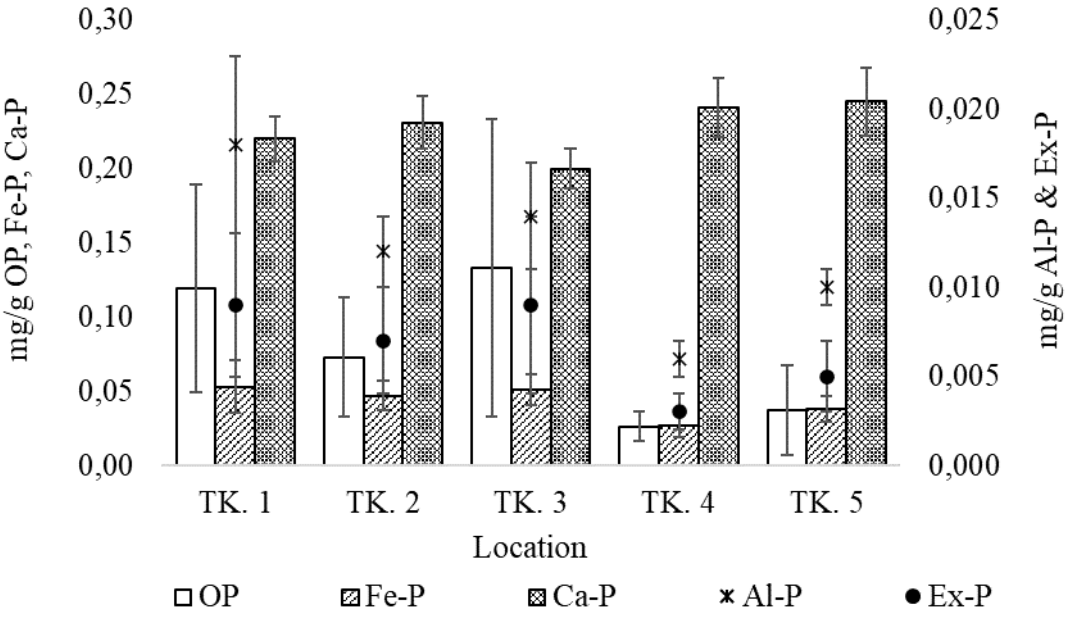

Figure 4. Distribution of phosphorus fraction

Inorganic phosphorus consists of Ca-P, Fe-P, Al-P, and Exchangeable Phosphates (Ex-P). Ca-P concentrations were in the range of 0.200 to 0.245 mgP/g, with an average contribution to TP of 63.13%. Ca-P is the main P fraction in Kendari Bay waters and generally comes from biogenic apatite (bones and teeth of dead marine organisms) (Zhuang *et al.,* 2014) and carbonate fluorapatite (CFA) (Hou *et al.*, 2009). Based on research by Zulham *et al.* (2017), the waters of Kendari Bay and its surrounding areas have a high production of fish and shellfish. Biogenic apatite and fluorapatite are almost insoluble in the physicochemical conditions of marine waters and remain stable both under oxidizing and reducing conditions, thereby rendering it impossible for them to be released from the sediment and enter the water column above it. Therefore, the P form in the Ca-P fraction will not be bioavailable, so it is not easily utilized by algae.

The high Ca-P concentrations are also associated mainly with excessive calcite saturation and coprecipitation of phosphates. In addition, the high carbonate adsorption capacity also contributed to the phosphorus fraction. It is known that calcite is produced at high salinity through precipitation reactions and biological activity. Therefore, calcite production in waters far from the coast will be higher than in waters near the coast. This can be seen in this study, where locations TK.4 and TK.5 have higher Ca-P values than locations TK.1, TK.2, and TK.3.

Fe-P concentrations were in the range of 0.027 to 0.053 mgP/g, with an average contribution to TP of 12%. Al-P and Ex-P concentrations have the same relative value of 0.003–0.009 mgP/g, with the smallest

contribution to TP being an average of 2%. The concentration of Fe-P tends to decrease from the location in the bay to the location at the mouth of the bay. Previous studies revealed that Fe-P concentrations decreased from brackish waters to waters with higher salinity due to the trapping of large amounts of phosphorus by Fe hydroxide/oxides in brackish water sediments (Kang *et al.*, 2017). Phosphorus that binds to Fe and Al is used to determine the availability of P for algae growth in waters (Ghaisas *et al.*, 2019).

The presence of Fe/Al-P in Kendari Bay sediments is important to understand eutrophication in the waters of this bay. This P fraction will release phosphate ions in anoxic environmental conditions due to the oxidation-reduction process (Yan *et al.*, 2017; Barik *et al.*, 2019; El Semary, 2022). The presence of the Fe/Al-P fraction in the waters of Kendari Bay is closely related to the content of Fe and Al, which can be seen from the values of the Pearson correlation coefficient, respectively, with r = 0.717 and r = 0.802 (P<0.05) as shown in Table 3.

Table 3. Correlation between phosphorus fraction and macro elements content in Sediment of Kendari Bay

	TP	IP	OP	Ex-P	Fe-P	Al-P	Ca-P	Al	Ca	Fe
TP	1									
IP	0,940*	1								
OP	0,656*	0,359	1							
Ex-P	0,953*	0,991*	0,414	1						
Fe-P	0,967*	0,986*	0,464	0,988*	1					
Al-P	0,762*	0,806*	0,301	0,735*	0,757*	1				
Ca-P	0,915*	0,997*	0,299	0,988*	0,973*	0,788*	1			
Al	0,590*	0,697*	0,073	0,654*	0,582*	0,802*	0,719*	1		
Ca	-0,260	-0,184	-0,305	-0,203	-0,322	0,051	-0,140	0,554	1	
Fe	0,559*	0,805*	-0,251	0,772*	0,717*	0,612*	0,845*	0,716*	0,088	1

*P<0.05

Ex-P is the fraction of sedimentary P that is loosely adsorbed Phosphorus so that it is easily released into the sediment-water interface. Therefore, this phosphorus fraction is often called the exchangeable phosphorus fraction (Ex-P). Its concentration in Kendari Bay sediments is relatively low, ranging from 0.003–0.009 mgP/g, with a contribution of 1.8% to TP.

Together with the OP, Fe-P, and Al-P fractions, Ex-P is the P compound in sediments that is biologically available (Bioavailability Phosphorus, BAP), which means it can be used directly for algae growth (Yang *et al.*, 2018). The availability of phosphorus in sediments is directly related to the amount of phosphorus that can be easily released. By knowing the various P fractions, the potentially available phosphorus can be determined. Calcium-phosphorus (Ca-P) is not expected to be a bioavailable fraction due to its insolubility in the brine environment, while Fe/Al-P cannot be released if the environmental conditions at the sediment-water interface are still aerobic. However, Ex-P and OP are considered potentially available fractions. Ex-P can be released gradually when the phosphate concentration in the water column is lower than in the pore water, and OP can be bioavailable through the demineralization process (Zheng *et al.*, 2022). In this study, Ex-P and OP contributed 10% to 35% of TP.

3.4. Kinetics of Phosphate Adsorption and Desorption

According to the experiment in the laboratory, the phosphate adsorption into sediment samples from all sampling locations indicated high and quick adsorption from the initial time until the sixth-hour experiment; however, after the sixth-hour experiment, the phosphate adsorption was getting slow (Figure 5). An average of 79% adsorption occurred during 6 to 36 hours, and an equilibrium process occurred after 36 hours. The adsorption progressed slowly because of the reduced active adsorption sites; almost no further adsorption could be found after 36

hours, indicating either that adsorption equilibrium had been reached or that desorption occurred as the consequence of the less active sites being available to P (Guo *et al.*, 2018). This pattern also occurs in the results of phosphate desorption kinetics experiments, which show the desorption rate in the first 0–6 hours. In the first few hours, the concentration in the surface water is lower, P is adsorbed quickly, and then the concentration of the overlying water increases, and the P desorption rate decreases. After 36 h, equilibrium desorption had been reached or adsorption might occur.

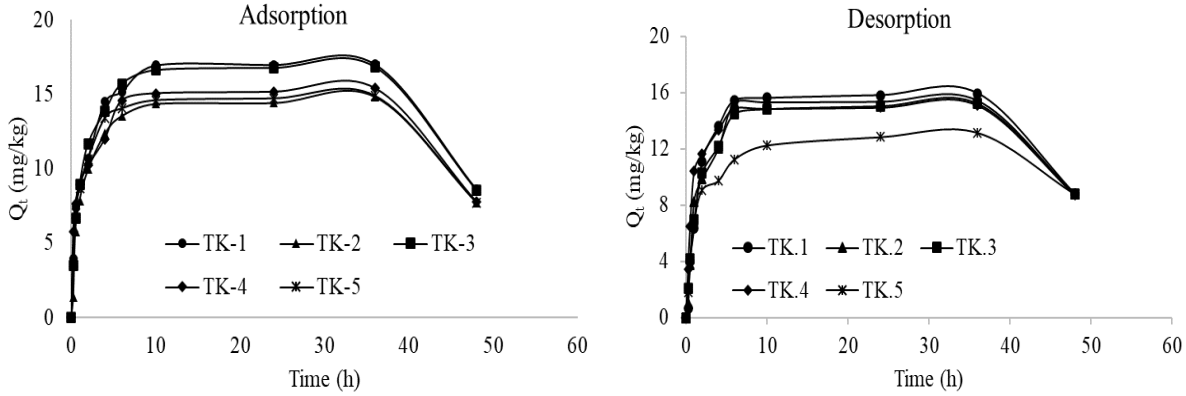

Figure 5. Adsorption and desorption rates of phosphate in sediments of Kendari Bay

The experimental results of the kinetic model showed that for both adsorption and desorption processes of phosphate by Kendari Bay sediments, the pseudo-second-order kinetic model gave a higher regression coefficient (R^2) value. The high value of the regression coefficient also shows that the adsorption capacity is proportional to the number of active sites contained in the adsorbent (Dim *et al.*, 2021). This indicated that adsorption and desorption in Kendari Bay sediments are controlled by chemisorption (Khamizov, 2020). The parameters of adsorption and desorption constants (k) and the amount of phosphate adsorbed (Q_e) are presented in Table 3. The adsorption and desorption rate constant values (k) have an average of 1.074 kg/mg/min and 0.878 kg/mg/min, respectively. Both k values are relatively the same as study results in Semarang coastal waters and higher than in Jepara coastal waters (Maslukah *et al.*, 2020).

Table 4. Adsorption and desorption kinetic parameters of psedo-second-order

Location	Adsorption			Desorption		
	K_a Kg/mg/min	Q_e mg/kg	R^2	K_d Kg/mg/min	Q_e mg/kg	R^2
TK.1	0.476	25.417	0.876	1.171	15.935	0.886
TK.2	0.674	24.699	0.896	1.015	15.423	0.898
TK.3	0.712	24.362	0.893	0.871	15.200	0.907
TK.4	1.157	20.924	0.936	0.675	15.084	0.910
TK.5	2.349	17.447	0.865	0.660	13.139	0.947
Average	1.074	22.570	0.893	0.878	14.956	0.910

K: adsorption and desorption constants, Q_e: adsorption and desorption capacity, R^2: regression coefficient

3.5. Isothermal adsorption

To describe the adsorption capacity at several different phosphate concentrations, isothermal adsorption experiment was carried out using the Langmuir and Freundlich isothermal adsorption models. The results showed that the adsorption rate tends to increase as the equilibrium concentration of phosphate increases and then reaches equilibrium after saturation conditions are reached (Figure 6).

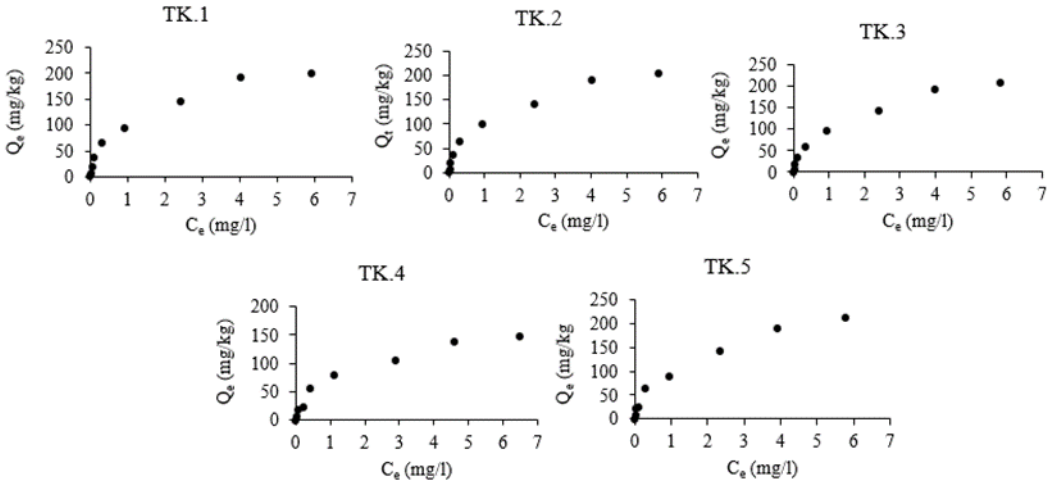

Figure 6 Phosphate isothermal adsorption of Kendari Bay sediments

Table 5. Isothermal adsorption parameters of Freundlich and Langmuir

Loca -tion	R^2 Freundlich	R^2 Langmuir	Q_{max} (mg/kg)	EPC_0 (mgP/L)
Tk.1	0.948	0.974	212.8	0.0029
Tk.2	0.939	0.968	212.8	0.0026
Tk.3	0.947	0.961	227.3	0.0033
Tk.4	0.950	0.968	156.3	0.0047
Tk.5	0.935	0.950	222.2	0.0028

R^2: regression coefficient, Q_{max}: maximum capacity of adsorption, EPC_0: zero equilibrium phosphate concentration.

Experimental results show that the Langmuir model equation provides slightly higher regression coefficient values compared to the Freundlich model equation (Table 5). But generally, both equations produce strong regression coefficients. This phenomenon showed that the phosphate adsorption process in Kendari Bay sediments occurs due to the presence of a monolayer and multilayer. From the Langmuir isothermal adsorption model, the maximum adsorption capacity (Q_{max}) value of Kendari Bay sediments was 156.3 mg/kg to 227.3 mg/kg. This value is lower than the results of research in the waters of Semarang Bay (347.2 mg/kg) and Jepara Bay (358.7 mg/kg) (Maslukah *et al.*, 2020). Yang *et al.* (2019) even found that the Q_{max} value of phosphate ions in sediment enriched with organic material in the concentration of 611.2 mg/kg.

There was a positive correlation between the Q_{max} values and the inorganic P fraction, specifically Fe-P (r = 0.797) and Al-P (r = 0.502) (Table 5). The Q_{max} value with the organic P fraction also produces a positive correlation coefficient value with r = 0.610. The high content of macro element-bound phosphorus in the sediment shows the great ability of the Kendari Bay sediment to adsorb phosphate ions.

Particle size and organic matter content are also important factors in sediment adsorption capacity. Sediment with fine particle size has a stronger adsorption capacity because of its larger specific surface area (Zhuang *et al.*, 2014). This can be seen from the research results, which obtained a positive correlation coefficient value between the Q_{max} value and clay particles (r = 0.998). Due to the large surface area, sediments with finer particles have stronger adsorption capacity (Vicente *et al.*, 2016; Kang *et al.*, 2017). Meng *et al.* (2015) also reported that the higher the composition of fine particles, the higher the specific surface area, and the stronger the surface energy in the adsorbed particles, the more phosphorus is absorbed. A positive correlation with organic matter content indicated a strong correlation coefficient value (r = 0.934). Yang *et al.* (2019) reported the maximum adsorption capacity value for sediment enriched with organic material (611.2 mg/kg).

Table 5. Correlation between maximum adsorption capacity (Q_{max}) with physicochemical characteristics and phosphorus fraction of Kendari Bay sediments

	OP	Ex-P	Fe-P	Al-P	Ca-P	Sand	Silt	Clay	OM	Q_{max}
OP	1									
Ex-P	0,966	1								
Fe-P	0,911	0,986	1							
Al-P	0,643	0,735	0,761	1						
Ca-P	-0,941	-0,842	-0,751	-0,358	1					
Sand	-0,717	-0,849	-0,905	-0,521	0,588	1				
Silt	-0,391	-0,498	-0,523	-0,451	0,274	0,612	1			
Clay	0,632	0,766	0,813	0,544	-0,494	-0,915	-0,879	1		
OM	0,740	0,882	0,937	0,732	-0,543	-0,952	-0,725	0,944	1	
Q_{max}	0,610	0,747	0,797	0,502	-0,482	-0,920	-0,869	0,998	0,934	1

Significant level (*P*) = 0,05

3.6. Equilibrium Phosphate - Concentration in Kendari Bay

Phosphate concentration at zero equilibrium (EPC_0) is an important parameter in determining the role of sediment resuspension in the phosphate adsorption-desorption process. When the phosphate concentration in the water is less than the EPC_0 value, sediment is expected to release phosphate from the sediment into the water column. On the other hand, if the phosphate concentration is greater than the EPC_0 value, the sediment will tend to adsorb phosphate (Wang *et al.*, 2018).

The waters of Kendari Bay are classified as an oligotrophic bay because the results of the SRP analysis in the Kendari Bay water body show a relatively low average value (0.001 mg/L), while the EPC_0 value resulting from isothermal adsorption experiments using the Langmuir equation is around 0.0026 mg/L to 0.0047 mg/L (Table 4). This indicated that Kendari Bay sediment potentially resuspends phosphate ions into the water column.

Although Kendari Bay sediments have the potential to release phosphate ions into water bodies based on the EPC0 value, the phosphate equilibrium mechanism in the environment is highly dependent on environmental conditions. Jiang *et al.* (2022) revealed that temperature and pH influence the concentration of phosphate. The low concentration of Ex-P in this study was less supportive of phosphate release. Furthermore, turbulence in the bay waters will disperse and dilute the released phosphate ions in seawater.

4. Conclusion

The adsorption-desorption kinetics of the Kendari Bay sediments were investigated using the pseudo-second-order rate equation, which indicated that the adsorption capacity is proportional to the number of active sites filled by P ions, with chemisorption being the rate limitation.

The maximum adsorption capacity (Q_{max}) value is influenced by particle size and phosphorus fraction. This is evident from the significant positive correlation between Q_{max} and the clay fraction, iron, Fe-P, and Al-P. Consequently, sediment in Kendari Bay exhibits a high adsorption capacity for phosphate ions due to its fine particle size and high Fe content. Despite the SRP value being smaller than the EPC_0 value, resulting in the resuspension of adsorbed phosphate ions, this process is limited by the very low Ex-P content. Therefore, Kendari Bay sediments have little potential to serve as a source of P input into Kendari Bay.

Furthermore, practical applications may involve incorporating sediment adsorption capacity data into ecosystem modeling frameworks to guide nutrient management practices and support sustainable coastal development initiatives in Kendari Bay and beyond.

Data availability statement
The data included and used in this study is not confidential and available upon request.

Funding Agencies
This research was funded by a research project of COREMAP-CTI BRIN 2021-2022 through the research activity "Projection of the Impact of Sediment Runoff on Terrestrial Ecosystems on Coral Reef Habitat in Climate Change Scenarios as a Basis for Strengthening Adaptation Strategies".

Conflict of interests
The authors declare no conflicts of interest.

Author contribution
SA designed the topic and research method, data collection and analysis, wrote the manuscript, **ARB** designed the topic and research supervision, **ER** and **MR** contributed to research supervision.

Acknowledgment
The authors would like to thank the Genomik Laboratory at the National Research and Innovation Agency for the sample processing and analysis. We are grateful to laboratory and field work assistance.

References
Alfiani N, Salihin LMI, Usman I, Khairisa NH. 2019. Analisis Geospasial Sedimentasi Teluk Kendari Akibat Perkembangan Lahan Terbangun. *Jurnal Geografi Aplikasi Dan Teknologi* 3 (2):79.

Armid A, Shinjo R, Sabarwai SH, Ruslan R. 2017. Pollution Assessment of Various Heavy Metals in the Surface Sediment of Kendari Bay. Indonesia. *J. Nature Environment and Pollution Technologi* 16(4): 1067-1074.

Asriyana N, Irawati. 2019. Assessment of the trophic status in Kendari Bay. Indonesia: a case study. *AACL Bioflux* 12(2):650–663.

Axinte O, Bădescu I, Stroe C, Neacsu V, Bulgariu L, Bulgariu D. 2015. Evolution of Trophic Parameters from Amara Lake. *Environmental engineering and management journal*. 14: 559-565.

Aydin I, Temel Z, Gunduzc B, Aydin F. 2018. Comparative determination of phosphorus fractionsin coastal surface sediment (NE Mediterranean Sea) by ICP-OES and UV/VIS Spectrometry. *Atomic Spectroscopy*. 39(5):193-197. http://doi.org/10.46770/AS.2018.05.003.

Barik SK, Bramh S, Bastia TK, Behera D, Mohanty PK, Rath P. 2019. Distribution of geochemical fractions of phosphorus and its ecological risk in sediment cores of a largest brackish water lake, South Asia. *Int. J. Sediment Res*. 34: 251–261.

Bramha S, Mohanty AK, Padhi R, Panigrahi S, Satpathy KK. 2014. Phosphorus speciation in the marine sediment of Kalpakkam coast. southeast coast of India. *Environmental Monitoring and Assessment*. 186: 6003–6015.

Cao X, Liu X, Zhu J, Wang L, Liu S, Yang G. 2016. Characterization of phosphorus sorption on the sediments of Yangtze River Estuary and its adjacent areas. *Mar. Pollut. Bull*. 114(1):277–284.

CBSSS (Central Bureau of Statistics. Southeast Sulawesi). 2015. *Southeast Sulawesi in Figures*. Indonesia

Dim PE, Mustapha LS, Termtanun M, Okafor JO. 2021. Adsorption of chromium (VI) and iron (III) ions onto acidmodified kaolinite: Isotherm, kinetics and thermodynamics studies. *Arabian Journal of Chemistry*. 14(4): 103064. http://doi.org/ 10.1016/j.arabjc.2021.103064

El Semary NA. 2022. Iron-Marine Algal Interactions and Impacts: Decreasing Global Warming by Increasing Algal Biomass. J. Sustainability. 14: 10372. http://doi.org/10.3390/ su141610372

Eviati and Sulaeman. 2009. Analisis Kimia Tanah, Tanaman, Air, dan Pupuk. In: Prasetyo. B.H.. Santoso D.. Retno. W.L. editor. *Petunjuk Teknis*. Balai Penelitian Tanah. 2: 234 pages.

Ghaisas NA, Maiti K, White JR. 2019. Coupled iron and phosphorus release from seasonally hypoxic Louisiana shelf sediment. *J. Estuaine, Coastal, and Shelf Science* 219: 81–89.

Gerard F. 2016. Clay minerals. iron/aluminum oxides. and their contribution to phosphate sorption in soils – a myth revisited. *Geoderma*. 262: 213–226

Guo CH, Li HX, Fang F, Ji YS, Xing YX, Fan YB, Liu Y. 2018. Study on distribution of phosphorus fractions and dsorption desorption characteristics in surface sediments of the Yellow River by molybdenum antimony spectrophotometry. *Spectrosc Spectr. Anal.* 38(1):218–223

Ho YS dan McKay G. 1999. Pseudo-second order model for sorption processes Process Biochem. 34(5):451-465. https://doi.org/10.1016/S0032-9592(98)00112-5.

Hou A, Chen P, Alloatti J, Mozzoni L, Zhang B, Shi A. 2009. Genetic variability of seed sugar content in worldwide soybean germplasm collections. *Crop Sci* 49:903–912.

Jiang Y, Ma XL, Wang B, Jiang BB, Wang WK, Wang YJ, Zhang CD. 2022: Effects of environmental factors on phosphorus adsorption capacity and release risk in lake sediments. *Plant Soil Environ*. 68: 186–194

Kang X, Song J, Yuan H, Shi X, Yang W, Li X, Li N, Duan L. 2017. Phosphorus speciation and its bioavailability in sediments of the Jiaozhou Bay. *Estuarine, Coastal, and Shelf Science* 188: 127–36.

Khamizov RK. 2020. A Pseudo-Second Order Kinetic Equation for Sorption Processes. Russ. *J. Phys. Chem.* 94:171–176. http://doi.org/10.1134/S0036024420010148

Li J, Reardon P, McKinley JP, Joshi SR, Bai Y, Bear K, Jaisi DP. 2017. Water column particulate matter: A key contributor to phosphorus regeneration in a coastal eutrophic environment, Chesapeake Bay. *J. Geophys. Res. Biogeosciences.* 122: 737–752. http://doi.org/10.1002/2016JG003572

Li P, Zhao C, Liu K, Xiao X, Wang Y, Wang Y, He D. 2021. Anthropogenic Influences on Dissolved Organic Matter in Three Coastal Bays, North China. *Journal Frontiers in Earth Science: section Biogeoscience.* 9: 697758. http://doi.org/10.3389/feart.2021.697758

Makkawaru A, Sideng U, Sufrianto. 2021. Interpretation of the Geological Romance of Kendari Bay Using Landsat 5 TM. *LaGeografia* 20:114.

Maslukah L, Wulandari SY, Yasrida A. 2017. Rasio Organik Karbon Terhadap Fosfor Dalam Sedimen Di Muara Sungai Banjir Kanal Barat. Semarang. *Buletin Oseanografi Marina* 6(1): 39-45.

Maslukah L, Sugianto D, Salma U, Zainuri M, 2019. Phosphorus Fractionation and Its Bioavailability in Panjang Island Jepara. *IOP Conference Series: Earth and Environmental Science* 246: 012051.

Maslukah L, Zainuri M, Wirasatriya A, Widiaratih R. 2020. Studi Kinetika Adsorpsi dan desorpsi Ion Fosfat (PO42-) di Sedimen Perairan Semarang dan Jepara. *J. Ilmu dan Teknologi Kelautan Tropis* 12(2): 383-394.

Meng J. Yao Q, Yu Z. 2014. Particulate phosphorus speciation and phosphate adsorption characteristics associated with sediment grain size. *Ecological Engineering* 70: 140–145.

Meng J, Yu Z, Yao Q, Bianchi TS, Paytan A. Zhao, B, Pan H, Yao P. 2015. Distribution, mixing behavior, and transformation of dissolved inorganic phosphorus and suspended particulate phosphorus along a salinity gradient in the Changjiang Estuary. *Marine Chemistry,* 168 : 124–134. http://doi.org/ 10.1016/ j. marchem.2014.09.016

Mucha AP, Vasconcelus MTSD, Bordalo AA. 2003. Macrobenthic community in the Douro Estuary relation with trace elements and natural sediment Characteristic. *Environmental Pollution* 12(2): 16-180

Omari H, Dehbi A, Lammini A, Abdallaoui A, 2019. Study of the Phosphorus Adsorption on the Sediments. *Journal of Chemistry*. 10 pages

Putra I, Mihardja DK, Trismadi T, Pranowo WS, Lazuardi R, Nugroho PE. 2021. Analisi Ketidaksimetrisan Pasang Surut Akibat Pengaruh Morfologi di Teluk Kendari: Study of Tidal Asymmetry as The Morfological Effect in Kendari Coastal Bay. *Jurnal Chart Datum*. 7(2):73–86. https://doi.org/10.37875/chartdatum.v7i2.210

Simanjuntak, N., Rifardi, A. Tanjung. 2020. Hubungan Karakteristik Sedimen dan Bahan Organik Sedimen dengan Kelimpahan Kerang Darah (Anadara granosa) di Perairan Tanjung Balai Asahan ProvinsiSumatera Utara. *J. Perikanan dan Kelautan*. 25(1): 6-17

Tu L, Jarosch KA, Schneider T, Grosjean M. 2019. Phosphorus fractions in sediments and their relevance for historical lake eutrophication in the Ponte Tresa basin (Lake Lugano, Switzerland) since 1959. *Science of the Total Environment.* 685:806-817.

U.S. EPA. 1996. METHOD 3050B. U.S. Environmental Protection Agency. Washington. D.C.. EPA 600/P-./001.

Van Diggelen JMH, Lamers LPM, Van Dijk G, Schaafsma MJ, Roelofs JGM, Smolders AJP. 2014. New insights into phosphorus mobilization from sulfur-rich sediments: time-dependent effects of salinization. *PLoS One* 9(11): e111106.

Veerasingam S dan Venkatachalapathy R. 2014. Estimation of carbonate concentration and characterization of marine sediments by Fourier Transform Infrared Spectroscopy. *Infrared Physics & Technology*. 66:136–140. http://doi.org/10.1016/j.infrared.2014.06.0

Vicente MAF, Melo GVD, Neto JAB, Oliveira ASD. 2016. Phosphorus Fractionation Distribution in Guapimirim estuary: SE Brazil. SpringerPlus. 5:1406. http://doi.org/ 10.1186/s40064-016- 3065-9

Wang LQ, Liang T, Chen Y. 2015. Distribution characteristics of phosphorus in the

sediments and overlying water of Poyang Lake. *Plos One* 10(5): e0125859.

Wang X, Wei J, Ba N, Cha H, Cao C, Zheng K, Liu Y. 2018. The phosphorus fractions and adsorption-desorption characteristics in the Wuliangsuhai Lake. China*. Environ Sci Pollut Res* 25: 20648–20661.

Yan Y, Gao B, Hao H, Zhou HD, Lu J. 2017. Nitrogen and phosphorus in sediments in China: A national-scale assessment and review. *Sci. Total Environ*. 576: 840–849

Yang B, Liu S, Zhang G. 2018. Geochemical Characteristics of Phosphorus In Surface Sediments From The Continental Shelf Region Of The Northern South China Sea. *Marine Chemistry.* 198: 44–55. https://doi.org/10.1016/j.marchem.2017.11.001

Yang, X., X. Chen, X. Yang. 2019. Effect of organic matter on phosphorus adsorption and desorption in black soil from Northeast China. *Soil and Tillage Research*. 187. 85-91.

Yilmaz E, Koc C. 2012. A Study On Seasonal Changes Of Phosphorus Fractions In Marine ¨ Kova Bay. Turkey Sediments of The Akyaka Beach in Gökova Bay, Turkey. *Clean Technologies and Environmental Policy* 14(2): 299–307.

Zhang WL, Zeng CS, Tong C, Zhai SJ, Lin X, Gao DZ. 2015. Spatial distribution of phosphorus speciation in marsh sediments along a hydrologic gradient in a subtropical estuarine wetland, China. *Estuar Coast Shelf Sci* 154:30–38.

Zheng Z, Wang X, Jin J, Hao J, Nie Y, Chen X, Mou J, Emslie SD, Xiaodong L. 2022. Fraction distribution and dynamic cycling of phosphorus in lacustrine sediment at Inexpressible Island, Antarctica. *Environ. Int.* 164:107228. http://doi.org/10.1016/j.envint.2022.107228

Zhuang W, Gao X, Zhang Y, Xing QG, Tosi L, Qin S. 2014. Geochemical characteristics of phosphorus in surface sediments of two major Chinese mariculture areas: The Laizhou Bay and the coastal waters of Zhangzi Island. *Mar. Pollut. Bull* 83: 343–351

Zhu H, Wang D, Cheng P, Zhong JBC. 2015. Effects of sediment physical properties on the phosphorus release in aquatic environment. *Sci. China Phys. Mech. Astron*. 58. 1–8

Zulham A, Subaryono, Mahulette. 2017. *Pengembangan Perikanan Tangkap Laut Kota Kendari*. Wudianto, Baskoro M, Wijopriono (Eds). : Rajawali Pers, 2017. xiv, 66 pages.

LIMNOTEK Perairan Darat Tropis di Indonesia
transforming into the Journal of Limnology and Water Resources
p-ISSN: 0854-8390 e-ISSN: 2549-8029
https://ejournal.brin.go.id/limnotek

Assessment of Heavy Metals Using the Enrichment Factor and Geoaccumulation Index in Menjer Lake, a Tropical Volcanic Lake

Lintang Nur Fadlillah[1], M. Widyastuti[1*], Alfina Ayu Rachmawati[2], Azura Ulfa[3]

[1]Laboratory of Hydrology and Environmental Climatology, Department of Environmental Geography, Faculty of Geography, Universitas Gadjah Mada, Yogyakarta 55281, Indonesia
[2]Department of Environmental Geography, Faculty of Geography, Universitas Gadjah Mada, Yogyakarta 55281, Indonesia
[3]Research Center for Remote Sensing, National Research and Innovation Agency, Jakarta, Indonesia

*Corresponding author's e-mail: mwiwik@ugm.ac.id

Received: 26 February 2024; Accepted: 31 May 2024; Published: 30 June 2024

Abstract: Lakes are recognized as vulnerable to pollution, including Menjer Lake, whose catchment area is dominated by agricultural lands and features floating net cages in the water body. The heightened contamination risk within the lake primarily stems from the accumulation of heavy metals, compounds known for their profound toxicity. The high-level concentration of heavy metal in sediment aligns with the level of water toxicity, underscoring the urgent need for thorough assessment and monitoring. The research focused on assessing heavy metal concentration and distribution through spatial analysis. Toxicity levels were evaluated using the enrichment factor (EF) and Geoaccumulation Index (Igeo). This study collected eight samples each during the rainy season of 2022 and 2023. The heavy metals were tested using an Atomic Absorption Spectrophotometer (AAS), including Pb, Cd, Cr, Fe, Al, and Cu. Comparatively, the mean concentration of heavy metals in 2023 was slightly higher for Fe and Al than in 2022. Moreover, Cd was not detected in either 2022 or 2023. The variety of land use and land cover has consequences on the spatial distribution of toxicity levels, showing an influential correlation between Al, Pb, and Fe metals with locations associated with cropland and floating net cages. Additionally, highly steep slopes significantly affected erosions that induced sediment from agricultural land use, further underscoring the multifaceted nature of environmental risk factors.

Keywords: environmental risk, ecological risk, heavy metals, lake hydrology, water pollution

DOI: https://doi.org/10.55981/limnotek.2024.3880

1. Introduction

Heavy metals are considered toxic owing to their ability to bind to sediments, accumulate over extended periods, and resist degradation (Yuan e*t al.*, 2022). These metals are commonly transported to water bodies through surface runoff and erosion processes and accumulate in the sediment. The natural sources of heavy metals are rock weathering and volcanic sediments. However, anthropogenic factors related to household activities, agriculture, and

industrial operations release large quantities of heavy metals into the environment (Looi *et al.*, 2019). The previous study found that heavy metals in sediments primarily originated from bedrock and land-based activities. However, lakes in the protected areas may be exposed to heavy metal pollution from forests, agriculture, and other anthropogenic land uses (Sojka *et al.*, 2022).

Menjer Lake is a volcanic lake located in Wonosobo City, serving multiple purposes such as tourism, hydropower generation, and fisheries. Moreover, agricultural activities are excessive in its catchment area. Agricultural activities, such as chili, potato, and cabbage farming, in the Menjer Lake catchment area have been identified as potential sources of heavy-metal pollutants. Metals commonly found in fertilizers, including Cr, Fe, Zn, and Cd, contribute to this pollution (Xu *et al.*, 2020). The extensive use of fertilizers, driven by intensive agricultural practices, may lead to these heavy metals (Alfarisy *et al.*, 2020). Additionally, Menjer Lake is fed by the Serayu River, potentially transporting metals along with dissolved sediments. Heavy metals usually found in lake-surface sediments are Fe, Pb, Cu, Zn, Cd, Hg, and Al (Bentley *et al.,* 2022). However, volcanic lake bedrock commonly contains metals such as Fe, Cu, and Pb.

One method to assess the presence of heavy metals in river sediments is to use the Enrichment Factor (EF) and Geoaccumulation Index (Igeo). The Igeo is used to determine metal contamination in sediments, with its calculation formula developed by Muller in 1969. Meanwhile, the EF assesses metal contamination resulting from anthropogenic activities. Both indices are crucial for identifying anthropogenic contaminants in sediment and surface soil (Barbieri, 2016). This method is essential because the metals accumulated in sediments can dissolve in water and undergo transfer to human bodies and animals (Hasimuna *et al.*, 2021). The EF and Igeo serve as metrics for evaluating the presence and extent of anthropogenic contaminants. The EF and Igeo are commonly utilized to assess metal concentrations of environmental concern. These indexes assess soil pollution levels, often based on similar soil fragments, using the numerical formula representing the bio-available fraction (Barbieri, 2016).

Research on assessing toxic metal levels in Indonesian lakes is currently limited. Several studies have been conducted on river sediments, including research by Wardhani *et al.* (2018) on reservoirs, Fadlillah *et al.* (2023) examining toxicity in water and sediments in the Winongo River, and Fadlillah *et al.* (2024) conducting research of ecological risk in nutrient and heavy metals in Menjer Lake using different methods without comparing to temporal changes between years. Conducting such research is crucial to address public concerns about heavy-metal accumulation in sediment. The study aimed to investigate the spatial variation, distribution, and sources of heavy metals (Pb, Cd, Cr, Fe, and Al) in Menjer Lake using the EF and Igeo across different years. Moreover, this research was conducted to create a basis for data on heavy metal concentration in lake sediment in Indonesia.

2. Materials and Methods

2.1 Study Area

Menjer Lake is situated in Maron Village, Garung District, Wonosobo, Central Java (Figure 1).This lake was formed at the base of Mount Pakuwaja due to volcanic eruptions and is positioned at 1300 m above sea level. Hence, it is characterized by extremely steep slopes (>40%). The water sources of Menjer Lake are from various rivers within the Menjer catchment areas, namely the Menjer, Siwedi, and Silumbu Rivers, as well as springs surrounding the lake (Bergen *et al.*, 2000). Additionally, this area experiences substantial rainfall, with the Menjer catchment area receiving an annual average rainfall of >3000 mm, classified as very high (Suhendro *et al.*, 2022).

2.2. Sampling collection and analysis

This investigation collected 16 surface sediment samples from Menjer Lake during the rainy season. Eight sampling sites (S1-S8) were carefully chosen to encompass different land uses, considering the potential introduction of heavy metals into the lake via runoff from diffuse sources. Field surveys were conducted in March 2022 and January 2023. The initial eight sediment samples were obtained in March 2022, and the remaining eight samples were collected in January 2023. Additionally, three soil samples were taken from the agricultural zone in January 2023 to investigate the correlation between surface sediment. Notably, the sampling sites were consistently maintained in the exact locations throughout the study period in 2022 and 2023 (Figure 1).

The Sediment samples from each site were gathered using a grab sampler for surface sediment, following the method outlined by Ahmed *et al.* (2022). Subsequently, the samples were placed in plastic bags, stored in ice boxes, and transported to the laboratory for analysis. Once there, they were naturally dried at ambient air temperature. Following drying, 0.3 g samples underwent digestion using HNO_3 and were analyzed for heavy metal content using an atomic absorption spectrophotometer (Varol, 2020). The heavy metals tested for Pb, Cd, Cr, Fe, and Al. All sediment analyses adhered to standard operating procedures in accordance with ISO 17025:2017. Calibration Curves were also prepared from a 1000-ppm stock standard solution to ensure quality control and assurance during the analyses.

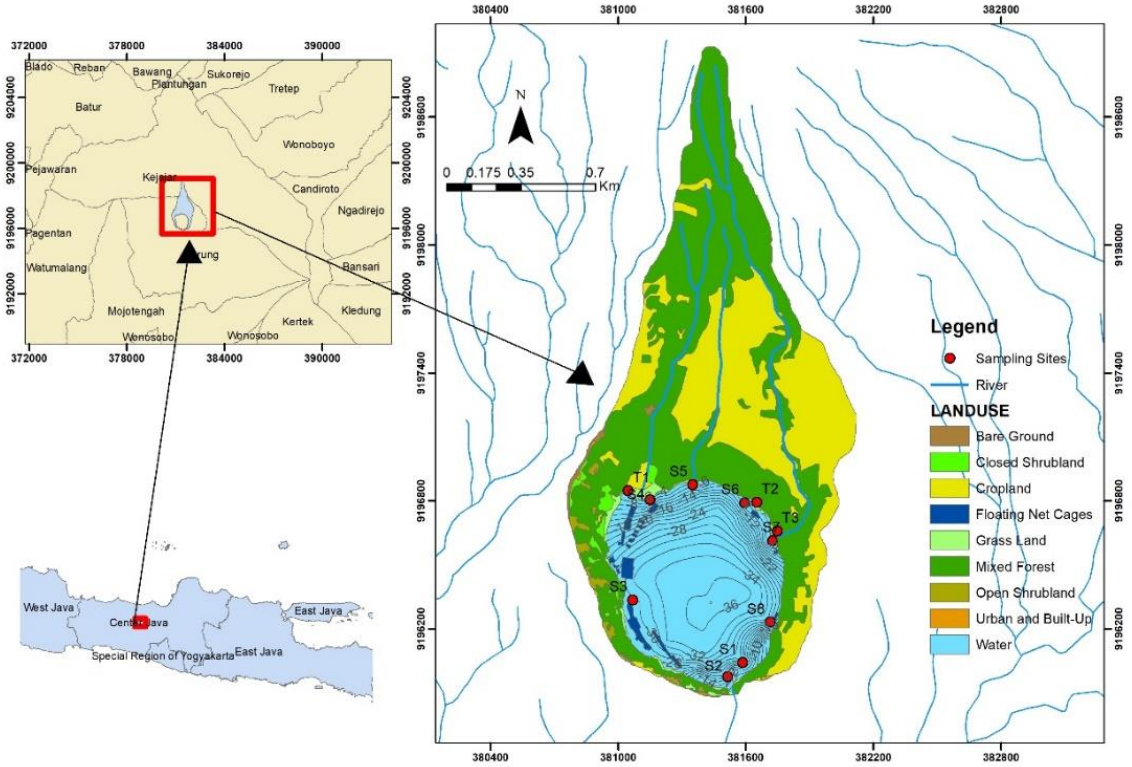

Figure 1. Location of Menjer Lake in Wonosobo, Central Java, Indonesia along with the designated sampling sites.

2.3. Heavy metal risk assessment analysis

2.3.1. *Enrichment Factor (EF)*

The EF is used to evaluate the contamination and pollution of heavy metals from anthropogenic activity (Li *et al.*, 2022). The EF is calculated using Equation 1:

$$\mathrm{EF} = \left(\left(\frac{\mathrm{A}}{\mathrm{B}}\right)\mathrm{sample}\right) / \left(\left(\frac{\mathrm{A}}{\mathrm{B}}\right)\mathrm{background}\right) \quad \text{....Eq 1.}$$

where A is the element concentration in the observed sample, while B is the reference element concentration in a sample. The value of EF is calculated by the ratio between the observed heavy-metal concentration ((A/B) sample) and the stable concentration of heavy metals with standard samples ((A/B) background). EF can be categorized by the value in sediment: EF < 1 indicates no enrichment; 1 < EF < 3 is low; 3 < EF < 5 is moderate; 5 < EF < 10 is moderately severe; 10 < EF < 25 is severe; 25 < EF < 50 is very severe; and up to 50 is highly severe (Yuan *et al.*, 2022).

2.3.2. *Geo-accumulation Index (Igeo)*

Most studies assess the environmental risk posed by sediment by considering the background concentration of heavy metals. The background concentration of heavy metals in lake sediment varies due to different geological settings and land use types (Birch, 2017; Xu *et al.*, 2020). Therefore, this study utilized Igeo to determine the level of heavy metal contamination in the sediment. The background values were adopted from previous research on rivers in volcanic areas (Fadlillah *et al.*, 2023). The (Igeo) was calculated using Equation 2:

$$\mathrm{Igeo} = \mathrm{Log2}\,\frac{\mathrm{Cn}}{1.5\,\mathrm{Bn}} \quad \text{....Eq 2.}$$

where Cn shows the metal concentration in sediment samples, while Bn is the metal concentration reference. The value of Igeo < 0 is unpolluted; 0 to 1 is lowly polluted; 1 to 2 is moderately polluted; 2 to 3 is moderate to highly polluted; 3 to 4 is highly polluted; 4 to 5 is high to extremely polluted; above 5 is extremely polluted (Xu *et al.*, 2020; Yuan *et al.,* 2022).

3. Results and discussion

3.1. Heavy-metal concentrations

The heavy metal concentrations in Menjer Lake were found to be significantly lower, approximately 40 times less, than those observed in other Indonesian lakes and reservoirs, such as the Saguling Reservoir, where anthropogenic and industrial activities contribute to higher pollution levels (Wardhani *et al.*, 2018). For instance, in the Saguling Reservoir, Pb, Cr, and Cd concentrations were measured at 40.2, 165.25, and 16.68 mg kg^{-1}, respectively. This contrast underscores Menjer Lake's relatively low exposure to pollution. Additionally, comparisons with international lakes reveal that Menjer Lake's concentrations of Pb, Cr, Fe, Al, and Cd are lower than those in lakes like Erhai Lake (Lin *et al.*, 2016) and Lake Taihu (Xu *et al.*, 2020), yet higher than Uchalli Lake in Pakistan (Aftab *et al.*, 2023), with Cd levels being the lowest among all metals in Menjer Lake.

Table 1 illustrates a slight decrease in metal concentrations in 2023, except for Fe and Al levels (Menjer Lake). Cr and Cd concentrations were undetectable due to their minimal amounts. Furthermore, no significant changes in watershed management or land use were observed across the different sampling years.

Table 1. Concentrations of heavy metals in the sediment of Menjer Lake

Name of sample	Heavy-metal Concentration (mg kg^{-1})	Pb	Cr	Fe	Al	Cd
Menjer Lake[a] (n = 8)	Mean	0.129	0.050	9.038	59.858	ND*
	Min	0.067	0.023	0.110	0.110	ND*
	Max	0.207	0.061	25.790	266.940	ND*
Menjer Lake[b] (n = 8)	Mean	0.085	ND*	24.234	35.473	ND*
	Min	0.030	ND*	0.880	5.177	ND*
	Max	0.149	ND*	82.740	105.720	ND*
Soil samples[C] (n = 3)	T1	0.101	ND*	88.100	64.517	ND*
	T2	0.134	ND*	92.500	96.043	ND*
	T3	0.100	ND*	67.040	72.066	ND*
Background value[d]		0.170	0.020	28.820	32.830	ND*

[a]Sediment samples taken in the year 2022. [b]Sediment samples taken in the year 2023. [c]Sediment samples taken from cropland in the catchment area of Menjer Lake. [d]Background value from previous research related to Winongo River (Fadlillah *et al.*, 2023). [e]Heavy metal concentrations in mean value. * Not detected

3.2. Spatial distribution of heavy metals in sediment

Menjer Lake is a deep volcanic lake with a maximum depth of over 36 m (Figure 1). The bathymetry of this lake, shown in Figure 1, displays a remarkably steep slope of lake topography, suggesting that sediments may have accumulated in the deep areas of the lake. The sediment sampling was conducted in the litoral zone up to 17 m depth of the lake due to the limitations of the grab sampler. The spatial distribution shows spatial consistency for each heavy metal related to the sampling sites and the corresponding land use from the samples taken in different years.

Table 2. Pearson correlation matrix for heavy metals in the lake-surface and cropland sediments in the year 2023

Heavy-metal correlations	Pb	Cr	Fe	Al	Cd
Pb	1				
Cr	-	-			
Fe	.86*	-	1		
Al	.88*	-	.72*	1	
Cd	-	-	-	-	-

The spatial distribution of heavy metals is shown in Figures 2 and 3. The highest Pb values in 2022 were recorded at points S3 and S5, while the highest Pb value in 2023 was observed at point S3. Meanwhile, the spatial distribution of Fe metal shows a similar pattern in 2022 and 2023. High Fe values are found at points S3 and S4, while low Fe values are found at points S6, S7, and S8. The highest values for Al metal in 2022 were found at points S4 and S5, whereas the highest values were at points S4 and S6 in 2023.

The results of the correlation analysis (Table 2) and the spatial distribution patterns indicate a strong correlation between locations with Al, Pb, and Fe metals. The high metal concentrations are observed in adjacent locations, specifically at points S3, S4, S5, and S6, which are influenced by floating net cages and agriculture (Wang *et al.*, 2018).

Regarding the distribution of Cr metal, the highest concentrations were found at points S4, S5, and S1 in 2022. Due to the instrument detection limit, the Cd metal results for 2022 and 2023 cannot be presented in spatial form. Similarly, the Cr value for 2023 cannot be presented spatially as well as cannot be calculated for EF and Igeo.

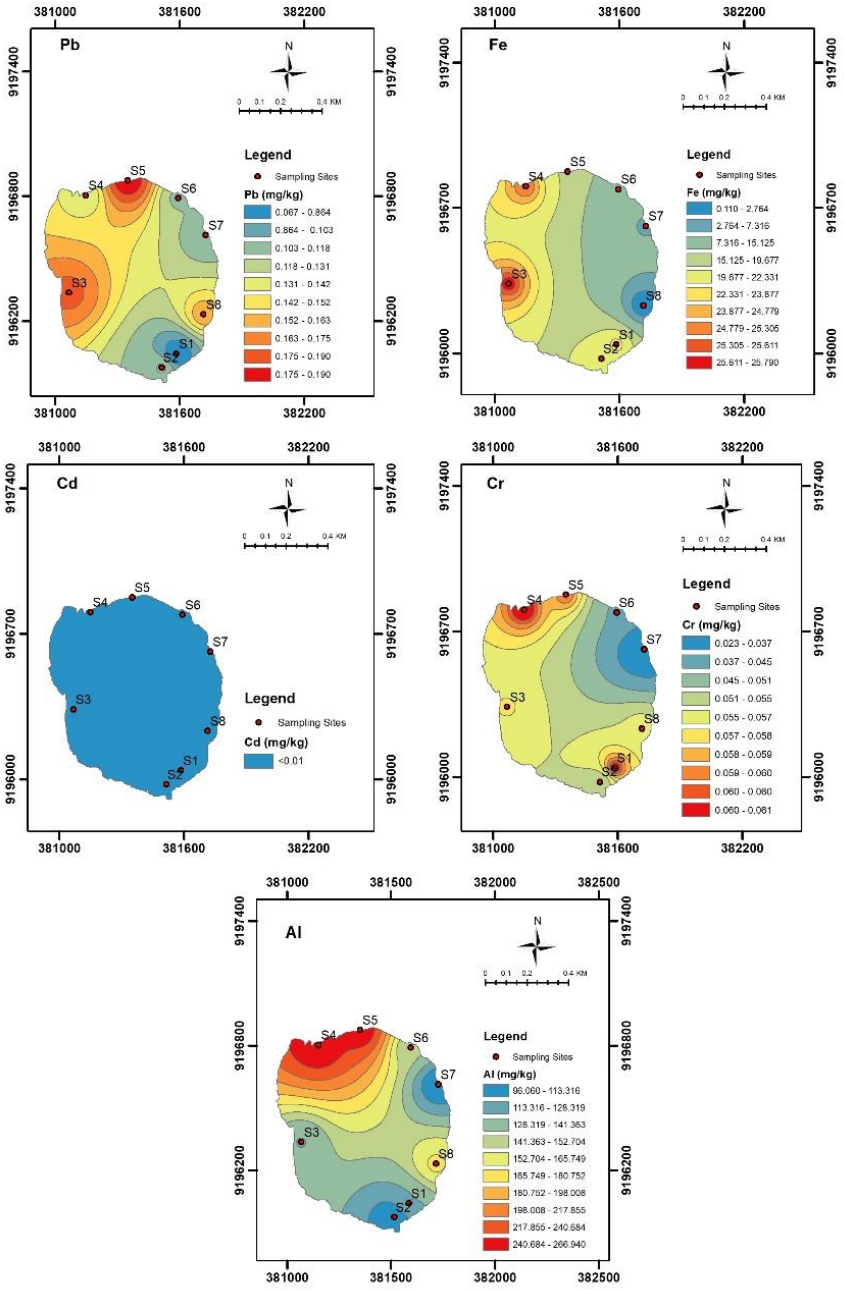

Figure 2. Spatial distribution of heavy metals in 2022

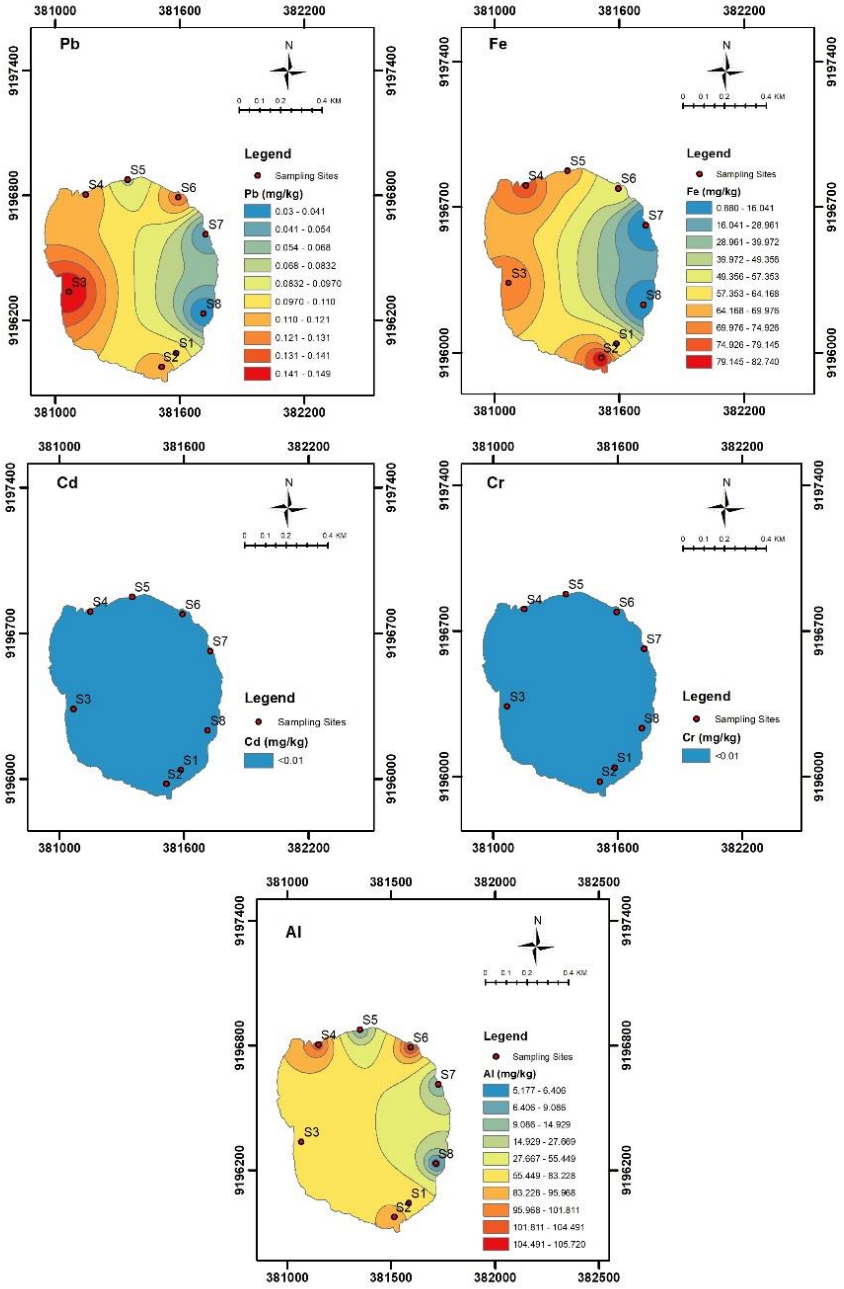

Figure 3. Spatial distribution of heavy metals in 2023

3.2. Assessment of heavy metal pollution in the sediments

The EF and Igeo methods are utilized in this research to characterize geochemical accumulations and compare them with background values from other regions (Tepe *et al.*, 2022). In this study, the background value for heavy metals is taken from the Winongo River (Fadlillah *et al.,* 2023), as there is limited research on heavy metals in lakes, especially volcanic lakes. The similar lithological settings between the river and

Menjer Lake suggest that they may receive similar concentrations from runoff originating from parent rocks rather than comparing them to reservoirs. Barbieri (2016) also states that the background values usually came from the natural substance of soil, which has a similar composition to mineralogy. That is why parent material or similar geological sources were more significant in choosing background values.

Table 3 displays the average EF values for 2022 and 2023, with the average heavy metals EF values ranked as follows: Al > Cr > Fe > Pb > Cd. Pollution levels in Menjer Lake are categorized as follows: no enrichment (Pb), low enrichment (Cr and Fe), and moderate enrichment (Al).

Table 3**.** EF and I_{geo} value for five heavy metals from lake-surface sediment

Name of sample	Heavy-metal Concentration (mg kg^{-1})	Pb	Cr	Fe	Al	Cd*
EF Value (n = 16)	mean	0.68	2.59	1.19	3.04	ND
	min	0.17	1.15	0.003	0.003	ND
	max	1.21	3.05	2.87	8.13	ND
	Pollution level	No Enrichment	Low Enrichment	Low Enrichment	Moderate Enrichment	ND
Igeo value (n = 16)	mean	−1.28	0.73	−1.54	−0.09	ND
	min	−3.08	−0.38	−8.61	−8.8	ND
	max	−0.3	1.02	0.93	2.43	ND
	Pollution level	Unpolluted	Lowly Polluted	Unpolluted	Unpolluted	ND

*ND Detection Limit: cannot proceed with the calculation.

Additionally, heatmaps were used to analyze the results of each sampling site analysis for each metal parameter. The EF heatmaps are presented in Figures 4 and 5, while the Igeo heatmaps are displayed in Figures 6 and 7. The EF and Igeo heatmaps for 2022 and 2023 exhibit variations, particularly in the Cr EF values. The EF value for Cr in 2023 falls within the low to moderate enrichment range, ranging from 1.15 to 3.05. For the other metal contents, such as Al and Pb, the EF in 2023 ranged from 0.003 to 8.13 and from 0.394 to 1.218 for Al and Pb, respectively, showing a slight decrease from the EF in 2022. The EF value in 2023 ranged from 0.158 to 3.22 and from 0.176 to 0.876 for Al and Pb, respectively. However, the Cr value in 2023 significantly decreased and went undetected. The primary sources of Cr metal in Menjer Lake potentially include soil weathering, as described in the study of Swarnalatha *et al.* (2013).

Furthermore, the Igeo value for Cr in 2022 also demonstrated unpolluted to lowly polluted (−0.4 to 1.0). The negative value indicates that the samples were low polluted or unpolluted (Xu *et al.*, 2020; Li *et al.*, 2021). The Igeo results for Al and Pb also display a significant decrease for Al and Pb. The values ranged from −8.9 to 2.4 and from −1.9 to −0.3 for Al and Pb in 2022, respectively, while the Igeo values ranged from −3.2 to 1.1 and from −3.1 to −0.8 for Al and Pb in 2023, respectively. Simultaneously, the Fe value 2023 exhibits a noticeable increase in EF and Igeo results. Meanwhile, Cd remains undetected.

The comparison of EF and Igeo values between different years (2022 and 2023) yielded similar results, as reflected in the consistent patterns shown in the heat maps for each heavy metal. Menjer Lake's pollution

level is classified as either unpolluted or lowly polluted, with a general trend toward decreasing pollution for Al, Pb, Cd, and Cr. This decrease in concentration could be attributed to changes in the sources of these metals (Zhou *et al.*, 2020). For instance, fertilizer use has been reduced in the areas surrounding the lake. Additionally, several agricultural zones in the lake's vicinity have been transformed into public spaces, contributing to the decrease in pollution levels observed. Conversely, the concentration of Fe is observed to be increasing over time. These fluctuations in heavy-metal concentrations across periods suggest alterations in lake bottom sediment due to resuspension, transport, and deposition processes (Ali *et al.*, 2022), likely influenced by hydrodynamic processes in the deep and steep lake (Broberg, 1994).

The pollution level in Menjer Lake is attributed to nonpoint sources and effluents directly entering the lake bodies (Swarnalatha *et al.*, 2013). However, in protected areas like Menjer Lake, the sources of heavy metal pollution are identified as limited. The surrounding land, primarily covered by forests, croplands, and fishing caged nets for aquaculture, exhibits minimal contamination from heavy metals (Sojka *et al.*, 2022).

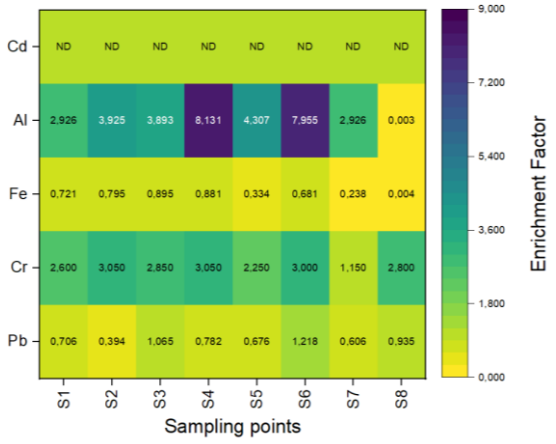

Figure 4. Enrichment factor heatmaps of heavy metals in Menjer Lake year 2022

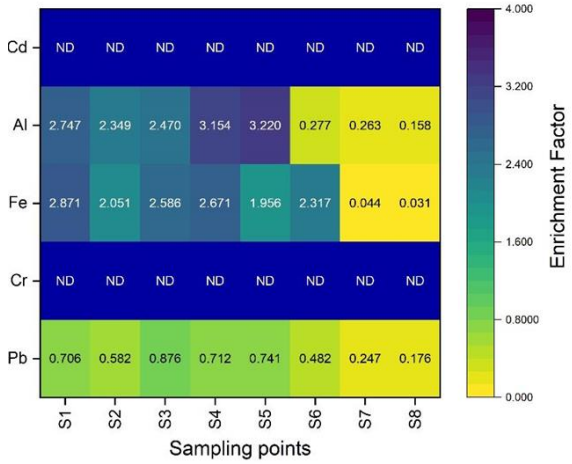

Figure 5. Enrichment factor heatmaps of heavy metals in Menjer Lake year 2023

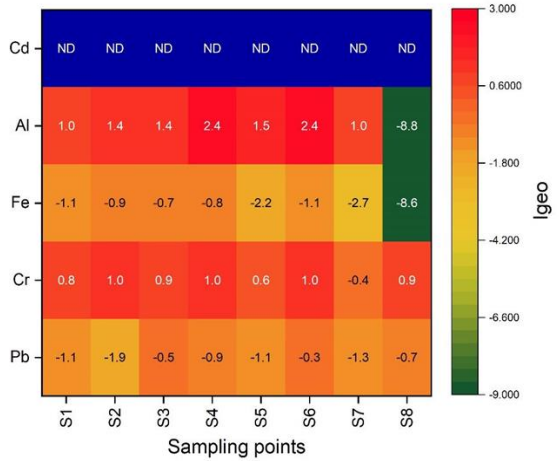

Figure 6. Igeo heatmaps of heavy metals in Menjer Lake year 2022

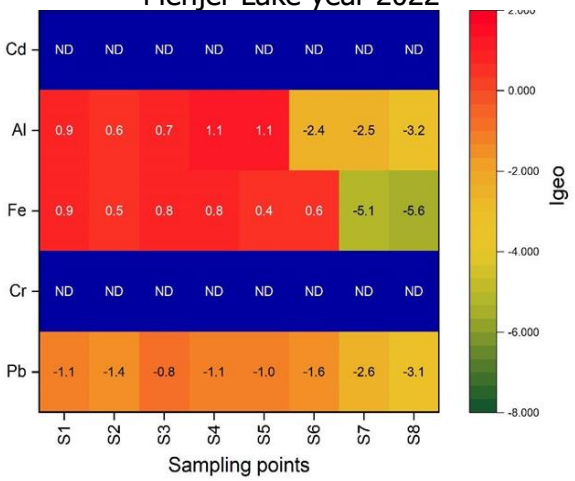

Figure 7. Igeo heatmaps of heavy metals in Menjer Lake year 2023

*)Please note that the scales depicted in the images differ.

4. Conclusion

The study delves into analyzing heavy metal spatial distribution, sources, and associated pollution risks, explicitly focusing on Pb, Cr, Fe, Al, and Cd concentrations in surface sediments within Menjer Lake. This investigation established correlations between sediment and agricultural soil samples, particularly for Pb, Cr, and Fe. The spatial analysis highlighted elevated heavy metal concentrations in areas like S3, S4, S5, and S6, attributed to activities such as floating net cages and agriculture. Furthermore, the lake's steep morphology contributed to the distribution pattern along its shores.

The Igeo analysis for 2022 and 2023 classified pollution levels as "unpolluted" and "lowly polluted," respectively, while EF results indicated varying degrees of enrichment from "no enrichment" to "moderate enrichment." Despite some pollution, Menjer Lake remains relatively unpolluted, mainly due to protective measures in its catchment area. Additionally, projections suggest a decrease in heavy metal pollution levels by 2023, particularly for Al, Cd, Cr, and Pb. Continued research into sediment-related risk assessments in Indonesian lakes is imperative. Sediment is a crucial environmental indicator, offering insights into pollution extents and accumulated contaminants, guiding future environmental management strategies.

Data availability statement

Data will be made available on request.

Funding Agencies

Funding support: Faculty of Geography, Gadjah Mada University, Indonesia (Contract number: 80/UN1/FGE/KPT/SETD/2023)

Conflict of interests

The authors declare they have no competing interests.

Acknowledgment

We would like to thank the Faculty of Geography, Gadjah Mada University, Indonesia, for supporting the data collection in this research. (Contract number: 80/UN1/FGE/KPT/SETD/2023)

Author Contributions

LNF provided the conceptual framework, conducted sampling, analyzed the data, and prepared the manuscript. **MW** contributed to sampling and reviewed the manuscript. **AAR** was responsible for mapping and writing the manuscript. **AU** was involved in land use mapping and writing the manuscript.

References

Aftab A, Aziz R, Ghaffar A, Rafiq MT, Feng Y, Saqib Z, Rafiq MK, Awan MA. 2023. Occurrence, source identification and ecological risk assessment of heavy metals in water and sediments of Uchalli Lake – Ramsar site, Pakistan. Environmental Pollution 334: 122117. DOI:10.1016/j.envpol.2023.122117

Ahmed ASS, Hossain MB, Babu SMO, Rahman M, Sun J, Sarker MSI. 2022. Spatial distribution, source apportionment, and associated risks of trace metals (As, Pb, Cr, Cd, and Hg) from a subtropical river Gomti Bangladesh. International Journal of Sediment Research, 37(1), 83–96. DOI: 10.1016/j.ijsrc.2021.07.001

Alfarisy FK, Andriyani I, Bowo C. 2020. Evaluation of water quality due to the use of intensive fertilizer on farmer level in the upstream of Bedadung Jember Watershed, East Java, Indonesia, Journal of Degraded and Mining Lands Management, Journal of Degraded and Mining Lands Management 7(4): 2301-2312. DOI:10.15243/jdmlm.2020.074.2301

Ali MM, Rahman S, Islam MS, Rakib MRJ, Hossen S, Rahman MZ, Kormoker T, Idris AM, Phoungthong K. 2022. Distribution of heavy metals in water and sediment of an urban river in a developing country: a probabilistic risk assessment. International Journal of Sediment Research 37(2): 173-187.

Barbieri M. 2016. The Importance of Enrichment Factor (EF) and Geoaccumulation Index (Igeo) to Evaluate the Soil Contamination., 5(1). DOI:10.4172/2381-8719.1000237

Bentley C, Junqueira T, Dove A, Vriens B. 2022. Mass-Balance Modeling of Metal Loading Rates in the Great Lake. Environmental Research 205, DOI: 10.1016/j.envres.2021.112557

Bergen van JM, Bernard A, Sumarti S, Sriwana T, Sitorus K. 2000. Creater lakes of Java: Dieng, Kelud, dan Ijen. Excursion Guidebook. IAVCEI General Assembly.

Birch GF. 2017. Determination of sediment metal background concentrations and enrichment in marine environments – A critical review. Science of the Total Environment, 580: 813-831, DOI:10.1016/j.scitotenv.2016.12.028

Broberg A. 1994. The Distribution and Characterization of 137Cs In Lake Sediments. Studies in Environmental Science, 62: 45-62. DOI:10.1016/S0166-1116(08)71699-6

Fadlillah LN, Utami S, Rachmawati AA, Jayanto GD, Widyatusti M. 2023. Ecological risk and source identifications of heavy metals contamination in the water and surface sediments from anthropogenic impacts of urban river, Indonesia. Heliyon 9 (4): e15485. DOI:10.1016/j.heliyon.2023.e15485

Fadlillah LN, Afifudin, Rachmawati AA. 2024. Spatiotemporal ecological risk evaluation and source identification of heavy metals and nutrients in the water and lake surface sediment in a protected catchment area of a volcanic lake. Environmental Monitoring and Assessment 196(3): 1-19. DOI: 10.1007/s10661-024-12432-5

Hasimuna OJ, Chibesa M, Ellender BR, Maulu S. 2021. Variability of selected heavy metals in surface sediments and ecological risks in the Solwezi and Kifubwa Rivers, Northwestern province, Zambia. Science African (12). DOI:10.1016/j.sciaf.2021.e00822

Li X, Wu P, Delang CO, He Q, Zhang F. 2021. Spatial-temporal variation, ecological risk, and source identification of nutrients and heavy metals in sediments in the peri-urban riverine system. Environmental Science and Pollution Research (28): 64739-64756, DOI:10.1007/s11356-021-15601-y

Li J, Zuo Q, Feng F, Jia H. 2022. Occurrence and Ecological Risk Assessment of Heavy Metals from Wuliangsuhai Lake, Yellow River Basin, China. Water, 14 (8): 1264, DOI:10.3390/w14081264

Lin Q, Liu E, Zhang E, Li K, Shen J. 2016. Spatial distribution, contamination and ecological risk assessment of heavy metals in surface sediments of Erhai Lake, a large eutrophic plateau lake in southwest China. Catena, 145, 193–203. DOI: 10.1016/j.catena.2016.06.003

Looi LJ, Aris AZ, Yusoff FM, Isa NM, Haris H. 2019. Application of Enrichment factor, Geoaccumulation Index, and Ecological Risk Index in assessing the elemental pollution status of surface sediments. Environmental Geochemical Health 41: 27-42, DOI:10.1007/s10653-018-0149-1

Muller G. 1969. Index of geo-accumulation in sediments of the Rhine River. *GeoJournal* 2(3): 108-118

Sojka M, Jaskuła J, Barabach J, Ptak M, Zhu S. 2022. Heavy metals in lake surface sediments in protected areas in Poland: concentration, pollution, ecological risk, sources and spatial distribution. Scientific Reports 12 (1): 15006. DOI:10.1038/s41598-022-19298-y

Suhendro I, Isnain MN, Wahyudi R. 2022. Rock characteristics of post-caldera volcanoes in Dieng volcanic complex (DVC), Central Java, Indonesia. Journal of Geoscience, Engineering, Environment, and Technology, 7(4), 151-157. DOI:10.25299/jgeet.2022.7.4.10015.

Swarnalatha K, Letha J, Ayoob S. 2020. Ecological Risk Assessment of a Tropical Lake System. Journal of Urban and Environmental Engineering 7(2): 323-329. DOI: 10.4090/juee.2013.v7n2.323329

Tepe Y, Simsek A, Ustaohlu F, Tas B. 2022. Spatial–temporal distribution and pollution indices of heavy metals in the Turnasuyu Stream sediment, Turkey. Environmental monitoring and assessment 194(11): 818, doi: 10.1007/s10661-022-10490-1Varol, M. 2020. Environmental, ecological and health risks of trace metals in sediments of a large reservoir on the Euphrates River (Turkey). Environmental Research, 187 p. 109664.

Wang J, Cheng Q, Xue S, Rajendran M, Wu C, Liao J. 2018. Pollution characteristics of surface runoff under different restoration types in manganese tailing wasteland. Environmental Science and Pollution Research, 25(10): 9998-10005.

Wardhani E, Notodarmojo S, Roosmini D. 2018. Sediment Quality Assessment by Using Geochemical Index at Saguling Reservoir West Java Province Indonesia. Energy and Environmental Research 8(2): 34 – 44. DOI:10.5539/eer.v8n2p34

Xu M, Wang R, Yang X, Yang H. 2020. Spatial distribution and ecological risk assessment of heavy metal pollution in surface sediments from shallow lakes in East China. Journal of Geochemical Exploration 213: 196490. DOI:10.1016/j.gexplo.2020.106490

Yuan Y, Liu B, Liu H. 2022. Spatial distribution and source identification for heavy metals in surface sediments of East Dongting Lake, China. Scientific Reports 12(1): 1 – 9, DOI:10.1038/s41598-022-12148-x

Zhou Q, Yang N, Li Y, Ren B, Ding X, Bian H, Yao X. 2020. Total concentrations and sources of heavy metal pollution in global river and lake water bodies from 1972 to 2017. Global Ecology and Conservation 22: e00925. DOI:10.1016/j.gecco.2020.e00925

LIMNOTEK Perairan Darat Tropis di Indonesia
transforming into the Journal of Limnology and Water Resources
p-ISSN: 0854-8390 e-ISSN: 2549-8029
https://ejournal.brin.go.id/limnotek

Assessment of Natural Bentonite Efficacy for Dye Removal in Textile Wastewater Treatment: Implications for Mitigating River Citarum Pollution

Azriel Fathan Nabhani[1], Zahidah[1], Heti Herawati[1], Fifia Zulti[2*]

[1]Department of Fisheries, Faculty of Fisheries and Marine Science, Padjadjaran University, Jatinangor, West Java, Sumedang, Indonesia
[2]Research Center for Limnology and Water Resources, National Research and Innovation Agency (BRIN), Indonesia

*Corresponding author's e-mail: fifi003@brin.go.id

Received: 15 April 2024; Accepted: 31 May 2024; Published: 30 June 2024

Abstract: Textile industries contribute significantly to the economy but release harmful pollutants into the environment, especially rivers. The effluent from the textile industry contains toxic dyes that can harm the river ecosystem. Several studies have been conducted to reduce toxic dyes in a river system using bentonite as an adsorbent to reduce river pollution effectively. However, the effectiveness of bentonite still needs to be tested again using textile liquid waste that has not gone through any waste processing at all. Citarum is one of the main rivers on Java Island, which suffers from textile effluent, especially azo dyes which are toxic, mutagenic, and carcinogenic which can harm the aquatic ecosystem. Therefore, this study aims to implement natural bentonite as an adsorbent to remove dyes from textile wastewater. We performed a laboratory test to adsorption on bentonite and textile wastewater considering the variation of adsorbent weight of 10 g and 20 g in 100 mL of textile wastewater stirred in an Erlenmeyer flask at room temperature for 0-300 minutes. The initial concentration of textile wastewater used was 10%, 30%, and 50%. We found that the maximum dye removal efficiency was 91.25% with 10% initial concentration treatment, 20 g adsorbent weight, and 60 minutes contact time. Longer contact time will increase the removal efficiency and adsorption capacity, while higher adsorbent dosage will decrease the concentration of dyes in wastewater. Efficient textile wastewater treatment has improved water quality, effectively meeting river water quality standards and environmental regulations.

Keywords: Natural Bentonite, Dye removal, Textile wastewater, Adsorption, River pollution, River Citarum

DOI: https://doi.org/10.55981/limnotek.2024.4848

1. Introduction

The textile sector is a major force behind commerce, innovation, and employment growth on a worldwide scale. Unquestionably, it has fueled economic expansion by supporting millions of people and increasing consumer demand for a wide variety of textile and clothing products (Rahman & Tabassum, 2024). Instead due to the textile industry's rapid expansion and intensification, there are now a lot more environmental risks, especially those related to water contamination. Pollution in aquatic bodies is caused by the release of untreated or improperly treated wastewater, which contains a range of toxins, including synthetic dyes. These dyes are essential for producing vibrant color in textiles, but they pose a significant environmental risk due to their toxicity, persistence, and tendency to bioaccumulate in aquatic habitats (Kuśmierek *et al.*, 2023).

To date, the dye removal process in textile liquid waste has been widely carried out using several processes, namely physics, chemistry,

and biology, as well as a combination of these three processes. Some methods that have been developed include coagulation, sedimentation, activated sludge, and adsorption methods. Adsorption is the easiest way to apply (Suryawan *et al.*, 2018). In practice, adsorption requires an adsorbent as a binder or contaminant absorber. Bentonite is one of the adsorbents that can be easily found and cheap. Bentonite can reduce dye levels in textile liquid waste. Bentonite content consists of illite, montmorillonite, and quartz, where 85% of the content is montmorillonite (Aichour & Zaghouane-Boudiaf, 2020; Dhar *et al.*, 2023; Khan *et al.*, 2023). The unique property of natural bentonite is that it has the ability to swell and form colloids when put into water. The swelling ability of bentonite is quite large. This swelling ability makes bentonite an adsorbent with a greater adsorption capacity than other adsorbents (Tahari *et al.*, 2022). Therefore, bentonite is suitable for use as an adsorbent in reducing dyes in textile liquid waste. Apart from its low cost, it is also abundant in nature. Research on bentonite used as an adsorbent in degrading dye levels has proven its versatility. Bentonite is able to reduce methylene blue (Boukerroui, 2020) as well as cation and anion dyes Li *et al.*, 2018). Natural bentonite is proven to be able to reduce dyes from various kinds of artificial waste such as methylene blue solution with an adsorption capacity of 73.25 mg/g and congo red 73.25 mg/g using natural bentonite from Algeria (Oussalah *et al.*, 2019), while natural bentonite from Iraq can reduce methylene blue by 256 mg/g (Jawad *et al.*, 2023), reducing dyes from Rodhamine solution by 142.86 mg/L(Priatna *et al.*, 2023). Of all these studies, no research has tested natural bentonite directly on the original waste. The condition of textile wastewater in the final reservoir is a collection of several production processes that not only contain one dye but a combination of various types of dyes used during the production process.

One glaring illustration of the detrimental impact of textile effluent pollution is the Citarum River in Indonesia. Thousands of businesses along the Citarum River watershed in the Bandung area of West Java are engaged in the textile industry (Susanti *et al.*, 2023). The river used to have clear water and abundant biodiversity but has now been severely contaminated due to the overflow of wastewater from the surrounding companies. The wastewater from these companies contains many contaminants such as heavy metals, dyes, and other chemicals, that are discharged directly into the river without treatment. As a result, the Citarum River has poor water quality, which has resulted in the destruction of aquatic habitats, deterioration of human health, and disruption of community livelihoods (Prayoga *et al.*, 2022). The urgency in conducting this research is to address the underlying causes of contamination and implement effective remediation procedures to restore the integrity and health of the Citarum River. This urgency is further emphasized by Presidential Regulation No. 15/2018, which underscores the government's commitment to controlling pollution and protecting watersheds.

Based on the urgent need to mitigate textile wastewater pollution in the Citarum River, the objectives of this study are to determine the performance of bentonite as a natural adsorbent in adsorbing textile effluent dyes in terms of removal efficiency, adsorption capacity, and its effect on water quality. This study's results will serve as a reference for the textile industry in adopting waste treatment technologies that minimize environmental impact, thus promoting sustainable practices and reducing pollution discharges into the Citarum River and similar water bodies. Therefore, while the primary focus of the study may not be directly on the Citarum River, its findings have significant implications for mitigating pollution in this critical waterway and addressing the broader environmental challenges associated with textile wastewater contamination.

2. Materials and Methods

2.1. Materials

This research was conducted at the Testing Laboratory in the Research Center for Limnology and Water Resources, BRIN, Bogor, from January to March 2023. The tools used include a rotary shaker, UV-Vis spectrophotometer Shimadzu 1800, analytical balance, volumetric pipette, Erlenmeyer, 100 mL bottle sample, aspirator, filter paper, test

tube, 100 mesh sieve, tray, beaker glass and water quality checker (WQC). The materials used include powdered bentonite, textile liquid waste, and dyestuff analyzers. Untreated textile liquid waste was taken from PT. X in Bandung, West Java. PT. X is one of the large-scale textile industries, with tens of millions of meters of fabric produced annually. Waste from the production process has been partially processed, but it is still thick in color (Figure 1), which, if discharged directly into the river, will pollute the waters.

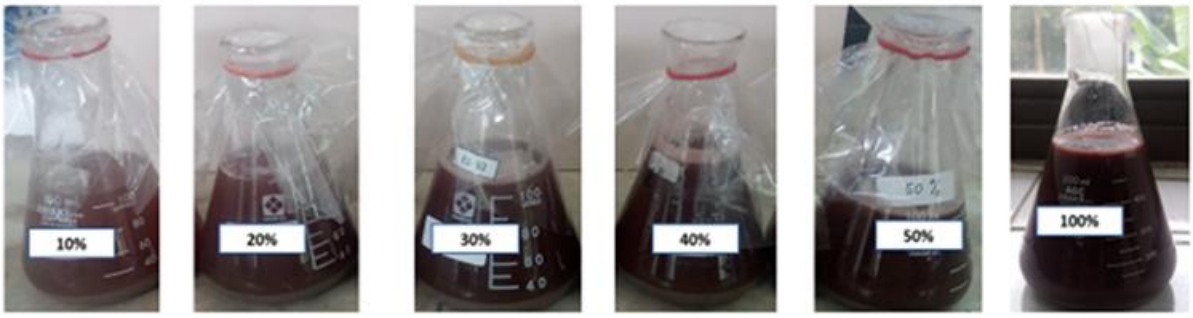

Figure 1. Visualization of textile wastewater from PT. X in Bandung, West Java

2.2. Batch Adsorption

Testing for dye reduction was carried out in batches by adding 10 g and 20 g of bentonite to 100 ml of diluted wastewater with three variations, namely 10%, 30%, and 50%. The solution was stirred at 125 rpm for intervals of 10, 30, 60, 90, 120, 150, 180, 210, 240, 270 and 300 minutes. The suspension was then filtered using a cellulose nitrate filter with a pore size of 0.45 µm and the dye concentration in the supernatant with Pt-Co standard solution using a UV-Vis Spectrophotometer at a wavelength of 456.2 nm. The literature reports on dye adsorption were the basis for selecting these process variables and value ranges (Jamil *et al.*, 2023). The schematic of the batch adsorption process is illustrated in Figure 2. The dye removal efficiency was calculated using Equation 1 and the adsorption capacity was calculated using Equation 2.

$$\%R = \frac{C_i - C_t}{C_i} x\ 100\ \% \quad ....(1)$$

$$q = (C_i - C_t)\frac{V}{m} \quad ....(2)$$

where Ci and Ct are the initial concentration of dye in the waste and at time t (mg/L), %R is the absorption efficiency, q is the adsorption capacity (mg/g), m is the adsorbent mass (g), and V is the wastewater volume (L).

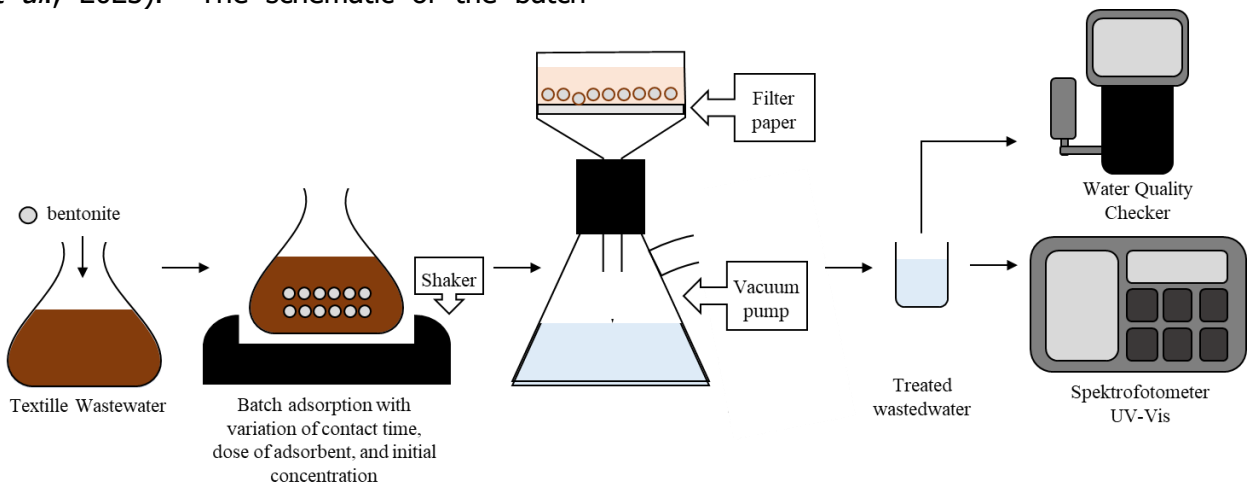

Figure 2. Schematic of dyes adsorption process using bentonite

The study in this research limits the testing of color reduction from textile effluents at a laboratory scale. Batch adsorption studies provide useful insights at laboratory scale but may not directly translate to large-scale industrial applications. Limitations in this research include not accounting for the effects of pH changes on bentonite adsorption capacity and not addressing bentonite regeneration and reuse. Variations in pH can significantly affect adsorption efficiency, and the lack of consideration for bentonite reuse affects the assessment of the feasibility and economic sustainability of the process in real-world applications.

3. Results and discussion

In this research, we focused on the analysis of textile waste obtained from the local textile processing industry because it has a characteristic of a striking red solid color, representing a significant problem in industrial waste management. We managed to measure the concentration of dyes in the waste, with results reaching 2,720.67 Pt-Co units. The intense red color observed in textile wastewater indicated the presence of intense and possibly persistent dyes in the environment. Some textile dyes that often produce red liquid waste include reactive, acidic, direct, and azo dyes, which can significantly negatively impact the environment and human health (Al-Tohamy *et al.*, 2022).

The high concentration of this liquid waste required dilution measures to facilitate further analysis and testing. This study showed textile effluent dilution ranging from 10% to 50%, as illustrated in Figure 1. Textile wastewater exhibits varying characteristics depending on the dilution concentration (Table 1). Dilutions in the 10-100% range at relatively the same temperature and pH conditions in each condition have very high color concentrations. Therefore, three concentrations were chosen that represent the performance of bentonite in reducing dyes, namely at dilution concentrations of 10%, 30%, and 50% with concentration values of 445.67 Pt-Co, 1,122.33 Pt-Co, and 1,774 Pt-Co, respectively. Wastewater with a concentration of 100%—meaning the original waste without additional solvent (distilled water)—was not tested because it is highly concentrated, with a dye concentration of 2,720.67 Pt-Co, and may require pre-treatment to avoid clogging and damage to the adsorbent. The pH conditions of the solution can affect the adsorption process between bentonite and dyes in effluent (Priatna *et al.*, 2023). In the pH range of 6.87 to 8.67 observed in this study, these conditions are generally favorable for dye adsorption by bentonite. At higher pH, there is usually an increase in the number of hydroxyl groups on the bentonite surface, which facilitates interaction with dyes that tend to be acidic. In addition, higher pH can also increase the ionization of dyes, which can increase the electrostatic attraction between dyes and bentonite surfaces (Patanjali *et al.*, 2022).

Table 1. Characteristics of initial wastewater

Dilution Concentration (%)	Dyes (Pt-Co unit)	T (°C)	pH
10	445.67	25.02	8.67
20	529.00	25.10	8.50
30	1,122.33	25.31	8.27
40	1,430.67	25.88	6.64
50	1,774.00	25.97	6.87
100	2,720.67	26.00	6.03

3.1. Effect of Contact Time on Dye Removal Efficiency in Textile Wastewater

At the start of the contact time, the effectiveness of removing dye from liquid waste textiles grows exceptionally quickly. It then keeps getting better throughout each phase of the contact time until it reaches its peak, after which it starts to decline. Adsorption increases with increasing contact time due to increased interaction between adsorbent and adsorbate so that the allowance efficiency value can increase to the equilibrium point (Marella 2019). The equilibrium condition is usually characterized by the point at which the absorption or adsorption of a particular substance by the adsorbent reaches its maximum point before reaching saturation (Parlindungan *et al.*, 2019; Vithalkar & Jugade, 2020). In this study, it was seen that the reduction efficiency rose steadily until 150 minutes, after which the concentration slowly

continued to fall. The rapid change in the initial contact time is due to the large number of active sites on the bentonite adsorbent surface. The slowing down of the adsorption process as contact time increases due to the active sites on the adsorbent beginning to be occupied by dye molecules so that the adsorption process becomes constant and tends to decrease (Chauhdary *et al.*, 2022; Huang *et al.*, 2017).

Adding 20 g of bentonite gives a higher efficiency value than 10 g (Fig. 3), with a maximum value of 91.25% in 60 minutes. The increase in color removal efficiency value with increasing adsorbent weight occurs due to a larger surface area and the availability of more adsorption sites (Guezzen *et al.*, 2023; Jawad *et al.*, 2023). Relatively low removal effectiveness resulted from the adsorbent's surface becoming saturated with dyes when its weight is low, even when the concentration of dyes in textile liquid waste remains high.

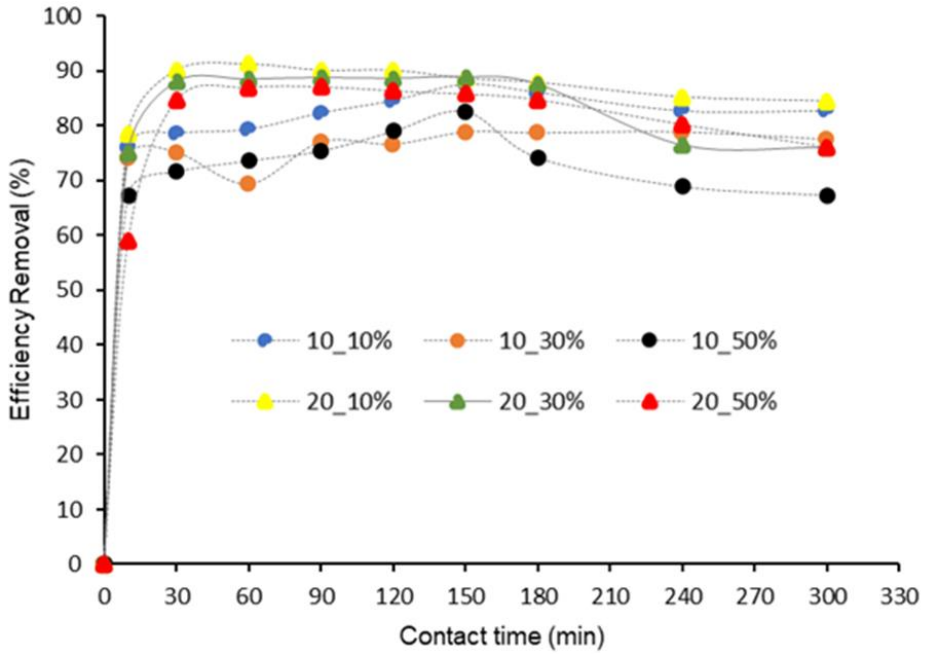

Figure 3. Effect of contact time for dye efficiency removal in textile wastewater

3.2. Effect of Dose for Dyes Adsorption Capacity by Bentonite

The adsorption capacity decreases when larger adsorbent weights are used. The addition of bentonite by 10 g showed that an increase in solution concentration had a significant impact on the rise in bentonite adsorption capacity in absorbing dyes, while the addition of weight by 20 g presented that the increase in solution concentration did not significantly affect the adsorption capacity (Figure 4). This occurred because increasing the amount of adsorbent minerals led to particle aggregation, resulting in a decrease in surface area and an increase in diffusion path length. In addition, increasing the amount of adsorbent causes the number of saturated sites per unit adsorbent to decrease, decreasing adsorbent capacity (Majiya et al., 2023). This implied that a portion of the adsorbent surface remained exposed.

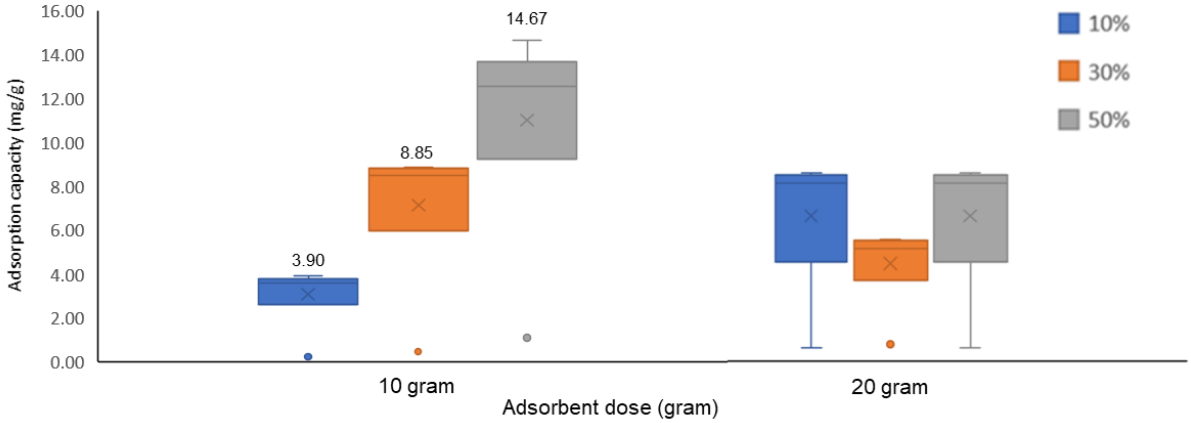

Figure 4. Effect of adsorbent dose to dyes adsorption capacity by bentonite

At equilibrium conditions, namely within 150 minutes, it can be seen how the initial concentration of waste affects the reduction efficiency and adsorption capacity. The two graphs in Figure 5 indicate that the greater the percentage value of the initial concentration of textile liquid waste, the increased adsorption capacity value while the allowance efficiency value decreases. The adsorption capacity increases to a specific concentration along with the increase in the initial concentration of effluent, which aligns with previous research (Albadarin *et al.*, 2017; De Gisi *et al.*, 2016). The increase in adsorption capacity revealed that active sites are still available on the adsorbent surface that can adsorb textile liquid waste dye molecules. Decreased obstruction of mass transfer between adsorbents and adsorbates when there is a greater concentration difference can also be a cause (Moosavi *et al.*, 2020). At the beginning of the adsorption process, the number of adsorbate molecules competing to reach the active side on the surface is very high. While at low concentrations, the adsorption yield (the amount of substance successfully absorbed by the sorbent in the adsorption process) becomes higher due to the small ratio between the dye molecules and the available active side. Moreover, at high concentrations, the pushing force of the adsorbate molecules is higher, so the number of adsorbed molecules is greater.

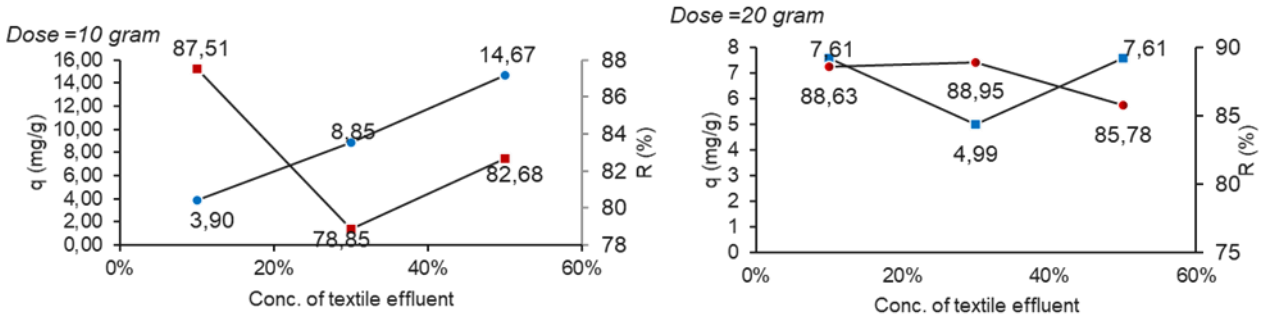

Figure 5. Effect of concentration on removal efficiency and adsorption capacity

3.2. Enhancement of Water Quality

The results revealed that wastewater quality improved after being treated with bentonite. Water quality parameters after treatment were measured under maximum efficiency conditions, namely 10% solution concentration, 20 g dose, and 60 minutes. The analysis showed that the color concentration decreased from 445.67 Pt-Co units to 39 Pt-Co units (%R= 91.25%), so water turbidity also reduced from 648 NTU to 330 NTU. The dissolved oxygen content also rose to 9.77 mg/L, TDS to zero. These parameter values follow class 3 water quality standards intended for fishery activities based on Government Regulation 22 of 2021(Table 2).

Table 2. Water Quality of textile wastewater before and after treatment

Parameter	Unit	Before treatment	After treatment	Threshold*)
Dyes	Pt-Co unit	445.67	33.00	100
Turbidity	NTU	648.00	330.00	400
Total Dissolved Solid (TDS)	mg/L	198.00	0.00	1,000
Dissolved Oxygen (DO)	mg/L	5.13	9.77	3
ORP	mV	20.00	-69.00	-

*)Class 3 water quality threshold based on Government Regulation No. 22 of 2021

Based on this water quality analysis, we can also predict the mechanism of dye absorption by bentonite. Bentonite is a clay mixture of montmorillonite, kaolinite, smectite, and mica. Montmorillonite is one of the main minerals found in natural bentonite, and it has many hydroxyl (OH) and oxygen (O) ions as well as interchangeable cations(Kumari & Mohan, 2021). The high content of hydroxyl and oxygen groups in bentonite provides several advantages in its application as an adsorbent or in cation exchange processes (Dehghani *et al.*, 2018). The change in ORP (Oxygen Reduction Potential) value from 20 mV to -69 mV after textile wastewater treatment with bentonite can be explained by bentonite's ability as a reducing agent that reduces oxidative compounds in the effluent, either through cation exchange processes, adsorption of these compounds, or a decrease in the concentration of ions that tend to increase the ORP value, such as heavy metal ions (Daily, 2019). Therefore, treatment with bentonite effectively reduces the oxidation ability of textile wastewater and improves the overall quality of wastewater by lowering pollution levels. The increased dissolved oxygen concentration in water after being treated with bentonite can be caused by the large number of oxygen ions in its structure that can interact with compounds dissolved in wastewater (Ma *et al.*, 2021; Oktaviyani *et al.*, 2023). This process may cause the release of dissolved oxygen into the water due to reactions between hydroxide ions on the bentonite surface and organic or inorganic compounds in the waste or due to adsorption and cation exchange processes that occur during treatment. Therefore, the rise in dissolved oxygen in water after treatment with bentonite may result from a complex interaction between the oxygen and hydroxide ions in the bentonite structure and compounds in the wastewater. The results of this study, especially regarding the Citarum River, have important implications for the remediation of pollutants from textile effluent. The pre-treatment wastewater quality indicated that dissolved oxygen levels were within acceptable limits for Class 3 water, which is deemed suitable for agricultural and fishery activities according to Indonesian Government Regulation Number 22 of 2021 on Environmental Protection and Management. However, the concentrations of dyes, turbidity, and total dissolved solids (TDS) significantly exceeded the permissible thresholds. Following treatment, all water quality parameters improved to favorable levels for use in fisheries and agriculture.

Natural bentonite can effectively eliminate dye contaminants from wastewater, providing a cost-effective and environmentally friendly solution to reduce river pollution. To maximize the efficiency of bentonite-based treatment systems in industrial settings, addressing various challenges and considerations is essential. These include overcoming issues related to wastewater reuse and adsorbent regeneration and optimizing operational parameters such as pH, temperature, and adsorbent dosage. Additionally, further research through pilot-scale studies and economic analyses is necessary to evaluate the scalability and cost-effectiveness of bentonite-based treatments.

4. Conclusion

The performance evaluation of bentonite as a natural adsorbent to adsorb textile effluent dyes resulted in 91.25% removal efficiency, and the highest adsorption capacity is 14.667 mg/g. Post-treatment analysis showed that the wastewater met river water quality standards and complied with relevant environmental

regulations. This research highlights the importance of natural bentonite's function as an effective adsorbent for dye removal in textile wastewater, thus offering a sustainable and cost-effective solution to reduce pollution in rivers such as the Citarum River. The results of this study provide valuable insights for real-world applications, highlighting the need for further optimization of operational parameters and exploration of synergies with other treatment technologies.

Data availability statement

The data included and used in this study is not confidential and is available upon request.

Funding Agencies

All fund for data collection, data analysis, and other aspects of the publication of this manuscript is provided by *Rumah Program Manajemen Sumber Daya Air dan Danau Prioritas 2023*, Research Organization for Earth Sciences and Maritime, National Research and Innovation Agency (BRIN).

Conflict of interests

Every author has stated that there is no conflict of interest to the manuscript's writing or submission.

Acknowledgment

We convey our gratitude to the distinguished reviewer(s) and the editor (s) for their significant support during the publication process.

Author Contributions

AFN and **FZ,** as the main contributors, conceptualized the study and data analysis and wrote the original article. **Z** and **HW** participated in the manuscript review process. All the writers approved the final manuscript.

References

Aichour A Zaghouane-Boudiaf H. 2020. Synthesis and characterization of hybrid activated bentonite/alginate composite to improve its effective elimination of dyes stuff from wastewater. *Applied Water Science, 10*(6), 1–13. https://doi.org/10.1007/s13201-020-01232-0

Al-Tohamy R, Ali SS, Li F, Okasha KM, Mahmoud YAG, Elsamahy T, Jiao H, Fu Y, Sun J. 2022. A critical review on the treatment of dye-containing wastewater: Ecotoxicological and health concerns of textile dyes and possible remediation approaches for environmental safety. *Ecotoxicology and Environmental Safety, 231*, 113160. https://doi.org/10.1016/j.ecoenv.2021.113160

Albadarin AB, Collins MN, Naushad M, Shirazian S, Walker G, Mangwandi C. 2017. Activated lignin-chitosan extruded blends for efficient adsorption of methylene blue. *Chemical Engineering Journal, 307*, 264–272. https://doi.org/10.1016/j.cej.2016.08.089

Chauhdary Y, Hanif MA, Rashid U, Bhatti IA, Anwar H, Jamil Y, Alharthi FA, Kazerooni EA. 2022. Effective removal of reactive and direct dyes from colored wastewater using low-cost novel bentonite nanocomposites. *Water, 14*, 1–20. https://doi.org/10.3390/w14223604

Daily J. 2019. Water, Water Everywhere: The Importance of pH and ORP Measurement in Potable Water. https://www.southforkinst.com/importance-of-ph-orp/

De Gisi S, Lofrano G, Grassi M, Notarnicola M. 2016. Characteristics and adsorption capacities of low-cost sorbents for wastewater treatment: A review. *Sustainable Materials and Technologies, 9*, 10–40. https://doi.org/10.1016/j.susmat.2016.06.002

Dehghani MH, Zarei A, Mesdaghinia A, Nabizadeh R, Alimohammadi M, Afsharnia M, McKay G. 2018. Production and application of a treated bentonite–chitosan composite for the efficient removal of humic acid from aqueous solution. *Chemical Engineering Research and Design, 140*, 102–115. https://doi.org/10.1016/j.cherd.2018.10.011

Dhar AK, Himu HA, Bhattacharjee M, Mostufa MG, Parvin F. 2023. Insights on applications of bentonite clays for the removal of dyes and heavy metals from wastewater: a review. *Environmental Science and Pollution Research, 30*(3). Springer Berlin Heidelberg. https://doi.org/10.1007/s11356-022-24277-x

Guezzen B, Medjahed B, Benhelima A, Guendouzi A, Didi MA, Zidelmal S, Abdelkrim Boudia R, Adjdir M. 2023. Improved pollutant management by kinetic and Box-Behnken design analysis of HDTMA-modified bentonite's adsorption of indigo carmine dye. *Journal of Industrial and Engineering Chemistry, 125*, 242–258. https://doi.org/10.1016/j.jiec.2023.05.034

Huang Z, Li Y, Chen W, Shi J, Zhang N, Wang X, Li Z, Gao L, Zhang Y. 2017. Modified bentonite adsorption of organic pollutants of dye wastewater. *Materials Chemistry and Physics, 202*, 266–276. https://doi.org/10.1016/j.matchemphys.2017.09.028

Jamil T, Yasin S, Ramzan N, Aslam HMZ, Ikhlaq A, Zafar AM, Aly Hassan A. 2023. Bentonite-Clay/CNT-Based Nano Adsorbent for Textile Wastewater Treatment: Optimization of Process Parameters. *Water.Switzerland, 15*(18). https://doi.org/10.3390/w15183197

Jawad AH, Saber SEM, Abdulhameed AS, Farhan AM, ALOthman ZA, Wilson LD. 2023. Characterization and applicability of the natural Iraqi bentonite clay for toxic cationic dye removal: Adsorption kinetic and isotherm study. *Journal of King Saud University - Science, 35*(4), 102630. https://doi.org/10.1016/j.jksus.2023.102630

Khan S, Ajmal S, Hussain T, Rahman MU. 2023. Clay-based materials for enhanced water treatment: adsorption mechanisms, challenges, and future directions. *Journal of Umm Al-Qura University for Applied Sciences*. https://doi.org/10.1007/s43994-023-00083-0

Kumari N Mohan C. 2021. Basics of Clay Minerals and Their Characteristic Properties. In Clay and Clay Minerals. *IntechOpen*. https://doi.org/10.5772/intechopen.97672

Kuśmierek K, Fronczyk J, Świątkowski A. 2023. Adsorptive removal of Rhodamine B dye from aqueous solutions using mineral materials as low-cost adsorbents. *Water, Air, and Soil Pollution, 234*(8). https://doi.org/10.1007/s11270-023-06511-5

Li W, Ma Q, Bai Y, Xu D, Wu M, Ma H. 2018. Chemical Engineering Research and Design Facile fabrication of gelatin/bentonite composite beads for tunable removal of anionic and cationic dyes. *Chemical Engineering Research and Design, 134*, 336–346. https://doi.org/10.1016/j.cherd.2018.04.016

Ma C, Qiao Y, Bin L, Yao Y. 2021. Performance of hybrid-constructed floating treatment wetlands in purifying urban river water: A field study. *Ecological Engineering, 171*(April), 106372. https://doi.org/10.1016/j.ecoleng.2021.106372

Majiya H, Clegg F, Sammon C. 2023. Bentonite-Chitosan composites or beads for lead (Pb) adsorption: Design, preparation, and characterization. *Applied Clay Science, 246* (September),107180. https://doi.org/10.1016/j.clay.2023.107180

Moosavi S, Lai CW, Gan S, Zamiri G, Akbarzadeh Pivehzhani O, Johan MR. 2020. Application of efficient magnetic particles and activated carbon for dye removal from wastewater. *ACS Omega, 5*(33), 20684–20697. https://doi.org/10.1021/acsomega.0c01905

Oktaviyani D, Pratiwi NTM, Krisanti M, Susanti E. 2023. Floating treatment wetlands using Vetiveria zizanioides and Heliconia psittacorum in aquaculture wastewater treatment. *IOP Conference Series: Earth and Environmental Science, 1201*(1). https://doi.org/10.1088/1755-1315/1201/1/012074

Oussalah A, Boukerroui A, Aichour A, Djellouli B .2019. Cationic and anionic dyes removal by low-cost hybrid alginate/natural bentonite composite beads: Adsorption and reusability studies. *International Journal of Biological Macromolecules, 124*, 854–862. https://doi.org/10.1016/j.ijbiomac.2018.11.197

Parlindungan JY, Pongkendek JJ, Wairara S, Abdullah N. 2019. Encapsulation powder skin duck eggshells on alginate as adsorbent methylene blue. *IOP Conference Series: Earth and Environmental Science, 343*(1). https://doi.org/10.1088/1755-1315/343/1/012194

Patanjali P, Mandal A, Chopra I, Singh R. 2022. Adsorption of cationic dyes onto biopolymer-bentonite composites: kinetics and isotherm studies. *International Journal of Environmental Analytical Chemistry, 102*(19), 8467–8489. https://doi.org/10.1080/03067319.2020.1849660

Priatna SJ, Hakim YM, Wibyan S, Sailah S, Mohadi R. 2023. Interlayer modification of West Java natural bentonite as hazardous dye Rhodamine B adsorption. *Science and Technology Indonesia, 8*(2), 160–169. https://doi.org/10.26554/sti.2023.8.2.160-169

Rahman M, Tabassum Z. 2024. Biotechnological Approach to Treat Textile Dyeing Effluents: A Critical Review Analysing the Practical Applications. *Textile Leather Review.* 7(January), 125–152. https://doi.org/10.31881/TLR.2023.189

Suryawan IWK, Helmy Q, Notodarmojo S. 2018. Textile wastewater treatment: Colour and COD removal of reactive black-5 by ozonation. *IOP Conference Series: Earth and Environmental Science, 106*(1). https://doi.org/10.1088/1755-1315/106/1/012102

Tahari N, de Hoyos-Martinez PL, Izaguirre N, Houwaida N, Abderrabba M, Ayadi S, Labidi J. 2022. Preparation of chitosan/tannin and montmorillonite films as adsorbents for Methyl

Orange dye removal. *International Journal of Biological Macromolecules, 210*, 94–106. https://doi.org/10.1016/j.ijbiomac.2022.04.231

Vithalkar SH, Jugade RM. 2020. Adsorptive removal of crystal violet from aqueous solution by cross-linked chitosan coated bentonite. *Materials Today: Proceedings, 29*, 1025–1032. https://doi.org/10.1016/j.matpr.2020.04.705

LIMNOTEK Perairan Darat Tropis di Indonesia
transforming into the Journal of Limnology and Water Resources
p-ISSN: 0854-8390 e-ISSN: 2549-8029
https://ejournal.brin.go.id/limnotek

UAV Mapping for Flood Routing in Steep and Densely Vegetated Areas: Insights from the Contok River Basin, Garang Watershed, Indonesia

Fahrudin Hanafi[1*], Edi Kurniawan[1], Dwi Priakusuma[1], Katarzyna Kubiak-Wojcicka[2]

[1]Department of Geography, Faculty of Social and Political Sciences, Universitas Negeri Semarang, Indonesia
[2]Department of Hydrology and Water Management, Faculty of Earth Sciences and Spatial Management, Nicolaus Copernicus University in Torun (UMK), Poland

*Corresponding author's e-mail: fahrudin.hanafi@mail.unnes.ac.id

Received: 28 May 2024; Accepted: 26 June 2024; Published: 30 June 2024

Abstract: This research utilizes photogrammetry to assess flood routing dynamics in the Contok river basin, a sub-watershed with a challenging landscape characterized by steep slopes, dense vegetation, and meandering patterns. The objectives are to assess Unmanned Aerial Vehicle (UAV) mapping accuracy, evaluate the river's capacity for design flood volumes, quantify the impact of land cover changes on surface runoff, and provide insights for early warning systems and watershed conservation strategies. The study area, encompassing the Contok River Basin, a sub-watershed of the Garang Watershed, covers 7,413 km² and includes a stream length of 5,274 meters in Semarang City, Central Java, Indonesia. This research employed image processing of aerial photographs and satellite imagery. Aerial photos captured using UAV data were utilized to derive elevation data and cross-sectional profiles of the Contok River, essential for understanding channel morphology and hydraulic characteristics. Concurrently, satellite imagery was used for land cover analysis, identifying vegetation and built-up areas that influence surface runoff dynamics. Hydrological analysis was performed to quantify discharge magnitudes, simulated against river cross-sections to evaluate flood behavior under varying scenarios. Our proposed UAV mapping provides adequate accuracy for small and local areas. Furthermore, it remains reliable for flood routing analysis. We discovered that the capacity of the Contok River channel in the downstream area allows it to convey design flood discharges up to a 50-year return period, contrary to the upstream area, it overflows. Notably, the shift from vegetated to built-up and agricultural areas significantly contributes to the 10.6% increase in surface runoff. This research highlights the role of UAV-based photogrammetry in assessing and mitigating flood hazards amidst evolving land cover patterns. It also enhances the understanding of flood dynamics and thus provides insights that will serve as a reference for flood early warning systems, flood management practices, and watershed conservation.

Keywords: UAV-Mapping, Photogrammetry, Flood-Routing, Surface-Runoff, Land-Cover-Changes

DOI: https://doi.org/10.55981/limnotek.2024.5028

1. Introduction

Water resources management is the effort to plan, implement, monitor, and evaluate the administration of water resource conservation, utilization, and control of water damage (Indonesia, 2019). According to Triatmodjo (2008), water resources management is divided into two main activities: utilization and regulation of water. Utilization of water resources focuses on using water for fulfilling needs such as clean water supply, irrigation, hydropower generation, water transportation, and so on. On the other hand, water regulation is oriented towards controlling water damage, ensuring that excess water does not lead to disasters (Triatmodjo, 2008).

The common phenomenon extensively studied regarding excess water is flooding. Flooding is a condition where the flow of a river exceeds the capacity of its channel, resulting in overflow or inundation (BSN, 2022). Suripin (2004) defines flooding as a condition where water exceeds the drainage channel's capacity or the flow of water in drainage channels is obstructed. Excess water can be caused by various factors, one of which is an increase in rainfall intensity, characterized by a dynamic and significant rise in precipitation (Kodoatie & Sugiyanto, 2002).

Floods are one of the disasters that occur quite frequently in Indonesia. Floods ranked third with a frequency of occurrence of 320 times, with the highest occurrence being 1,625 for forest and land fires followed by landslides with 360 occurrences (BNPB, 2023). Knowledge of potential flood threats is essential to provide early warnings, which can help in estimating community preparedness (BSN, 2022).

To estimate the potential flood threat, flood routing is commonly conducted. Flood routing is a method used to determine the timing and flow rate (hydrograph) at a specific point in the flow based on the upstream hydrograph (Triatmodjo, 2008). The determination of flow discharge is often approached using volume conservation, as seen in the Muskingum method for flood routing (Fenton, 2019). A simple method in flood routing uses a volume conservation approach, where the flow is considered as a prism. This method requires data on the flow discharge and the cross-sectional area of the stream (Fenton, 2019).

Accurate river cross-section data is necessary for flood routing. However, conducting geodetic terrestrial surveys for cross-section mapping is time-consuming, labor-intensive, and costly (Uysal et al., 2015). Consequently, there is a lack of data on challenging landscapes characterized by steep slopes, dense vegetation, and meandering river patterns. Our Study area, the Contok Watershed, is situated on the lower slopes of Mount Ungaran, at an elevation ranging from 191 to 367 meters above sea level, with an average slope of 15% and a maximum slope of 35%. The river's total length across all orders is 9.246 kilometers, exhibiting a dendritic drainage pattern. Based on remote sensing image analysis, nearly 60% of the Contok Watershed is covered with dense vegetation. Furthermore, 80% of the river channel is beneath the canopy cover, making direct aerial observations of the river channel are challenging.

The photogrammetry approach offers a solution for mapping in a remote, challenging landscape, and poorly mapped area. Photogrammetry combines art, science, and technology to obtain reliable information from photographic images (Lillesand & Kiefer, 1998; Rachmanto & Ihsan, 2020). Additionally, the use of photogrammetry with UAVs/drones is particularly suitable for large-scale measurement and mapping (Harfan *et al.*, 2019). In river morphometric data acquisition, photogrammetry processes overlapping aerial photos to create orthophoto maps and line maps (Marjuki *et al.*, 2019).

An orthomosaic procedure, as part of photogrammetry, corrects aerial photos geometrically to display objects accurately (Ikhwan *et al.*, 2021). Its primary purpose is to provide up-to-date visual information, identify specific objects, and monitor infrastructure conditions (Park *et al.*, 2022). Furthermore, orthomosaic techniques are valuable for large-scale mapping, including infrastructure, urban areas, disaster management, water resources, coastal regions, and forestry.

UAV-based photogrammetry efficiently captures detailed images of land cover, especially in small areas with low flight heights (Turner *et al.*, 2015). It can meet the demand for acquiring elevation data and ortho-photomosaic with a high spatial resolution of up to 10 cm (Rusnák, et al., 2018). Consequently, it has become an ideal method for assessing vegetation dynamics along riverbanks, analyzing river channel morphology after flooding, studying lateral river expansion, and reconstructing submerged channel topography (Dunford *et al.*, 2009; Hervouet *et al.*, 2011; Michez *et al.*, 2016; Tamminga *et al.*, 2015; Vericat *et al.*, 2009; Woodget *et al.*, 2014).

Mapping using UAV has significant importance in various scopes, such as cartography, environmental monitoring, and urban planning (Daud, *et al.*, 2022). The application of UAVs is also effective in erosion and flood surveys, as UAVs can continuously

produce 2D and 3D images in a short amount of time in the field (Duo *et al.*, 2018). Additionally, UAV can be used for continuous monitoring and mapping of natural disasters (Kim *et al.*, 2019).

Advanced technology, UAVs can assist in mapping by monitoring the elevation of the study area over time (Young *et al.*., 2021). In addition, UAVs are also considered more cost-effective with reasonably good accuracy compared to traditional surveys for spatial data collection (Hill, 2019).

The use of UAVs as data acquisition tools has been highly successful in the field of hydrology, particularly for modeling flood hydraulic characteristics. This success is bolstered by the high-resolution topographic data acquired from UAV mapping of river channels and floodplains (Feng *et al.*, 2015; Annis, *et al.*, 2020; Karamuz *et al.*, 2020). DEMs of topographic data are one of the primary sources used in hydraulic modeling and flood inundation mapping (Saksena & Merwade, 2015). DEM represents the elevation of the ground surface in the form of a digital model, which can be utilized to identify the slope or gradient of an area (Mabrur & Agustina, 2022). This data is essential for representing information about land surfaces that have been inundated or showing the direction of water flow during floods. Therefore, data acquisition using UAV platforms can enhance the effectiveness of preventive and systematic disaster management (Kim *et al.*, 2019).

Nevertheless, research on flood routing in steep, densely vegetated areas is limited. While many studies have examined flood dynamics across various terrains, the unique characteristics of regions with extreme slopes and dense vegetation are understudied. Previous research has focused on flat or moderately sloped areas, neglecting specific aspects such as the effects of steep slopes on infiltration, evapotranspiration, and flow resistance by vegetation. This study addresses this gap by using aerial photography for detailed hydrological and topographical analysis. There is an urgent need for more research to develop accurate aerial photo-based models and effective flood mitigation strategies for steep, vegetated regions.

Therefore, the research objectives are to: first, assess the accuracy of UAV mapping in a challenging setting, such as a steep and densely vegetated river basin; second, conduct a flood routing analysis to evaluate the storage capacity of the Contok River channel for the design flood volume; and third, quantify the impact of land cover changes on surface runoff. This research is expected to provide insights that will serve as a reference for early warning systems against flood threats and for watershed conservation.

2. Materials and Methods

This research employed two analyses: photogrammetric analysis, hydrological analysis. Photogrammetric analyses were used to determine the river's cross-sectional profile, while hydrological analysis will be conducted to obtain flood routing results. In addition, a remote sensing data series was used to identify the change in the runoff coefficient.

2.1 Study Area

The research location is Contok Watershed, which is a sub-watershed of the Garang Watershed. The Contok Watershed has an area of 7,413 km² with 5,274 km of stream length, located in Patemon and Sekaran Village, Gunungpati District, Semarang City, Central Java Indonesia. Figure 1 is the map of the study area.

2.2. Photogrammetric Analysis

In this study, photogrammetric mapping aims to establish a geometric relationship between an object and an aerial photograph/image and derive spatial information about the object under study from the photograph. The photogrammetry process yields data in the form of land features captured through aerial photography. Photogrammetry processes data quickly and with high quality (Sutjipto *et al.*,2017). According to Putra *et al.* (2023) The photogrammetric mapping resulting data includes various models such as the Digital Elevation Model (DEM), Digital Terrain Model (DTM), and Digital Surface Model (DSM).

The processing of aerial photos from UAVs was conducted using Agisoft Metashape software (https://www.agisoft.com/). This software was used for image processing of UAV acquisition data through the formation of

mosaics with automatic tie point input, the formation of three dimensions (point cloud), and the extraction of DEM from the orthophoto. The output produced is a three-dimensional representation of the surface with coordinates X, Y, and Z. The resulting orthomosaic is then tested using the root mean square error (RMSE) method, which involves comparing the total difference in point displacements to the number of sampled points. The accuracy values are classified according to the Regulation of the Indonesian Geospatial Information Agency (BIG) number 15 of 2014 (BIG, 2014) as shown in Table 1.

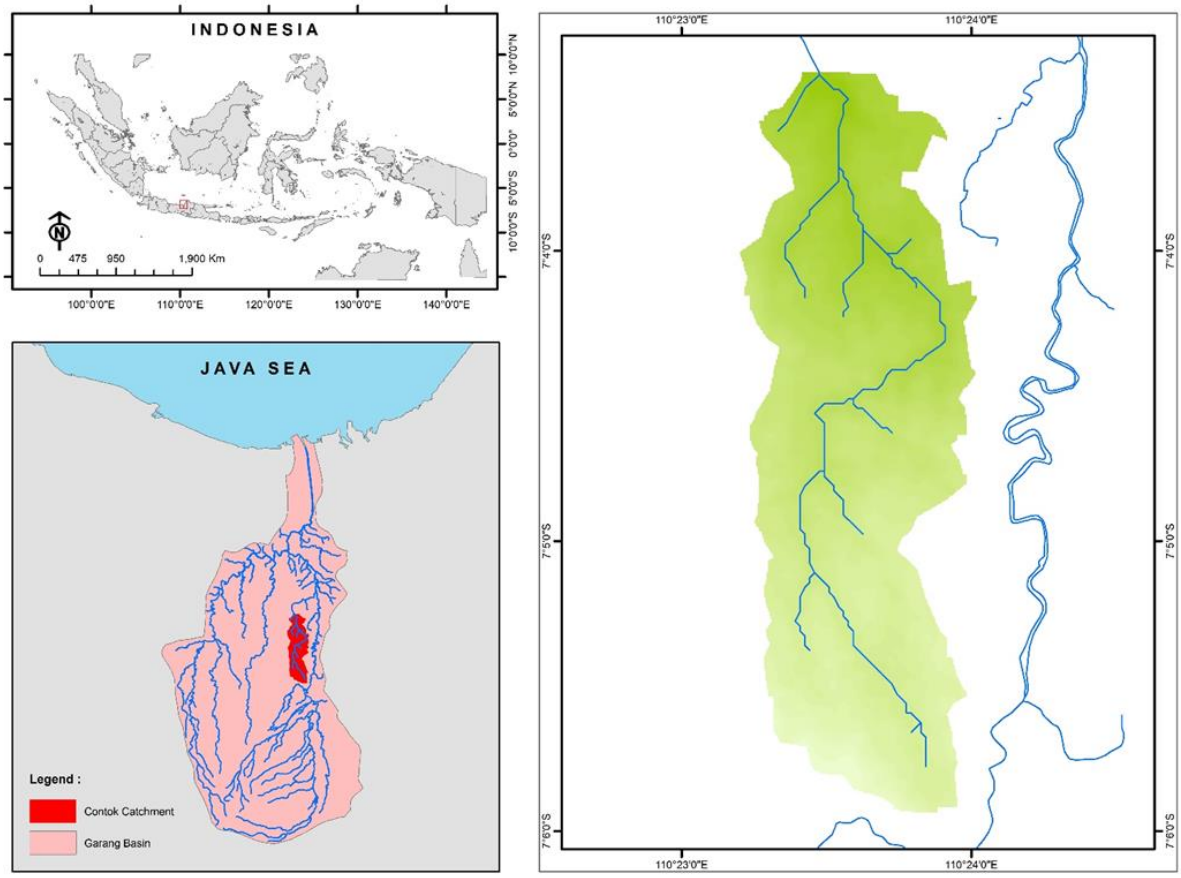

Figure 1. Map of the Study area, Contok River Basin, a Sub-Watershed of Garang Watershed, Indonesia

Table 1. Classification of Map Accuracy

No.	Scale	Accuracy Map of RBI		
		Class 1	Class 2	Class 3
		CE90 (m)	CE90 (m)	CE90 (m)
1	1: 1,000,000	200	300	500
2	1: 500,000	100	150	250
3	1: 250,000	50	75	125
4	1: 100,000	20	30	50
5	1: 50,000	10	15	25
6	1: 25,000	5	7,5	12,5
7	1: 10,000	2	3	5
8	1: 5,000	1	1.5	2.5
9	1: 2,000	0.5	0.75	1.25
10	1: 1,000	0.2	0.3	0.5

Source: (BIG, 2014)

2.3 Flood Routing

Flood routing was conducted using rainfall data from Climate Hazards Group InfraRed Precipitation with Station data (CHIRPS) covering 20 years, from 2003 to 2022, retrieved from the Climate Hazard Centre, UC Santa Barbara website (UCSB, 2023). The design flood was analyzed for 25-year and 50-year return periods, using the rational method calculation.

To track the river's storage volume in response to accommodate the design flood discharge, the Manning method was employed. By examining the flow velocity values based on the river bed slope and cross-sectional area, simulations were conducted to assess the river's storage capacity against 25 and 50-year design flood discharges.

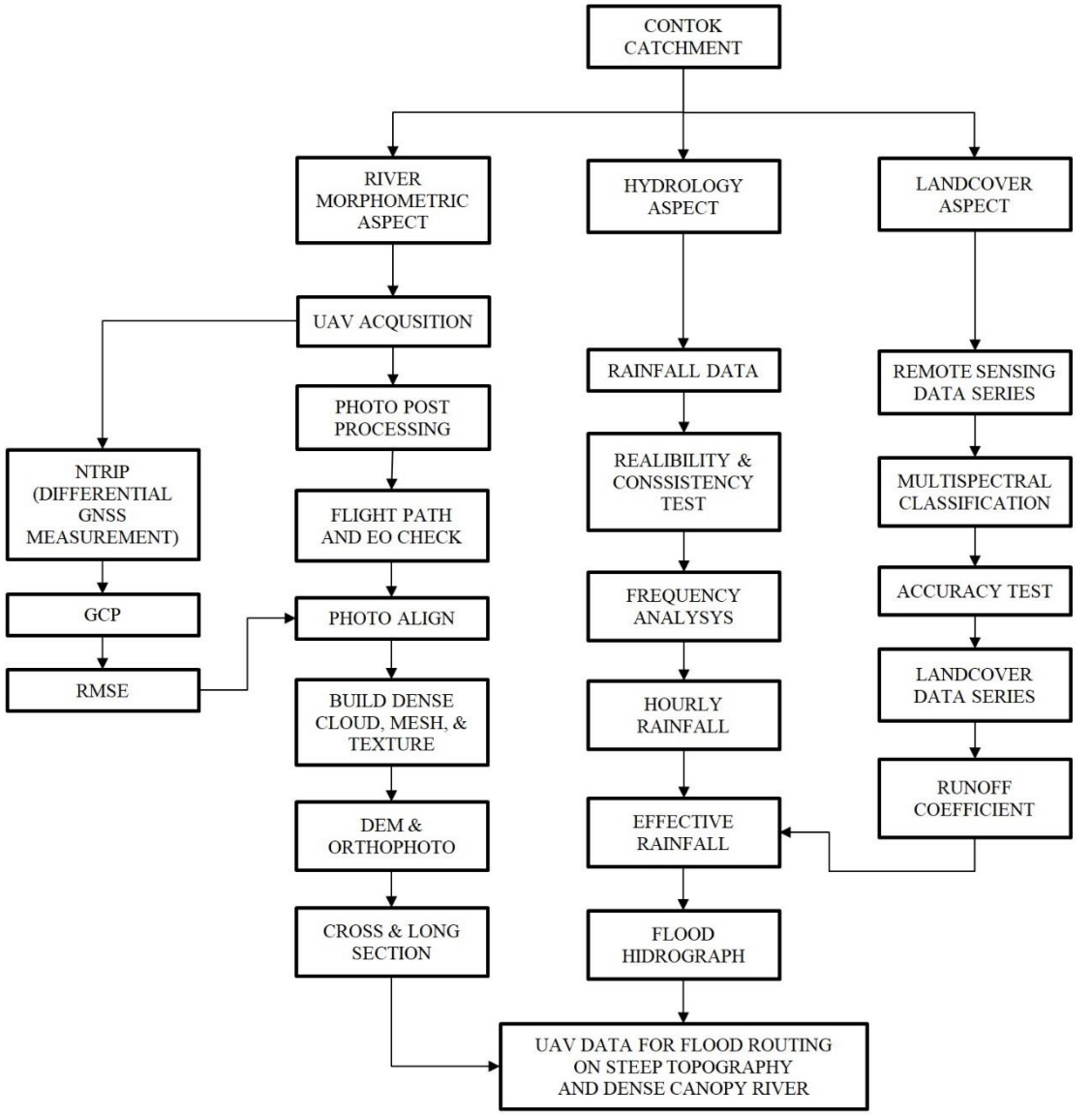

Figure 2. Flowchart diagram of the flood routing study using UAV data, precipitation data, and remote sensing data series in the steep and densely vegetated areas of the Contok river basin, a sub-watershed of the Garang Watershed, Semarang, Central Java, Indonesia

There are several methods used in design flood calculation, i.e. Mononobe method for effective rainfall calculation (Equation 1), Kirpich method for time of concentration calculation (Equation 2), Rational method for design flood calculation (Equation 3), Manning method for defining the stream velocity based on the steepness of the river cross-sectional profile and its natural condition (Equation 4). Generally, the more cross-sectional profiles will result in a more precise simulation.

$$I = \left[\frac{R_{24}}{24}\right] \times \left[\frac{24}{t_c}\right]^{2/3} \quad \text{....Eq. 1}$$

where, I: effective rainfall (mm), R_{24}: design rainfall (mm), t_c: time of concentration (hour).

$$t_c = 0{,}01947 \times L^{0{,}77} \times S^{-0{,}385} \quad \text{....Eq. 2}$$

where, t_c: time of concentration (hour), L: river/stream length (m), and S: riverbed steepness/slope.

$$Q = 0{,}278 \times C \times I \times A \quad \text{....Eq. 3}$$

where, Q: design flood (m^3/s), C: runoff coefficient I: effective rainfall (mm) A: catchment area (km^2).

$$v = \frac{1}{n} \times R^{2/3} \times S^{1/2} \quad \text{....Eq. 4}$$

where, v: stream velocity (m/s), n: Manning roughness coefficient, R: Hydraulic radius, S: slope.

Figure 2 shows a summary of each step used in this research. Image processing is conducted for both aerial photographs and satellite imagery. Aerial photographs were processed to obtain the elevation data and the cross-sectional profiles of the Contok river, while satellite imageries were used for land cover identification analysis. On the other hand, hydrological analysis was performed to determine the discharge magnitude and further simulated against the river cross-section profiles. This study serves as a flood mitigation effort, by identifying areas of the river with lower capacity due to variations in cross-sectional heights (velocity) in comparison to the flood magnitude.

3. Result and Discussion

3.1. River Morphometric aspect

The aerial images collected in this research total approximately 720 photos, captured over two flights to cover the entire study area as shown in Figure 3. Each flight was conducted with specifications of GSD: 2,73 cm/pixel, Flight altitude: 100 m, Flight area 965x346 m, Photo overlap: 70%, and Flight time: 15 minutes 30 seconds.

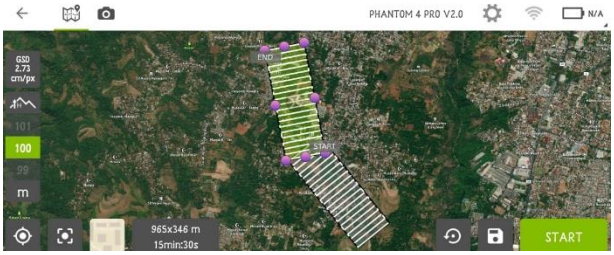

Figure 3. UAV flights path to cover the Contok River Basin, a sub-watershed of Garang River, Central Java Indonesia

Modeling and Ortho mosaicking processes from aerial photos resulted in a block photo of the research area with a DEM built based on UAV's inherent coordinate values. The orthomosaic data is in raster form, providing information in pixel-based form. To obtain more specific quantitative data, transforming raster data into vector data is necessary. This process converts the Orthomosaic raster data into vector data to identify the length and area of the studied objects. Figure 4 shows the results of the Ortho-mosaicking process.

Figure 5 provides spatial and elevation data resolution of 0.05m. The subsequent analysis conducted is planimetric testing to determine the data quality level from the post-processing of aerial photos. Planimetric testing is carried out by testing the positional accuracy referring to the actual coordinates at the test points on the ground surface. The control points used are Independent Control Points (ICP). The planimetric testing results are presented in Table 2.

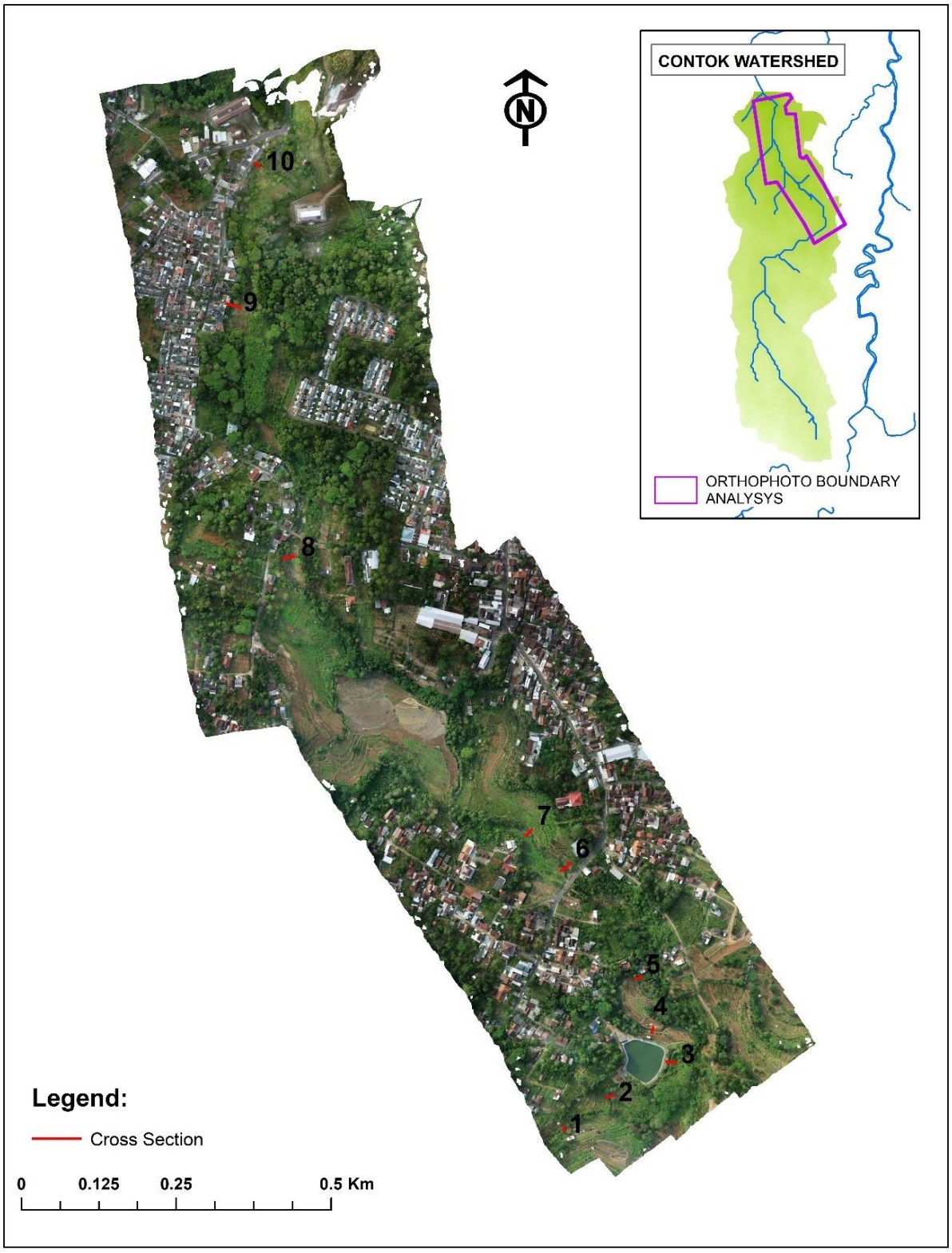

Figure 4. Orthomosaic and cross-sectional location (marked in Red) of Contok River Basin, a sub-watershed of Garang River, Central Java Indonesia

Table 2. Planimetric test

No	Image Distance (m)	Real Distance (m)	Difference (m)
1	4.249	4.395	0.146
2	3.757	3.840	0.083
3	4.341	4.435	0.094
4	3.604	3.640	0.036
5	4.330	4.435	0.105
6	4.000	4.045	0.045
7	4.859	4.890	0.031
8	4.215	4.395	0.180
Displacement Distant Total		0.720	
Planimetric Test Result		0.300	

The DEM extracted from the orthophoto post-processing after the 3D point cloud was generated, was then used to create cross-sectional data of the river within the most opened area. Figure 5 is the DEM map with the locations of the river cross-sections. Figure 6 is an example of the generated cross-sectional profile.

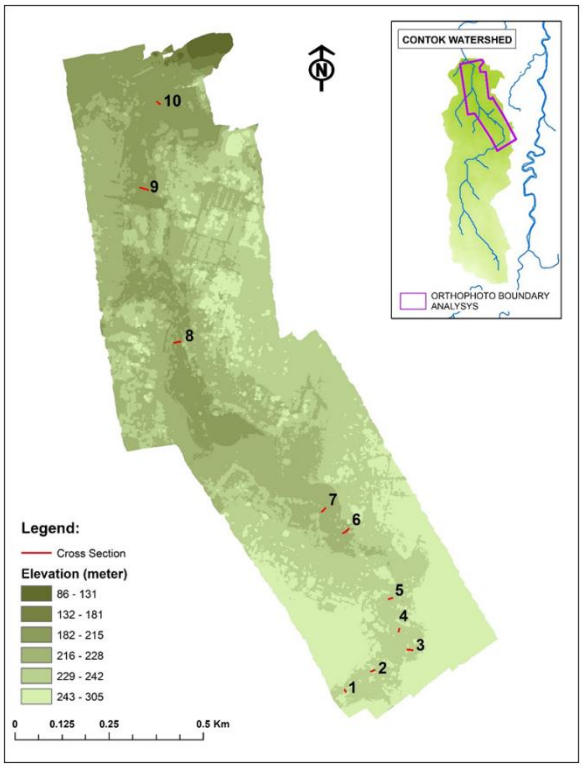

Figure 5. The Digital Elevation Model (DEM) map along with the locations of the river cross-sections.

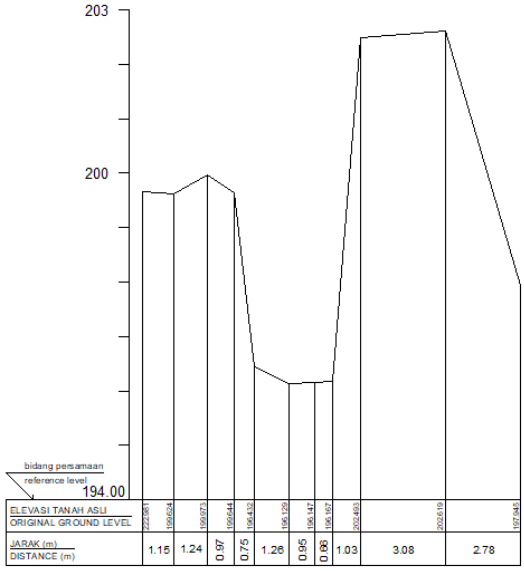

Figure 6. Cross Section on Control Point

The map produced from this research falls under the category of large-scale maps, namely 1:10,000. Referring to the standards of the BIG as shown in Table 1, the map resulting from orthomosaic processing in this study falls under Class 1 accuracy. The planimetric test applied through the ICP control method yields a displacement value of 0.3 m (Table 2), which is below the threshold of the BIG accuracy criteria, which is 2 m. ICP measurement was conducted by performing a manual survey using measuring tape on the easily recognized objects both in aerial photos and in the field. For example, the bridge width serves as a control point for the river section, as do the street corners at certain locations. Overall, eight places were measured as ICP.

The application of UAV mapping in this study involved Ground Control Points (GCPs) to align and scale the photogrammetric data correctly by providing reference points that the software uses to correct any distortions and ensure spatial accuracy. Good accuracy also can be achieved through favorable weather conditions, optimal flying altitude, and well-suited non-vegetative areas for control purposes. In this study, a total of 12 Ground Control Points (GCPs) were measured using the GNSS (Global Navigation Satellite System) NTRIP (Networked Transport of RTCM via Internet Protocol) method, with a Sokkia GRX-2 as the rover and the Telkom Simpang Lima CORS as the base station.

This study demonstrates that the use of ICP in photogrammetry remains effective for narrow river catchments. The advantage of the ICP method in narrow areas lies in the ease of field verification of objects that are easily recognizable both from aerial photos and on the ground. The use of GCP in this study was less effective due to the reliance on the NTRIP (stop and go) method, which depends on internet connectivity. In areas with moderate to steep slopes and dense vegetation cover, this dependence leads to signal distortion, resulting in poor location accuracy with intolerable RMSE (Root Mean Square Error). On the other hand, some of the GCPs are unseen from the aerial photos due to the densely vegetated area. Consequently, this study indicates that ICP is effective for photogrammetry in small areas, whereas GCP with static location measurement methods is required for larger areas.

3.2. Landcover and precipitation aspects

Land cover data in the Contok Watershed is required for the analysis of run-off coefficients in flood routing. Land cover is associated with the direction of river flow from upstream to downstream. Identification of land cover is conducted through the multispectral classification of Sentinel-2 imagery, using supervised classification maximum likelihood. This method falls under digital classification types because data processing is based on the digital values of images using specific software. The principle used is to group pixels with similar spectral characteristics into the same category or class for identification through a distinguishing color (Gibson & Power, 2000; Marini *et al.*, 2014). The Landcover map of 2013 and 2023 are shown in Figure 7, while the tabular comparison is shown in Table 3.

Table 3. Comparison of Land Cover in the Contok Watershed in 2013 and 2023

No	Land Cover	2013 (km^2)	2023 (km^2)
1	Built Area	1.416	1.914
2	Open Area	0.086	0.173
3	Agriculture	0.421	0.923
4	Vegetation	0.590	4.402
	Total	7.413	7.413

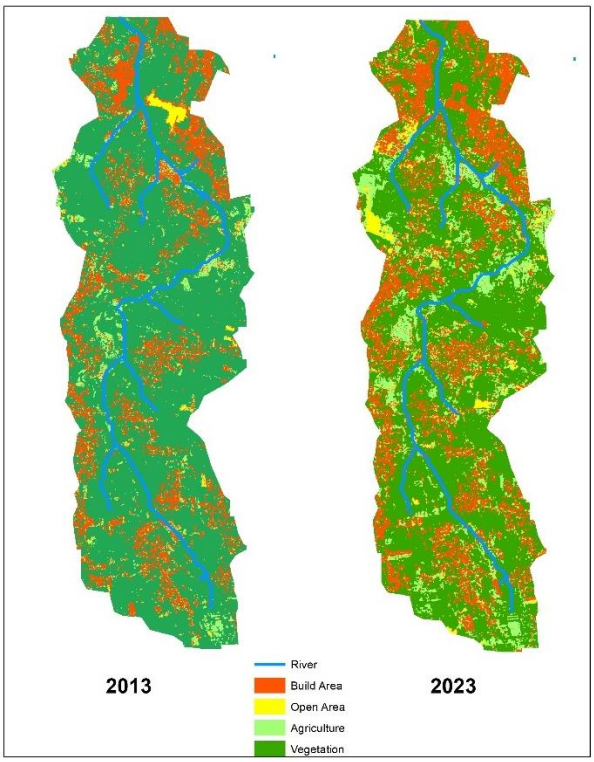

Figure 7. Comparison Land Cover in the Contok watershed in 2013 and 2023, resulted from the Sentinel-2 imagery multispectral classification

Frequency analysis was conducted on rainfall data from CHIRPS to obtain rainfall magnitudes with return periods of 25 and 50 years. Using watershed parameters of land cover (Table 3), the length of the river segment, riverbed slope, the coefficient of run-off analysis, concentration time, and effective rainfall are then analyzed and resulted in the runoff coefficient (C) of the Contok Watershed as shown in Table 4.

Table 4. The runoff coefficient (C) of the Contok Watershed

No	Land Cover	2013			2023		
		Area (km^2)	C	Composite	Area (km^2)	C	Composite
1	Built Area	1,416	0,5	0,098	1,914	0,5	0,129
2	Open area	0,086	0,3	0,004	0,173	0,3	0,007
3	Agriculture	0,421	0,3	0,017	0,923	0,3	0,037
4	Vegetation	5,490	0,2	0,148	4,402	0,2	0,119
	Total	7,413		0,264	7,413		0,292

3.2. Hydrology aspect

The Contok Watershed area has a length of 5,274 meters, with a riverbed (based on long section analysis) slope of 0.0207. The concentration-time value is determined to be 63.68 minutes or 1.06 hours. Based on this concentration time value, effective rainfall is analyzed using the Mononobe method (Equation 1). The effective rainfall values for each return period are obtained as shown in Table 5.

Table 5. The results of effective rainfall analysis and discharge

Return Period (year)	Rain (mm)	Effective Rain (mm)	Q 2013 (m^3/s)	Q 2023 (m^3/s)
25	118,088	39,354	21,418	23,698
50	130,463	43,468	23,662	26,181

The calculated design flood discharge results for the years 2013 and 2023 with return periods of 25 and 50 years are presented in Table 5. The Manning equation is used to simulate river storage based on cross-sectional profiles and flow velocities. The coefficient of roughness for the natural channel with vegetation obstruction is 0.07, and the cross-sectional area (Figure 5) is 12.06 m^2. Therefore, the channel storage capacity is 25.38 $m^3\ s^{-1}$.

The same storage capacity calculations were conducted for the other ten cross-section points, to determine the storage capacity representing the upstream, middle, and downstream of Contok Watershed.

Table 6 shows the river storage capacity analyzed at each cross-section based on the Manning equation (Equation 4). The storage capacity is then simulated against a discharge with a return period of 50 years in 2023. The simulation of storage volume at each cross-section is shown in Figure 8 to 17.

Table 6. Storage simulation for each cross-section

Location	Area (m2)	P (m)	V (m/s)	Capacity (m3/s)	Q25-2023 (m3/s)
CS 1	5.25	6.52	1.78	9.33	26.18
CS 2	7.90	7.41	2.14	16.94	26.18
CS 3	15.69	12.77	2.36	36.95	26.18
CS 4	8.57	9.42	1.93	16.52	26.18
CS 5	5.10	9.03	1.40	7.15	26.18
CS 6	25.58	16.69	2.73	69.84	26.18
CS 7	11.24	10.03	2.22	24.89	26.18
CS 8	15.95	11.64	2.53	40.42	26.18
CS 9	13.65	10.65	2.42	33.09	26.18
CS 10	12.06	9.73	2.37	28.58	26.18

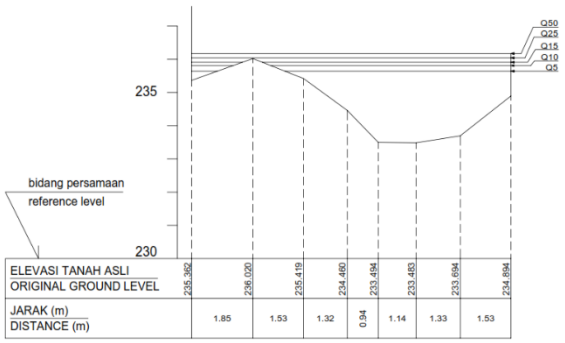

Figure 8. Storage simulation for cross-section 1

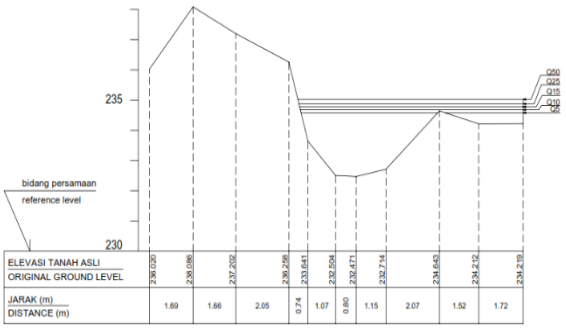

Figure 9. Storage simulation for cross-section 2

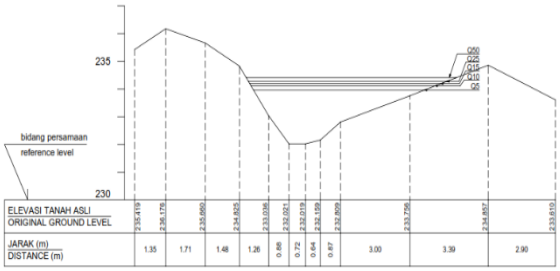

Figure 10. Storage simulation for cross-section 3

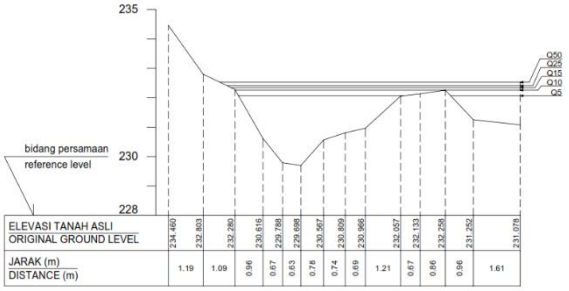

Figure 11. Storage simulation for cross-section 4

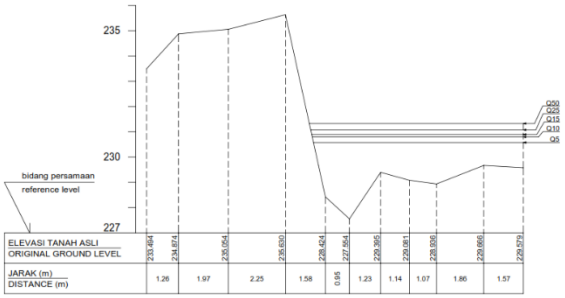

Figure 12. Storage simulation for cross-section 5

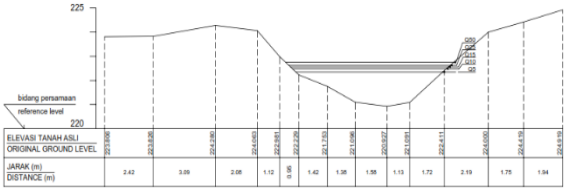

Figure 13. Storage simulation for cross-section 6

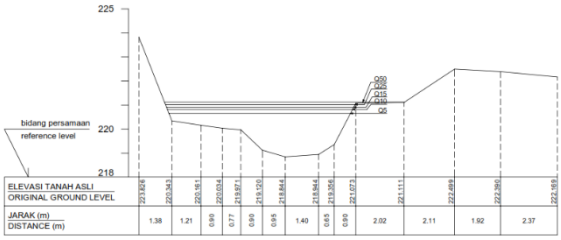

Figure 14. Storage simulation for cross-section 7

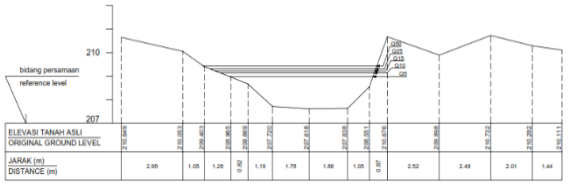

Figure 15. Storage simulation for cross-section 8

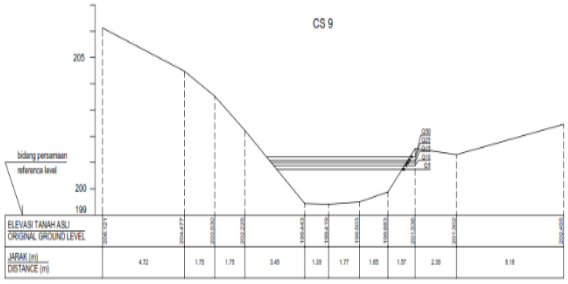

Figure 16. Storage simulation for cross-section 9

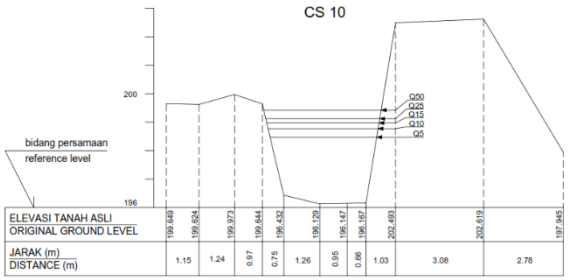

Figure 17. Storage simulation for cross-section 10

3.3. Landcover change aspect

Land cover changes are an important factor in increasing surface runoff. This is supported by several previous studies; deforestation and urbanization are the most influential factors in changing hydrological cycles and sedimentation (Siswanto & Frances, 2019). Changes in land cover, especially in built-up areas, greatly affect the magnitude of surface runoff (Sidiq, *et al.*, 2022).

Massive changes in land cover occur with a reduction in vegetation area of 1.01 km², converting it into built-up areas and agricultural land. These changes trigger changes in the runoff coefficient and increase the results of the design flood analysis by 10,6%. The downstream section of the Contok River in the study area is still capable of accommodating the 50-year return period flood discharge for the 2023 simulation, with overflow occurring only at cross-sections 1, 2, 4, and 5. This is due to field conditions, where the upstream area has small channels with banks that are either fallow land or have been utilized as fields, while in the downstream area, embankments have been constructed, along with river channel improvements.

4. Conclusion

The research findings indicate that UAV mapping without GCPs provides adequate accuracy for small and local areas. However, for larger areas with extensive flight paths, GCPs are necessary, especially for river mapping on steep slopes with dense vegetation, and meandering patterns. Special treatments are required to obtain sequential and continuous cross-sections with integrated elevation, during aerial photography and post-processing. Further research could focus on integrating multi-return LiDAR with photogrammetric point clouds to improve accuracy in dense vegetation areas. Developing automated algorithms for vegetation point filtering in photogrammetry, possibly using machine learning, would enhance efficiency. Comparative studies among LiDAR, filtered photogrammetry, and vegetation indices could validate their performance in varied environments. Exploring advanced remote sensing technologies like hyperspectral imaging or radar systems could further advance canopy removal and land elevation mapping capabilities.

The capacity of the Contok River channel in the downstream area is still able to convey design flood discharges up to a 50-year return period, while in the upstream area, it overflows. A significant factor in increasing surface runoff in this study is the change in land cover. The change in land cover from vegetated areas to built-up and agricultural areas increases surface runoff by 10.6%. To minimize flooding at specific cross-sections and return periods, it is necessary to construct river embankments and optimize reservoirs, considering land use changes beyond our control.

Data availability statement

The topographic data of the river and aerial photographs utilized in this study were obtained through direct measurements. Rainfall data were sourced from the Central Java Public Works Department and the UCSB Climate Hazards Center - CHIRPS website (https://www.chc.ucsb.edu/data/chirps).

Funding Agencies

This research was supported by the Department of Geography and the Faculty of Social and Political Sciences, Universitas Negeri Semarang, Indonesia.

Conflict of interests

All authors declare that there are no conflicts of interest in this study.

Acknowledgment

Special thanks to the Kobra Sekempol Survey Team and CV. Sembilan Samudera for their contributions in terms of equipment, effort, and expertise.

References

Annis A, Nardi F, Petroseli A, Apollonio C, Arcangeletti E, Tauro F, Grimaldi S. 2020. UAV DEMs for Small Scale Flood Hazard Mapping. *Water*. https://doi.org/10.3390/w12082232

Badan Informasi Geospasial-BIG. 2014. Peraturan Kepala BIG Nomor 15 Tahun 2014 tentang Pedoman Teknis Ketelitian Peta Dasar. Jakarta: BIG. In Bahasa

Badan Nasional Penganggulangan Bencana-BNPB. 2023. Data Informasi Bencana Indonesia.

Retrieved December 18, 2023, from https://dibi.bnpb.go.id/ In Bahasa

Badan Standarisasi Nasional-BSN. 2022. SNI 8840-3:2022 Sistem Peringatan Dini Bencana - Bagian 3: Banjir. Jakarta: Badan Standarisasi Nasional. In Bahasa

Daud SM, Yusof MY, Heo CC, Khoo LS, Singh MK, Mahmood MS, Nawawi H. 2022. Applications of Drone in Disaster Management: A Scooping Review. *Science Justice, 62*, 30-42. https://doi.org/10.1016/j.scijus.2021.12.001

Dunford R, Michel K, Gagnage M, Piégay H, Trémelo ML. 2009. Potential and Constraints of Unmanned Aerial Vehicle Technology for The Characterization of Mediterranean Riparian Forest. *International Journal of Remote Sensing, 4915-4935*. https://doi.org/10.1080/01431160903023025

Duo E, Trembanis AC, Dohner S, Grottoli E, Caviola P. 2018. Local-scale Post-event Assessments with GPS and UAV-based Quick-response Surveys: A Pilot Case From The Emilia-Romagna. Italy) Coast. *Natural Hazard and Earth System Sciences, 18*(11), 2969-2989. https://doi.org/10.5194/nhess-18-2969-2018

Feng Q, Liu J, Gong J. 2015. Urban Flood Mapping Based on Unmanned Aerial Vehicle Remote Sensing and Random Forest Classifier—A Case of Yuyao, China. *Water*. https://doi.org/10.3390/w7105377

Fenton JD. 2019. Flood Routing Methods. *Journal of Hydrology, 570*, 251-264. https://doi.org/10.1016/j.jhydrol.2018.12.073

Gibson PJ, Power CH. 2000. Introductory Remote Sensing: Digital Image Processing and Applications. New York: Routledge.

Harfan A, Yudhatama D, Bachrodin I. 2019. Pemanfaatan Metode Fotogrametri Untuk Pengukuran Garis Pantai dan Identifikasi Objek-objek Tematik dengan Menggunakan Wahana UAV. Unmanned Aerial Vehicle. Studi Kasus Pengukuran Garis Pantai di Pangkalan TNI AL Pondok Dayung. *Jurnal Chart Datum*, 71-84. In Bahasa

Hervouet A, Dunford R, Piégay H, Belletti B, Trémélo ML. 2011. Analysis of Post-flood Recruitment Patterns in Braided-Channel Rivers at Multiple Scales Based on an Image Series Collected by Unmanned Aerial Vehicles, Ultra-light Aerial Vehicles, and Satellites. *GIScience Remote Sensing, 50-73*. https://doi.org/10.2747/1548-1603.50.1.50

Hill AC. 2019. Economical Drone Mapping For Archeology: Comparion of Efficiency and Accuracy. *Journal of Archeological Science: Reports, 24*, 80-91. https://doi.org/10.1016/j.jasrep.2018.11.021

Ikhwan M, Ratnaningsih A, Lestari I, Ikhsani H. 2021. Aplikasi Teknologi Unmanned Aerial Vehicle. UAV) untuk Mengidentifikasi Tutupan Hutan dan Lahan di Universitas Lancang Kuning. *Wahana Forestra Jurnal Kehutanan*, 86-101. https://doi.org/10.20886/jphh.2020.38.1.41-53 In Bahasa

Indonesia. 2019. Undang-undang Nomor 17 Tahun 2019 tentang Sumber Daya Air. Jakarta: Kementerian Hukum dan HAM. In Bahasa

Karamuz E, Romanowicz RJ, Doroszkiewicz J. 2020. The Use of Unmanned Aerial Vehicles in Flood Hazard Assessment. *Journal of Flood Risk Management*. https://doi.org/10.1111/jfr3.12615

Kim SS, Kim TH, Sim JS. 2019. Applicability Assessment of UAV Mapping for Disaster Damage Investigation in Korea. *The International Archives of the Photogrammetry Remote Sensing and Spatial Information Science, 209-214*. https://doi.org/10.5194/isprs-archives-XLII-3-W6-209-2019

Kodoatie RJ, Sugiyanto. 2002. Banjir: Beberapa Penyebab dan Metode Pengendaliannya dalam Perspektif Lingkungan. Yogyakarta: Pustaka Pelajar. In Bahasa

Lillesand TM, Kiefer RW. 1998. Penginderaan Jauh dan Interpretasi Citra. 4 ed. Yogyakarta: Gadjah Mada University Press. In Bahasa

Mabrur AY, Agustina F. 2022. Pemetaan Orthophoto untuk Rencana Pembuatan Peta Rawan Longsor. *Jurnal Ilmiah Universitas Batanghari Jambi, 408-411*. https://doi.org/10.33087/jiubj.v21i2.1630 In Bahasa

Marini Y, Emiyati, Hawariyah S. 2014. Perbandingan Metode Klasifikasi Supervised Maximum Likelihood dengan Klasifikasi Berbasis Objek untuk Inventarisasi Lahan Tambak di Kabupaten Maros. *Prosiding Seminar Nasional Penginderaan Jauh 2014*, 505-516. In Bahasa

Marjuki B, Astutik S, Hartini KS, Wijanarko SR, Prananingtyas SR, Ridha MR, Ananda R. 2019. Pemetaan menggunakan UAV. Pusdatin Kementerian PUPR Indonesia.

Michez A, Piégay H, Lisein J, Claessens H, Lejeune P. 2016. Classification of Riparian Forest Species and Health Condition Using Multi-temporal and Hyperspatial Imagery from Unmanned Aerial System. *Environmental Monitoring and Assessment*. https://doi.org/10.1007/s10661-016-5282-0

Park J, Cho YK, Kim S. 2022. Deep learning-based UAV image segmentation and inpainting for generating vehicle-free orthomosaic. *International Journal of Applied Earth*

Observation and Geoinformation. https://doi.org/10.1016/j.jag.2021.102520

Putra RS, Riani D, Silitonga SP. 2023. Pembuatan Digital Elevation Model Universitas Palangka Raya Menggunakan Drone dan GPS Geodetik. *Jurnal Basement, 1*, 33-40. https://doi.org/10.1016/j.basment.2023.01.004 In Bahasa

Rachmanto DH Ihsan M. 2020. Pemanfaatan Metode Fotogrametri Untuk Pemetaan Skala 1: 1000. Studi Kasus: Universitas Pendidikan Indonesia. *Jurnal ENMAP*, 81-86. https://doi.org/10.30630/enmap.v2i2.34

Rusnák M, Sládek J, Kidová A, Lehotský M. 2018. Template for high-resolution river landscape mapping using UAV technology. *Measurement, 139-151*. https://doi.org/10.1016/j.measurement.2018.02.036

Saksena S, Merwade V. 2015. Incorporating the effect of DEM resolution and accuracy for improved flood inundation mapping. *Journal of Hydrology, 180-194*. https://doi.org/10.1016/j.jhydrol.2015.08.021

Sidiq W, Hanafi F, Priakusuma D, Haruman W, Sumarso M, Setyowati N. 2022. Analisis Banjir Genangan di Kawasan Tembalang dan Sekitarnya. *Jurnal Riptek, 137-144*. https://doi.org/10.31289/riptek.v2i1.4261

Siswanto SY, Frances F. 2019. How land use/land cover changes can affect water, flooding and sedimentation in a tropical watershed: a case study using distributed modeling in the upper Citarum Watershed, Indonesia. *Environmental Earth Sciences, 78*(17), 1-15. https://doi.org/10.1007/s12665-019-8575-7

Suripin. 2004. Sistem Drainase Perkotaan yang Berkelanjutan. Yogyakarta: Andi Offset. In Bahasa

Sutjipto AT, Purwiyono TT, Azizi MA. 2017. Monitoring Pergerakan Massa Batuan Dengan Metode Terestris Menggunakan Total Station Dan Metode Fotogrametri Di Kaliwadas, Kebumen, Jawa Tengah. Workshop Seminar Nasional Geomekanika 4. Padang. In Bahasa

Tamminga AD, Eaton BC, Hugenholtz CH. 2015. UAS-based remote sensing of fluvial change following an extreme flood event. *Earth Surface Processes and Landforms*, 1464-1476. https://doi.org/10.1002/esp.3940

Triatmodjo B. 2008. Hidrologi Terapan. Cetakan Kedua ed.. Yogyakarta: Beta Offset.

Turner D, Lucieer A, De-Jong SM. 2015. Time Series Analysis of Landslide Dynamics Using an Unmanned Aerial Vehicle. UAV. *Remote Sensing*, 1736-1757. https://doi.org/10.3390/rs70301736

UCSB Climate Hazards Center. 2023. Climate Hazards Group InfraRed Precipitation with Station data. CHIRPS. Retrieved from https://www.chc.ucsb.edu/data/chirps last accessed on Jan 16, 2024

Uysal M, Toprak A, Polat N. 2015. DEM generation with UAV Photogrammetry and accuracy analysis in Sahitler hill. *Measurement*, 539-543. https://doi.org/10.1016/j.measurement.2015.02.018

Vericat D, Brasington J, Wheaton J, Cowie M. 2009. Accuracy assessment of aerial photographs acquired using lighter-than-air blimps: low-cost tools for mapping river corridors. River Research and Applications, 985-1000. https://doi.org/10.1002/rra.1243

Woodget AS, Carbonneau PE, Visser F, Maddock IP. 2014. Quantifying submerged fluvial topography using hyperspatial resolution UAS imagery and structure from motion photogrammetry. *Earth Surface Processes and Landforms*, 47-64. https://doi.org/10.1002/esp.3418

Young SS, Rao S, Dorey K. 2021. Monitoring The Erosion and Accretion of A Human-built Living Shoreline With Drone Technology. *Environmental Challenges, 5*. https://doi.org/10.1016/j.envc.2021.100252

p-ISSN: 0854-8390
e-ISSN: 2549-8029
LIMNOTEK
Perairan Darat Tropis di Indonesia,
***transforming into the* Journal of Limnology and Water Resources**

Volume 30, Number 1, June 2024

Published by:

National Research and Innovation Agency (BRIN)

Indonesian Limnology Society (MLI)